The Astrophysical Journal Supplement Series, 137:21–73 2001 November

THE UCSD HIRES/KECK I DAMPED Lyα ABUNDANCE DATABASE. I. THE DATA

Jason X. Prochaska,[1,2] Arthur M. Wolfe,[1,3] David Tytler,[1,3] Scott Burles,[1,4] Jeff Cooke,[1,3] Eric Gawiser,[1,3] David Kirkman,[1,3] John M. O'Meara,[1,3] and Lisa Storrie-Lombardi[1,5]

Received 2001 April 27; accepted 2001 June 14

ABSTRACT

We present new chemical abundance measurements of 16 damped Lyα systems at $z > 1.5$ and update our previous abundance analyses. The entire database presented here was derived from HIRES observations on the Keck I telescope, reduced with the same software package, and analyzed with identical techniques. Altogether, we present a large, homogeneous database of chemical abundance measurements for protogalaxies in the early universe, ideal for studying a number of important aspects of galaxy formation. In addition, we have established an on-line directory for this database and will continuously update the results.

Subject headings: galaxies: abundances — galaxies: evolution — nuclear reactions, nucleosynthesis, abundances — quasars: absorption lines

On-line material: color figures, machine-readable table

1. INTRODUCTION

Since their discovery nearly 20 years ago (Wolfe et al. 1986), the damped Lyα (DLA) systems have provided an extraordinary means for probing the properties of high-redshift galaxies. For example, Wolfe and his collaborators have lead a number of observing programs to trace the universal neutral baryonic content, a study made possible by the fact that the DLA systems are the dominant neutral gas reservoirs at every epoch (e.g., Wolfe et al. 1995; Lanzetta, Wolfe, & Turnshek 1995; Storrie-Lombardi, Irwin, & McMahon 1996; Storrie-Lombardi & Wolfe 2000). Through accurate metallicity measurements, DLA studies also provide an examination of the chemical enrichment history of the universe (Pettini et al. 1994, 1997; Prochaska & Wolfe 2000; Prochaska, Gawiser, & Wolfe 2001, hereafter PGW01). In addition, the advent of high-resolution echelle spectrographs on 10 m class telescopes has enabled researchers to trace the relative chemical abundances of these systems, measurements that provide direct insight into processes of nucleosynthesis and dust depletion in the early universe (Lu et al. 1996, hereafter L96; Prochaska & Wolfe 1999, hereafter PW99; Pettini et al. 2000).

In this paper we build on previous observations of the chemical abundances of DLA systems. In particular, we introduce new measurements of over 15 DLA systems and revise the measurements of our previously analyzed systems (PW99). The principle goal of this paper is to provide the community with a uniform, homogeneous database of $z > 1.5$ DLA abundances. To this end, we have created a Web site[6] where we will continuously update our observations and possibly include measurements from throughout the community. Our new observations include spectra with wavelength coverage extending blueward of Lyα where elements like Ar, P, S, N, and O can be examined. In the second paper in this series (Prochaska & Wolfe 2001, hereafter Paper II), we address the implications of the complete data set on chemical evolution, dust depletion, dust obscuration, and nucleosynthesis. In several companion papers, we address the N/O abundance of the DLA systems, examine the kinematic characteristics of the full sample (J. X. Prochaska & A. M. Wolfe 2001, in preparation), infer the star formation rate of the DLA systems (Wolfe, Prochaska, & Gawiser 2001), and investigate the observational evidence for photoionization in these systems.

2. OBSERVATIONS AND ANALYSIS

All of the observations presented in this paper were acquired with the High Resolution Echelle Spectrometer (HIRES; Vogt et al. 1994) on the Keck I 10 m telescope. The HIRES spectrograph is mounted at the Nasmyth focus of Keck I and is equipped with an image rotator, two collomators (red and blue sensitive), and a Tektronix 2048 × 2048 CCD. For each observation, we implemented either a 1″.1 or a 0″.8 slit, which provides a resolution of FWHM ≈ 8.4 and 6.3 km s^{-1}, respectively. The HIRES spectrograph affords ≈2500 Å of wavelength coverage per setting with continuous coverage below $\lambda \approx 5100$ Å. Table 1 summarizes all of the new observations; refer to PW99 for previous observations.

All of the data were reduced with the MAKEE package as tailored for HIRES observations by T. Barlow.[7] This package flat-fields the exposures, optimally extracts the spectra from the two-dimensional images traced by a standard star or pinhole image, removes cosmic rays, and wavelength calibrates the spectra by cross-correlating each object's Th-Ar calibrations with a large database of calibrated HIRES data. We then continuum fitted each spectrum with an in-house routine similar to the IRAF task

[1] Visiting Astronomer, W. M. Keck Telescope. The Keck Observatory is a joint facility of the University of California and the California Institute of Technology.

[2] The Observatories of the Carnegie Institute of Washington, 813 Santa Barbara Street, Pasadena, CA 91101.

[3] Department of Physics and Center for Astrophysics and Space Sciences, University of California, San Diego, C-0424, La Jolla, CA 92093-0424.

[4] Experimental Astrophysics Department, Fermi National Accelerator Laboratory, MS 127, P.O. Box 500, 500 Wilson Road, Batavia, IL 60637-1433.

[5] SIRTF Science Center, California Institute of Technology, MS 100-22, Pasadena, CA 91125.

[6] http://kingpin.ucsd.edu/~hiresdla.

[7] http://spider.ipac.caltech.edu/staff/tab/makee.

TABLE 1

JOURNAL OF NEW OBSERVATIONS

QSO	z_{em}	Wavelength (Å)	Date	Exposure (s)	Resolution (km s^{-1})	S/N ($pixel^{-1}$)
J0255+00	4.02	5100–8160	F99, F00	20200	6.3	15
Q0336−01	3.22	3940–6390	F99	5400	8.2	10
Q0347−38	3.23	3600–5900	F98	4500	8.2	6
HS 0741+4741	3.20	3600–5900	F98, S00	10800	8.2	25
		5050–7470	F00	5400	6.3	30
BRI 0951−04	4.37	5720–8150	F99	7200	8.2	10
BRI 0952−0115	4.43	5700–8150	S99	28800	8.2	15
PSS 0957+33	4.25	6440–8760	F00	7200	6.3	15
BRI 1108−0747	3.92	5950–8340	F98, F99	12600	8.2	20
Q1210+17	2.54	3760–6170	S00	7200	8.2	20
Q1223+17	2.92	4780–7160	S98	19600	8.2	30
		3560–5900	S98	5000	8.2	7
BRI 1346−0322	3.99	4280–6600	S00	7200	8.2	4
PSS 1443+27	4.41	6070–8500	S99	25200	8.2	20
		6790–9180	S00	11000	8.2	15
Q1759+75	3.05	3500–5800	S00	22200	8.2	30
Q1946+7658	2.99	3470–5055	F98	47970	8.2	50
Q2344+12	4.30	3400–4985	F98	4000	8.2	12
Q2348−01	3.01	5060–7480	F99, F00	16200	8.2	15

CONTINUUM. For quasars with multiple exposures, the individual spectra were co-added (weighting by signal-to-noise ratio [S/N] and rejecting bad pixels) to produce a single one-dimensional spectrum with 2 km s^{-1} pixels.

3. IONIC COLUMN DENSITIES

In this section we present ionic column density measurements for all of the new systems as well as a number of transitions excluded in PW99. All of the ionic column densities were derived with the apparent optical depth method (AODM; Savage & Sembach 1991). This technique corrects for hidden saturation by comparing the apparent column density, N_a, for multiple transitions from a single ion. This technique also gives an efficient means of calculating total column densities for each ion. The analysis involves calculating $N_a(v)$ for each pixel from the optical depth equation

$$N_a(v) = \frac{m_e c}{\pi e^2} \frac{\tau_a(v)}{f\lambda} , \quad (1)$$

where $\tau_a(v) = \ln [I_i(v)/I_a(v)]$, f is the oscillator strength, λ is the rest wavelength (see Table 2), and I_i and I_a are the incident and measured intensities. By summing over the velocity profile of a given transition, one calculates the total column density,

$$N_T = \sum N_a(v) \Delta v , \quad (2)$$

and a 1 σ error on the column density through standard error propagation

$$\sigma^2(N_T) = \sum \left(\frac{m_e c}{\pi e^2 f\lambda}\right)^2 \frac{\sigma^2[I_a(v)]}{I_a^2(v)} \Delta v^2 . \quad (3)$$

In previous papers (Wolfe et al. 1994; Prochaska & Wolfe 1996, 1997), we showed that the DLA profiles are not contaminated by hidden saturation. Furthermore, we demonstrated that the total column densities derived with the AODM agree very well with line profile fitting, which should give a more accurate measure of the ionic column densities when hidden saturation is negligible. As the AODM is easier to apply to a large data set, we have chosen to use this technique to measure the ionic column densities for the DLA sample.

Tables 3–40 present the results of the abundance measurements including an estimate of the 1 σ error. For those transitions where the profile saturates, i.e., $I_a/I_i < 0.05$ in at least 1 pixel, the column densities are listed as lower limits. The values reported as upper limits are 3 σ limits except in the cases in which we set an upper limit due to significant line blending. We have ignored continuum error in our analysis that may dominate the measurements of very weak transitions, especially those blueward of Lyα emission. We estimate a systematic error of $\approx 10\%$ in most cases. The 3 σ statistical limits are conservative, however, and are likely to account for the continuum error in all but the noisiest and/or crowded absorption regions. In the following subsections we comment briefly on each DLA system, plot the metal line profiles, and tabulate column densities for each profile. We adopt ionic column densities from these measurements by calculating the weighted mean. In the velocity plots, $v = 0$ is chosen arbitrarily and corresponds to the redshift listed in the figure caption. We indicate regions of blending, primarily through blends with other metal line systems or the Lyα forest, by plotting with dotted lines. For those systems previously analyzed in PW99, we report only upon the changes made since publication. For completeness, when we include the measurement of a new transition (e.g., Ni II λ1317), we report other measurements of the same ion and the new adopted ionic column density.

Throughout the paper we adopt the wavelengths and oscillator strengths presented in Table 2. When possible, we have adopted laboratory values for the oscillator strengths. Since PW99 there have been several new measurements of f-values that impact the abundances of the DLA systems, including new Ni II and Ti II oscillator strengths, which have significantly revised the abundances of these elements. Most importantly, however, is the adoption of new oscillator strengths for the majority of Fe II transitions and in particular the Fe II $\lambda\lambda$1608, 1611 transitions. In this paper we adopt $f(1608) = 0.0580$ from the laboratory measurement of Ber-

TABLE 2

Atomic Data

Transition	λ	f	Reference
H I–19 λ914	914.0390	0.00019700	1
H I–18 λ914	914.2860	0.00023000	1
H I–17 λ914	914.5760	0.00027000	1
H I–16 λ914	914.9190	0.00032100	1
H I–15 λ915	915.3290	0.00038600	1
N II λ915	915.6120	0.14490000	1
H I–14 λ915	915.8240	0.00046900	1
H I–13 λ916	916.4290	0.00057700	1
P III λ917	917.1180	0.40490000	1
H I–12 λ917	917.1806	0.00072260	1
H I–11 λ918	918.1294	0.00092100	1
H I–10 λ919	919.3514	0.00120000	1
H I–9 λ920	920.9631	0.00160500	1
O I λ921	921.8600	0.00117300	2
O I λ922	922.2000	0.00242000	2
H I–8 λ923	923.1504	0.00221600	1
O I λ924	924.9520	0.00153400	2
O I λ925	925.4420	0.00350000	2
H I–7 λ926	926.2257	0.00318300	1
O I λ929	929.5168	0.00226370	2
O I λ930	930.2566	0.00532000	2
H I–6 λ930	930.7483	0.00481400	1
S VI λ933	933.3780	0.44140000	1
O I λ936	936.6295	0.00373500	1
H I–5 λ937	937.8035	0.00779900	1
S VI λ944	944.5230	0.21810000	1
O I λ948	948.6855	0.00644600	1
H I–4 λ949	949.7431	0.01394000	1
O I λ950	950.8846	0.00157100	1
P II λ963	963.8010	1.45800000	1
N I λ963	963.9903	0.01837000	1
N I λ964	964.6256	0.01180000	1
N I λ965	965.0413	0.00580100	1
O I λ971	971.7380	0.01480000	1
H I–G λ972	972.5368	0.02900000	1
O I λ976	976.4481	0.00330000	1
C III λ977	977.0200	0.76200000	1
O I λ988a	988.5778	0.00051460	1
O I λ988b	988.6549	0.00771200	1
O I λ988	988.7734	0.04318000	1
N III λ989	989.7990	0.10660000	1
Si II λ989	989.8731	0.13300000	1
S III λ1012	1012.5020	0.03550000	1
Si II λ1020	1020.6989	0.02828000	1
H I–B λ1025	1025.7223	0.07912000	1
O I λ1025	1025.7620	0.02030000	1
O VI λ1031	1031.9261	0.13290000	1
C II λ1036	1036.3367	0.12310000	1
O VI λ1037	1037.6167	0.06609000	1
O I λ1039	1039.2304	0.00919700	1
Ar I λ1048	1048.2199	0.24410000	1
Fe II λ1055	1055.2617	0.00751400	3
Fe II λ1062	1062.1520	0.00380000	1
S IV λ1062	1062.6620	0.03999000	1
Fe II λ1063	1063.1760	0.06000000	1
Fe II λ1064	1063.9718	0.00371800	3
Ar I λ1066	1066.6600	0.06652000	1
Fe II λ1081	1081.8748	0.01400000	1
N II λ1083	1083.9900	0.10310000	1
Fe II λ1096	1096.8769	0.03240000	3
Fe II λ1106	1106.3596	0.00150000	1
Fe II λ1112	1112.0480	0.00629000	3
P V λ1117	1117.9770	0.47320000	1
Fe II λ1121	1121.9748	0.02020000	3
Fe III λ1122	1122.5260	0.16200000	4
Fe II λ1125	1125.4478	0.01600000	3

TABLE 2—*Continued*

Transition	λ	f	Reference
P V λ1128	1128.0080	0.23450000	1
Fe II λ1133	1133.6650	0.00550000	3
N I λ1134	1134.1653	0.01342000	1
N I λ1134	1134.4149	0.02683000	1
N I λ1134	1134.9803	0.04023000	1
C I λ1139	1139.7930	0.01410000	1
Fe II λ1142	1142.3656	0.00420000	3
Fe II λ1143	1143.2260	0.01770000	3
Fe II λ1144	1144.9379	0.10600000	3
P II λ1152	1152.8180	0.23600000	1
C I λ1157	1157.1857	0.02440000	1
S III λ1190	1190.2080	0.02217000	1
Si II λ1190	1190.4158	0.25020000	1
Si II λ1193	1193.2897	0.49910000	1
Mn II λ1197	1197.1840	0.15660000	1
Mn II λ1199	1199.3910	0.10590000	1
N I λ1199	1199.5496	0.13280000	1
N I λ1200	1200.2233	0.08849000	1
N I λ1200	1200.7098	0.04423000	1
Si III λ1206	1206.5000	1.66000000	1
H I–A λ1215	1215.6701	0.41640000	1
N V λ1238	1238.8210	0.15700000	1
N V λ1242	1242.8040	0.07823000	1
S II λ1250	1250.5840	0.00545300	1
S II λ1253	1253.8110	0.01088000	1
S II λ1259	1259.5190	0.01624000	1
Si II λ1260	1260.4221	1.00700000	1
Fe II λ1260	1260.5330	0.02500000	1
C I λ1277	1277.2450	0.09665000	1
P II λ1301	1301.8740	0.01730000	1
O I λ1302	1302.1685	0.04887000	1
Si II λ1304	1304.3702	0.09400000	5
Ni II λ1317	1317.2170	0.07786000	6
C I λ1328	1328.8333	0.05804000	1
C II λ1334	1334.5323	0.12780000	1
C II* λ1335	1335.7077	0.11490000	1
O I λ1355	1355.5977	0.00000124	1
Ni II λ1370	1370.1310	0.07690000	6
Si IV λ1393	1393.7550	0.52800000	1
Si IV λ1402	1402.7700	0.26200000	1
Ga II λ1414	1414.4020	1.80000000	2
Ni II λ1454	1454.8420	0.03230000	7
Co II λ1466	1466.2120	0.03100000	8
Ni II λ1467	1467.2590	0.00990000	7
Ni II λ1467	1467.7560	0.00630000	7
Si II λ1526	1526.7066	0.12700000	9
C IV λ1548	1548.1950	0.19080000	1
C IV λ1550	1550.7700	0.09522000	1
C I λ1560	1560.3092	0.08041000	1
C I* λ1560	1560.6822	0.06030000	1
Co II λ1574	1574.5503	0.02500000	8
Ge II λ1602	1602.4863	1.35000000	1
Fe II λ1608	1608.4511	0.05800000	10
Fe II λ1611	1611.2005	0.00136000	11
C I λ1656	1656.9283	0.14050000	1
C I* λ1657a	1657.3792	0.03512000	1
C I* λ1657b	1657.9068	0.04681000	1
Al II λ1670	1670.7874	1.88000000	1
Ni II λ1703	1703.4050	0.00600000	7
Ni II λ1709	1709.6000	0.03240000	7
Ni II λ1741	1741.5490	0.04270000	7
Ni II λ1751	1751.9100	0.02770000	7
Si II λ1808	1808.0126	0.00218000	12
Si I λ1845	1845.5200	0.22900000	1
Al III λ1854	1854.7164	0.53900000	1
Al III λ1862	1862.7895	0.26800000	1

TABLE 2—*Continued*

Transition	λ	f	Reference
Fe II λ1901	1901.7730	0.00010090	1
Ti II λ1910a	1910.6000	0.20200000	13
Ti II λ1910b	1910.9700	0.09800000	13
Co II λ1941	1941.2852	0.03400000	8
Co II λ2012	2012.1664	0.03679000	8
Zn II λ2026	2026.1360	0.48900000	14
Cr II λ2026	2026.2690	0.00471000	2
Mg I λ2026	2026.4768	0.11200000	1
Cr II λ2056	2056.2539	0.10500000	14
Cr II λ2062	2062.2340	0.07800000	14
Zn II λ2062	2062.6640	0.25600000	14
Cr II λ2066	2066.1610	0.05150000	14
Fe II λ2249	2249.8768	0.00182100	15
Fe II λ2260	2260.7805	0.00244000	15
Fe II λ2344	2344.2140	0.11400000	4
Fe II λ2374	2374.4612	0.03130000	4
Fe II λ2382	2382.7650	0.32000000	4
Mn II λ2576......	2576.8770	0.35080000	1
Fe II λ2586	2586.6500	0.06910000	4
Mn II λ2594......	2594.4990	0.27100000	1
Fe II λ2600	2600.1729	0.23900000	4
Mn II λ2606......	2606.4620	0.19270000	1
Mg II λ2796	2796.3520	0.61230000	16
Mg II λ2803	2803.5310	0.30540000	16
Mg I λ2852	2852.9642	1.81000000	1
Ti II λ3073	3073.8770	0.10910000	1
Ti II λ3230	3230.1310	0.05860000	1
Ti II λ3242	3242.9290	0.18320000	1
Ti II λ3384	3384.7400	0.34000000	1

NOTE.—Table 2 is also available in machine-readable form in the electronic edition of the *Astrophysical Journal Supplement*.

REFERENCES.—(1) Morton 1991. (2) Verner, Barthel, & Tytler 1994. (3) Howk et al. 2000. (4) D. C. Morton 2001, in preparation. (5) Tripp, Lu, & Savage 1996. (6) Fedchak & Lawler 1999. (7) Fedchak, Wiese, & Lawler 2000. (8) Mullman et al. 1998. (9) Schectman, Povolny, & Curtis 1998. (10) Bergeson et al. 1996. (11) Raassen & Uylings 1998. (12) Bergeson & Lawler 1993a. (13) Wiese, Fedchak, & Lawler 2001. (14) Bergeson & Lawler 1993b. (15) Bergeson, Mullman, & Lawler 1994. (16) Verner 1996.

geson et al. (1996) and $f(1611) = 0.00136$ from Raassen & Uylings (1998). In general, these values revise the abundance of Fe^+ downward by $\approx$0.1 dex. Finally, we adopt solar meteoritic abundances from Grevesse, Noels, & Sauval (1996).

To assess the accuracy of our measurements and the reliability of the error analysis, one can compare the column density measurements from two transitions for the same ion with very accurately known relative oscillator strengths. The majority of our DLA systems exhibit absorption from the high-ion C^{+3} (Wolfe & Prochaska 2000), which exhibits a pair of resonance absorption lines at $\lambda \approx 1550$ Å as a result of the spin-orbit coupling of the $2p$ electronic level. Because the physics of spin-orbit coupling is well understood, we have high confidence that the relative oscillator strengths of the $\lambda\lambda$1548, 1550 transitions have a ratio of 2:1. Figure 1 plots the $N(1550)$ value versus $N(1548)$ for all of the DLA systems where the transitions are unsaturated and unblended. One notes that the agreement in the values is excellent even out to $N(C^{+3}) \approx 14.5$ where saturation could affect the stronger C IV λ1548 transition. In short, Figure 1 demonstrates that the AODM provides a reasonably accurate measure of the column densities and 1 σ errors for our analysis.

We now comment on the individual systems noting revisions from previous works where applicable.

3.1. *Q0000−26*, $z = 3.390$

We presented metal abundances for this system in PW99 but missed the Ni II λ1454 profile (Fig. 2 and Table 3). Furthermore, we have identified a telluric blend with the Ni II λ1751 profile, which led to an overestimate of Ni for this system. The Ni II λ1454 column density is in excellent agreement with the Ni abundance derived by Molaro et al. (2000) and further clouds the nucleosynthetic interpretation of this system (Molaro et al. 2001). Owing to the higher S/N of the UVES spectrum, we now adopt the Fe^+ column density from Molaro et al. (2000) but revise it downward to

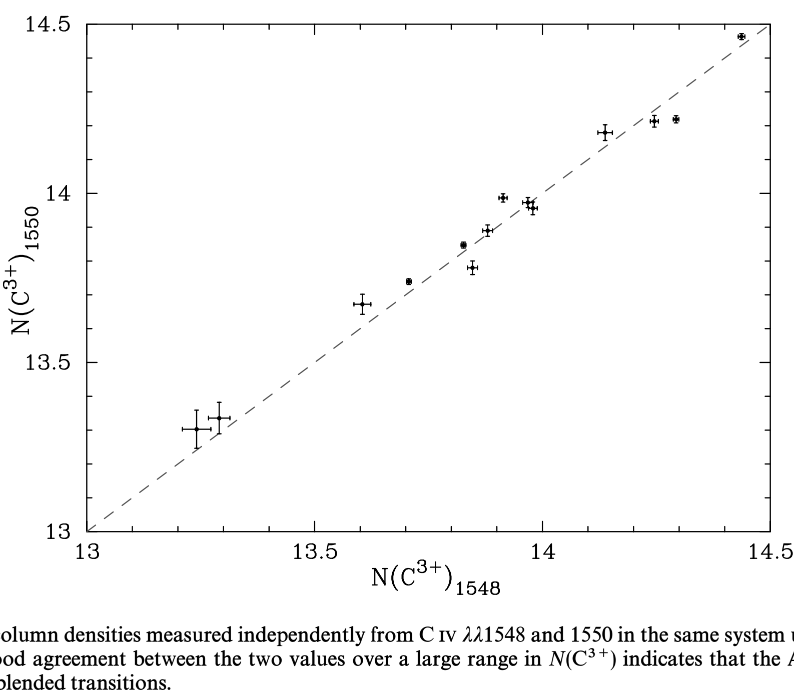

FIG. 1.—Comparison of C^{3+} column densities measured independently from C IV $\lambda\lambda$1548 and 1550 in the same system using the AODM. The dashed line traces the line of equality. The good agreement between the two values over a large range in $N(C^{3+})$ indicates that the AODM is an accurate method for measuring column densities in unblended transitions.

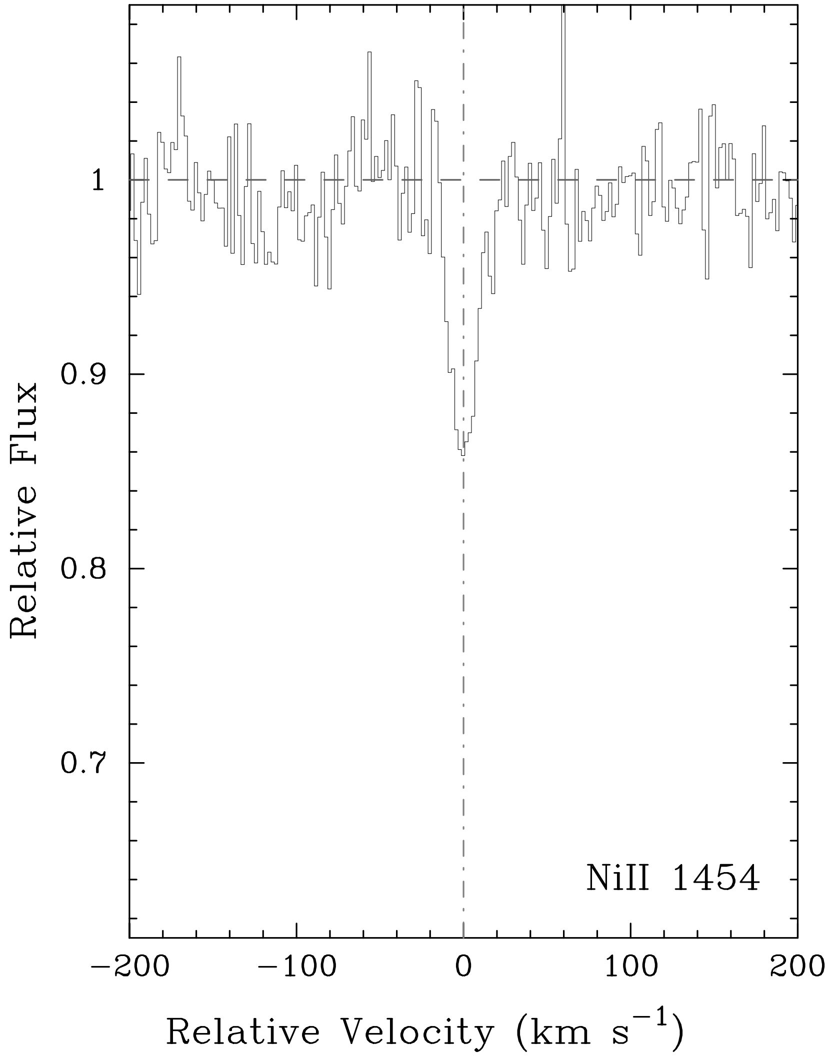

FIG. 2.—Velocity plot of the new metal line transition for the DLA system at $z = 3.390$ toward Q0000−26. The vertical line at $v = 0$ corresponds to $z = 3.3901$. [*See the electronic edition of the Journal for a color version of this figure.*]

$N(Fe^+) = 14.75 \pm 0.03$ as a result of the new Fe II λ1611 oscillator strength. This places the Fe^+ column density in reasonably good agreement with the $N(Ni^+)$ measurement and further supports the notion that the α-elements (O, Si) are enhanced in this system. We note in passing that the $N(Fe^+)$ value derived from our HIRES spectrum of Fe II λ1611 still significantly exceeds the UVES measurement for reasons we do not fully appreciate.

3.2. *BR 0019−15*, $z = 3.439$

This system was analyzed in PW99. Since publication, we have identified the C II* λ1335 profile (Fig. 3 and Table 4) and revised the Fe II λ1608 column density to a lower limit because the profile is mildly saturated. This revision accounts for the large Ni/Fe ratio reported in PW99.

3.3. *PH 957*, $z = 2.309$

This system was carefully studied in Wolfe et al. (1994) and subsequently in PW99. We present new limits on $N(Co^+)$ and $N(Ti^+)$, the latter of which places a tight constraint on the Ti/Fe ratio ([Ti/Fe] < −2.04 dex). We also present a measurement of $N(Mg^0)$ from the Mg I λ2026 transition. Figure 4 presents the new profiles as well as several Zn II and Cr II transitions that provide clarification

TABLE 3

IONIC COLUMN DENSITIES: Q0000−2619, $z = 3.390$

Ion	λ	AODM	N_{adopt}	[X/H]
H I	1215	21.410 ± 0.080	...	...
Ni II	1454	13.365 ± 0.045	13.365 ± 0.045	−2.295 ± 0.092
Ni II	1751	< 13.689	...	...

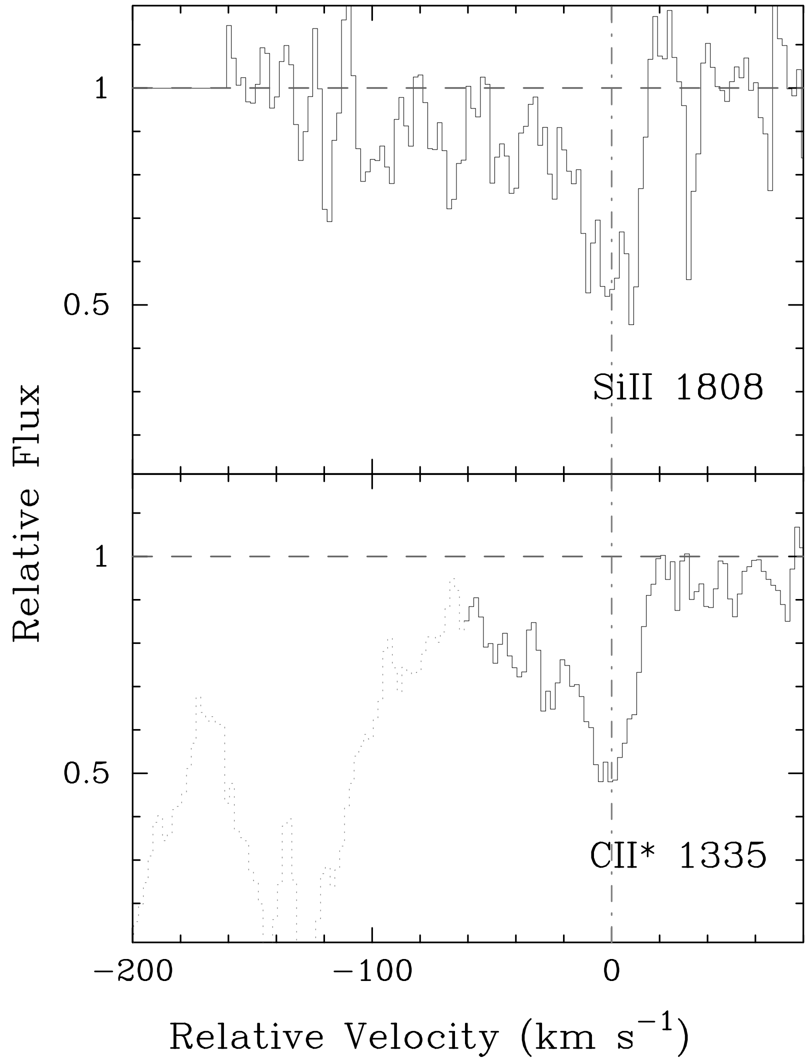

FIG. 3.—Velocity plot of the C II* λ1335 profile for the DLA system at $z = 3.439$ toward BR 0019−15. The Si II λ1808 profile is shown for comparison. The vertical line at $v = 0$ corresponds to $z = 3.4388$. [*See the electronic edition of the Journal for a color version of this figure.*]

with respect to the identification of Mg I λ2026. Table 5 lists the new values.

3.4. *Q0149+33*, $z = 2.140$

We have several changes to report on this system since PW99. Figure 5 and Table 6 present the Ni II λ1317 and Ti II λ1910 profiles that were overlooked in PW99. We have also revised the Si II λ1304 and Si II λ1526 column densities to lower limits and base the Si abundance solely on the unsaturated Si II λ1808 profile. For Cr, we now include the Cr II λ2062 profile in our analysis. Finally, we warn that the Fe II λ1608 column density might be considered a lower limit for $N(Fe^+)$, which would explain its underabundance relative to Cr and Ni. As noted in PW99, this system exhibits a supersolar Cr/Zn ratio ([Cr/Zn] $= 0.22 \pm 0.1$). Because of its low [Zn/H] and N(H I) values, this system has special significance in terms of dust depletion (Paper II, § 3).

3.5. *Q0201+36*, $z = 2.463$

This system was studied at length in Prochaska & Wolfe (1996), and we now include an upper limit on the Ti II λ1910

TABLE 4

IONIC COLUMN DENSITIES: BR 0019−15, $z = 3.439$

Ion	λ	AODM	N_{adopt}	[X/H]
H I	1215	20.920 ± 0.100	...	...
C II	1335	13.838 ± 0.018	...	...
Fe II	1608	>14.789	>14.789	>-1.631
Ni II	1709	13.607 ± 0.105	13.683 ± 0.040	-1.487 ± 0.108
Ni II	1741	13.701 ± 0.043	...	...

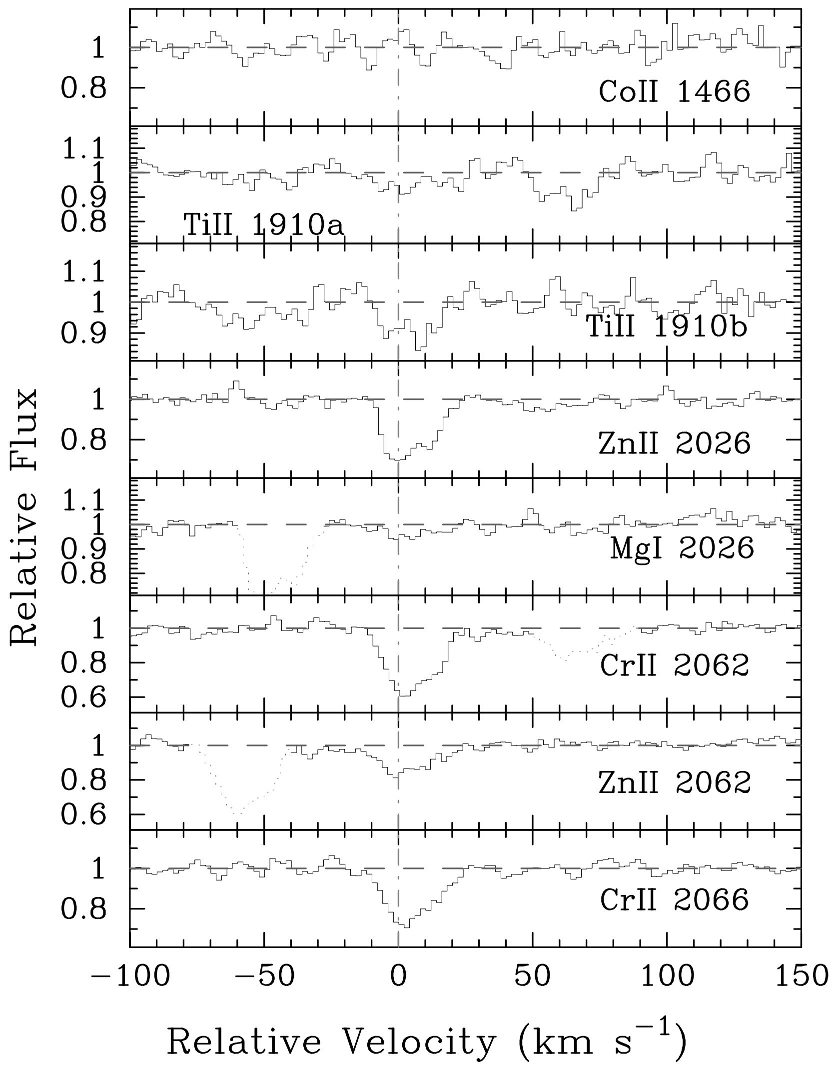

FIG. 4.—Velocity plot of several new metal line transitions for the DLA system at $z = 2.309$ toward PH 957. The vertical line at $v = 0$ corresponds to $z = 2.309$. [*See the electronic edition of the Journal for a color version of this figure.*]

transition and a measurement for the Ni II λ1454 profile (Fig. 6). To provide the best comparison with other objects in the complete sample, we adopt AODM column densities for all of the transitions (Table 7).

3.6. *J0255+00*, $z = 3.253$ *and* 3.915

The two DLA systems observed toward this faint Sloan Digital Sky Survey (SDSS) quasar ($r = 19.1$; Fan et al. 1999) were identified as part of a program designed to survey $z > 3$ DLA systems (A. M. Wolfe et al. 2001, in preparation). We measured the N(H I) column densities of the two systems with a Low Resolution Imaging Spectrometer (LRIS) spectrum and then acquired HIRES observations at wavelengths redward of the Lyα forest. Figures 7 and 8 present the metal line profiles for the two systems, and Tables 8 and 9 list the ionic column densities. For the system at $z = 3.915$, $N(Fe^+)$ is well constrained by the lower and upper limits from the Fe II λ1608 and Fe II λ1611 transitions, respectively, and we have adopted a column density by averaging the two limits: log $N(Fe^+) = 14.75 \pm 0.08$ dex.

3.7. *Q0336−01*, $z = 3.062$

This Large Bright Quasar Survey (LBQS) quasar is one of the few DLA systems at $z > 3$ with N(H I) $> 10^{21}$ cm^{-2}.

TABLE 5

IONIC COLUMN DENSITIES: PH 957, $z = 2.309$

Ion	λ	AODM	N_{adopt}	[X/H]
H I........	1215	21.400±0.050	...	...
Mg I......	2026	12.344±0.126	...	...
Ti II	1910	<12.207	<12.207	<−2.133
Co II......	1466	<13.164	<13.164	<−1.146

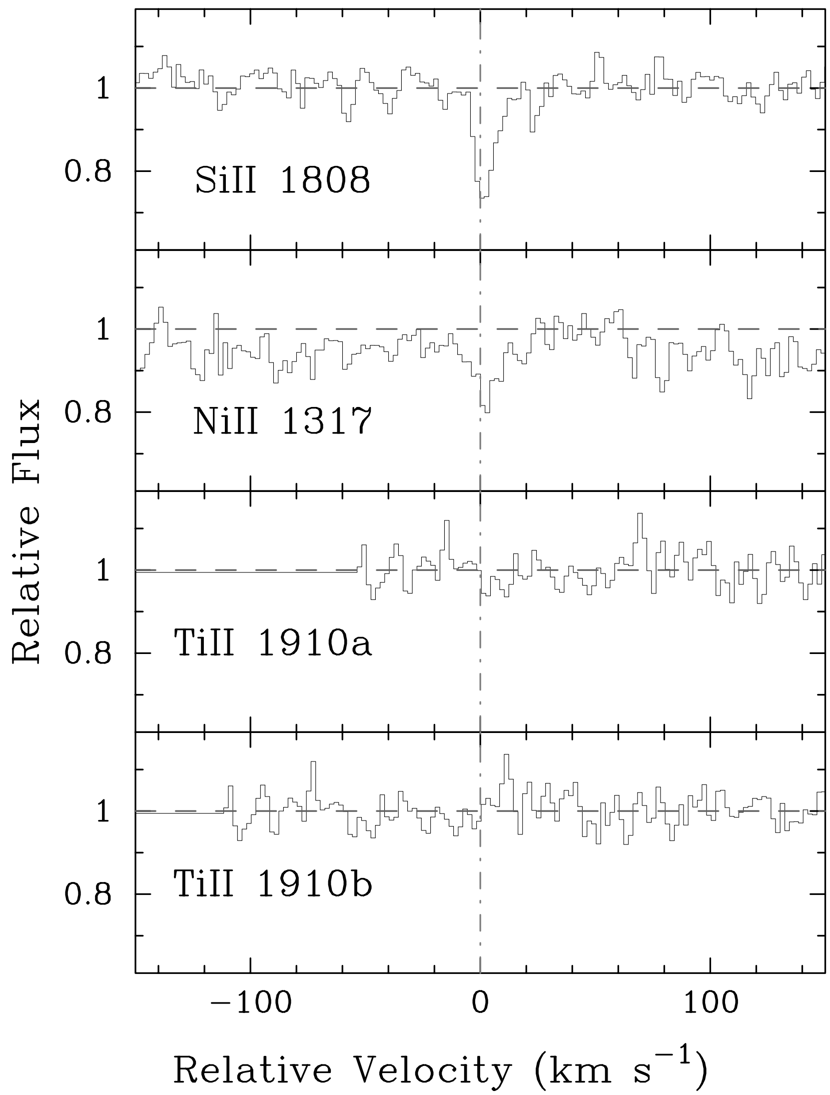

FIG. 5.—Velocity plot of several new metal line transitions for the DLA system at $z = 2.141$ toward Q0149+33. For comparison, we also plot the Si II λ1808 profile. The vertical line at $v = 0$ corresponds to $z = 2.140755$. [*See the electronic edition of the Journal for a color version of this figure.*]

TABLE 6

IONIC COLUMN DENSITIES: Q0149+33, $z = 2.141$

Ion	λ	AODM	$N_{\rm adopt}$	[X/H]
H I	1215	20.500 ± 0.100	...	...
Si II	1304	>14.432	14.572 ± 0.047	-1.488 ± 0.110
Si II	1526	>14.339	...	...
Si II	1808	14.572 ± 0.047	...	...
Ti II	1910	<12.169	<12.169	<-1.271
Cr II......	2056	12.793 ± 0.044	12.720 ± 0.035	-1.450 ± 0.106
Cr II......	2062	12.520 ± 0.090	...	...
Cr II......	2066	12.841 ± 0.062	...	...
Ni II......	1317	13.092 ± 0.071	13.169 ± 0.036	-1.581 ± 0.106
Ni II......	1370	13.192 ± 0.103	...	...
Ni II......	1703	<13.885	...	...
Ni II......	1709	13.184 ± 0.088	...	...
Ni II......	1741	13.250 ± 0.064	...	...
Ni II......	1751	13.179 ± 0.090	...	...

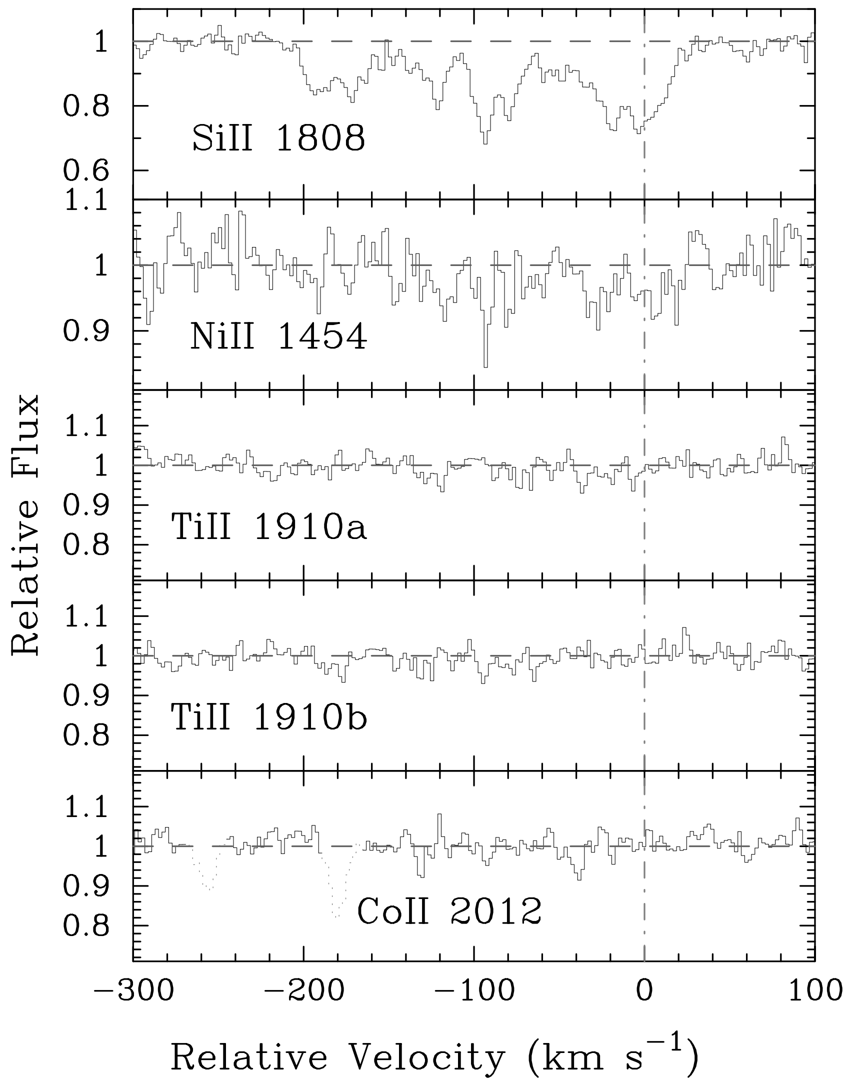

FIG. 6.—Velocity plot of several new metal line transitions for the DLA system at $z = 2.463$ toward Q0201+36. For comparison, we also plot the Si II λ1808 profile. The vertical line at $v = 0$ corresponds to $z = 2.4628$. [*See the electronic edition of the Journal for a color version of this figure.*]

TABLE 7

IONIC COLUMN DENSITIES: Q0201+36, $z = 2.463$

Ion	λ	AODM	$N_{\rm adopt}$	[X/H]
H I........	1215	20.380 ± 0.045	...	...
C IV	1550	14.612 ± 0.005	...	...
Al II	1670	> 14.133	> 14.133	> -0.737
Al III......	1862	13.601 ± 0.007	...	...
Si II	1808	15.534 ± 0.010	15.534 ± 0.010	-0.406 ± 0.046
Si IV	1393	> 14.071	...	...
Ti II	1910	< 12.196	< 12.196	< -1.124
Cr II	2056	13.266 ± 0.030	13.248 ± 0.029	-0.802 ± 0.054
Cr II	2066	13.132 ± 0.094	...	...
Fe II	1608	15.010 ± 0.004	15.010 ± 0.004	-0.870 ± 0.045
Co II......	2012	< 12.957	< 12.957	< -0.333
Ni II	1454	13.669 ± 0.073	14.022 ± 0.010	-0.608 ± 0.046
Ni II	1709	14.080 ± 0.021	...	...
Ni II	1741	14.021 ± 0.013	...	...
Ni II	1751	13.984 ± 0.021	...	...

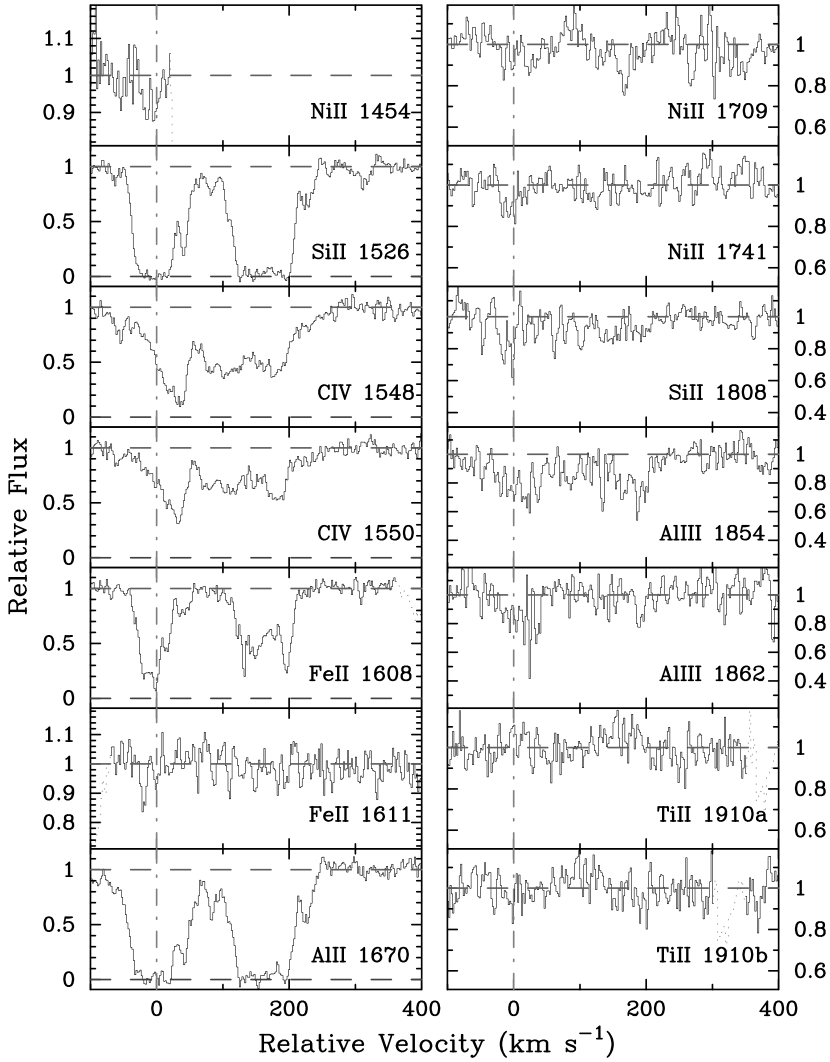

FIG. 7.—Velocity plot of the metal line transitions for the DLA system at $z = 3.253$ toward J0255+00. The vertical line at $v = 0$ corresponds to $z = 3.252931$. [*See the electronic edition of the Journal for a color version of this figure.*]

Although most of the transitions that we examine lie within the Lyα forest, we have carefully avoided lines that are clearly blended with forest clouds. Unfortunately, we only place a lower limit on $N(\mathrm{Si}^+)$ although we do report a reasonably secure value for $N(\mathrm{S}^+)$. The system also provides an accurate measurement of Ar I and a reasonable estimate of P II. Finally, we note a very large $N(\mathrm{O}^0)$ lower limit derived from the saturated O I λ988 transition. This limit

TABLE 8

IONIC COLUMN DENSITIES: J0255+00, $z = 3.253$

Ion	λ	AODM	N_{adopt}	[X/H]
H I	1215	20.700 ± 0.100	...	...
C IV	1548	14.437 ± 0.007	...	...
C IV	1550	14.463 ± 0.009	...	...
Al II	1670	>13.879	>13.879	>-1.311
Al III......	1854	13.277 ± 0.025	...	...
Al III......	1862	12.977 ± 0.102	...	...
Si II.......	1526	>15.119	15.323 ± 0.038	-0.937 ± 0.107
Si II.......	1808	15.323 ± 0.038	...	...
Ti II	1910	<12.805	<12.805	<-0.835
Fe II	1608	14.764 ± 0.010	14.764 ± 0.010	-1.436 ± 0.100
Fe II	1611	<14.832	...	...
Ni II	1709	13.771 ± 0.075	13.608 ± 0.066	-1.342 ± 0.120
Ni II	1741	13.473 ± 0.114	...	...

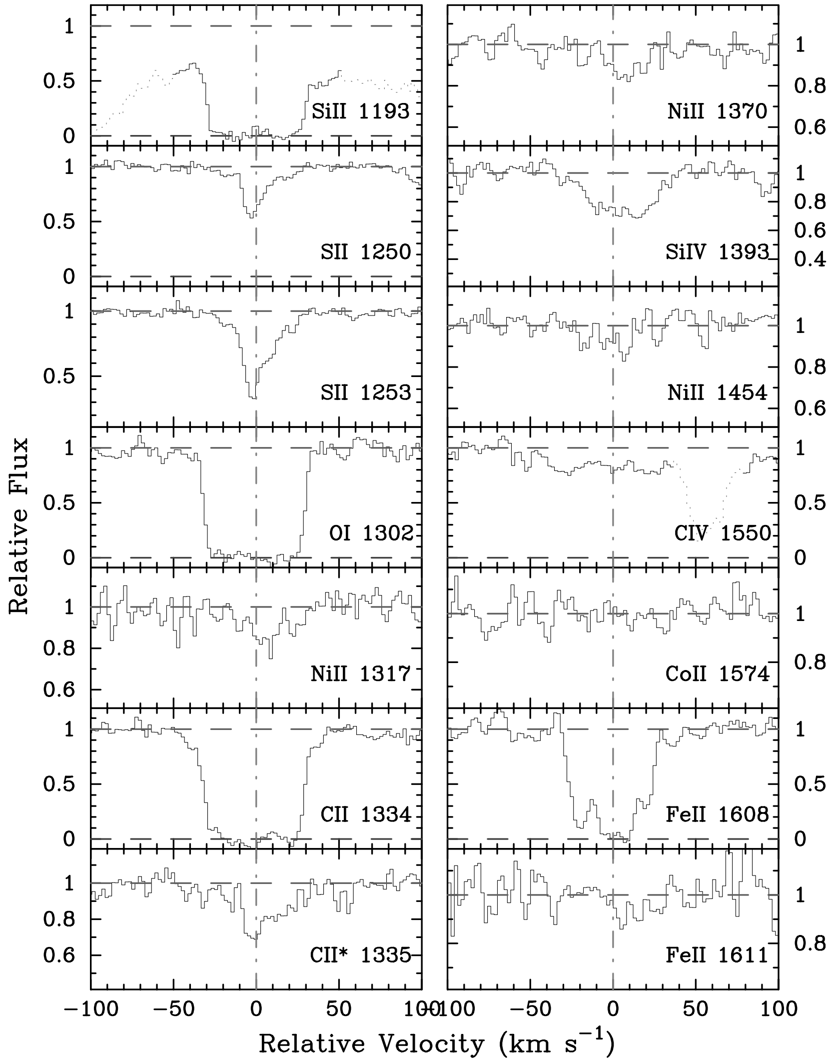

FIG. 8.—Velocity plot of the metal line transitions for the DLA system at $z = 3.915$ toward J0255+00. The vertical line at $v = 0$ corresponds to $z = 3.914617$. [*See the electronic edition of the Journal for a color version of this figure.*]

may be influenced by blending in the Lyα forest, but we have no reason to believe that this is the case at present (see Fig. 9 and Table 10).

3.8. *Q0347−38*, $z = 3.025$

Although this system was analyzed in PW99, we report a number of measurements and limits based on the original data and new observations taken with a second, blue setup. Table 11 presents the ionic column densities, and Figure 10 plots the new profiles. We also reclassify the sulfur abundance as an upper limit because this transition is blended with an Lyα forest cloud.

TABLE 9

IONIC COLUMN DENSITIES: J0255+00, $z = 3.915$

Ion	λ	AODM	$N_{\rm adopt}$	[X/H]
H I........	1215	21.300 ± 0.050	...	...
C II	1334	> 14.732	> 14.732	> −3.118
C II	1335	13.442 ± 0.040	...	...
O I........	1302	> 15.167	> 15.167	> −3.003
Si II	1193	> 14.193	> 14.193	> −2.667
Si IV	1393	12.856 ± 0.028	...	...
S II........	1250	14.763 ± 0.021	14.721 ± 0.011	−1.779 ± 0.051
S II........	1253	14.707 ± 0.013	...	...
Fe II	1608	> 14.707	14.750 ± 0.088	−2.050 ± 0.101
Fe II	1611	< 14.809	...	...
Co II......	1574	< 13.212	< 13.212	< −0.998
Ni II	1317	13.315 ± 0.052	13.271 ± 0.037	−2.279 ± 0.062
Ni II	1370	13.213 ± 0.058	...	...
Ni II	1454	13.387 ± 0.104	...	...

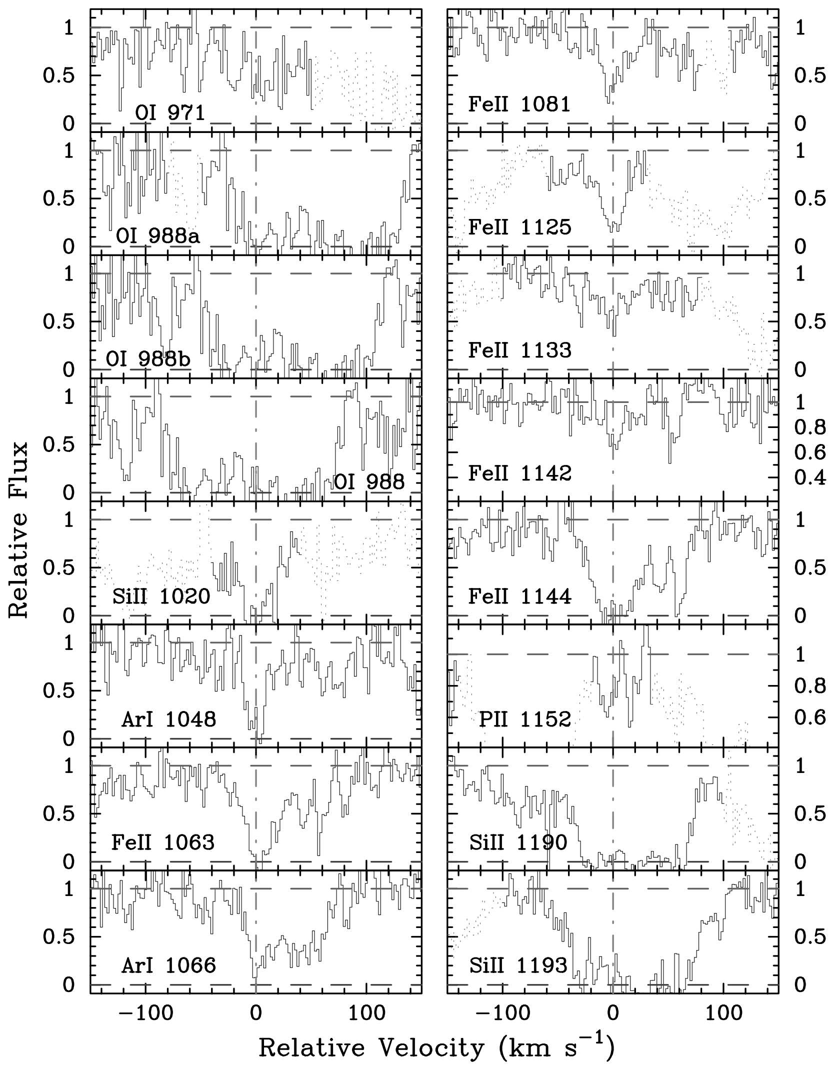

FIG. 9.—Velocity plot of the metal line transitions for the DLA system at $z = 3.062$ toward Q0336 − 01. The vertical line at $v = 0$ corresponds to $z = 3.062078$. [*See the electronic edition of the Journal for a color version of this figure.*]

3.9. *Q0458−02*, $z = 2.040$

In reviewing this system, we identified a number of transitions missed in PW99. Figure 11 presents the metal line profiles, and Table 12 shows the column densities. Most of these only yield upper limits on ionic column densities, but given the very large H I column density of this system, these limits are valuable. For example, the limit on Ti II λ1910 implies [Ti/Fe] < −0.45 dex, which is highly suggestive of dust depletion. As discussed in Paper II, § 2.1.6, we have revised the measurement of $N(\mathrm{Zn}^+)$ downward by 0.02 dex because of mild blending between the Zn II λ2026 and Mg I λ2026 profiles.

TABLE 10

IONIC COLUMN DENSITIES: Q0336−01, $z = 3.062$

Ion	λ	AODM	$N_{\rm adopt}$	[X/H]
H I	1215	21.200 ± 0.100	...	...
C II	1334	> 14.958	> 14.958	> −2.792
C II	1335	14.041 ± 0.025	...	...
C IV	1548	14.138 ± 0.016	...	...
C IV	1550	14.180 ± 0.023	...	...
O I	988	> 16.940	> 16.940	> −1.130
O I	1302	> 15.389	...	...
Si II	1020	> 15.141	> 15.141	> −1.619
Si II	1193	> 14.322	...	...
Si II	1304	> 14.926	...	...
Si IV	1393	13.767 ± 0.015	...	...
Si IV	1402	13.656 ± 0.032	...	...

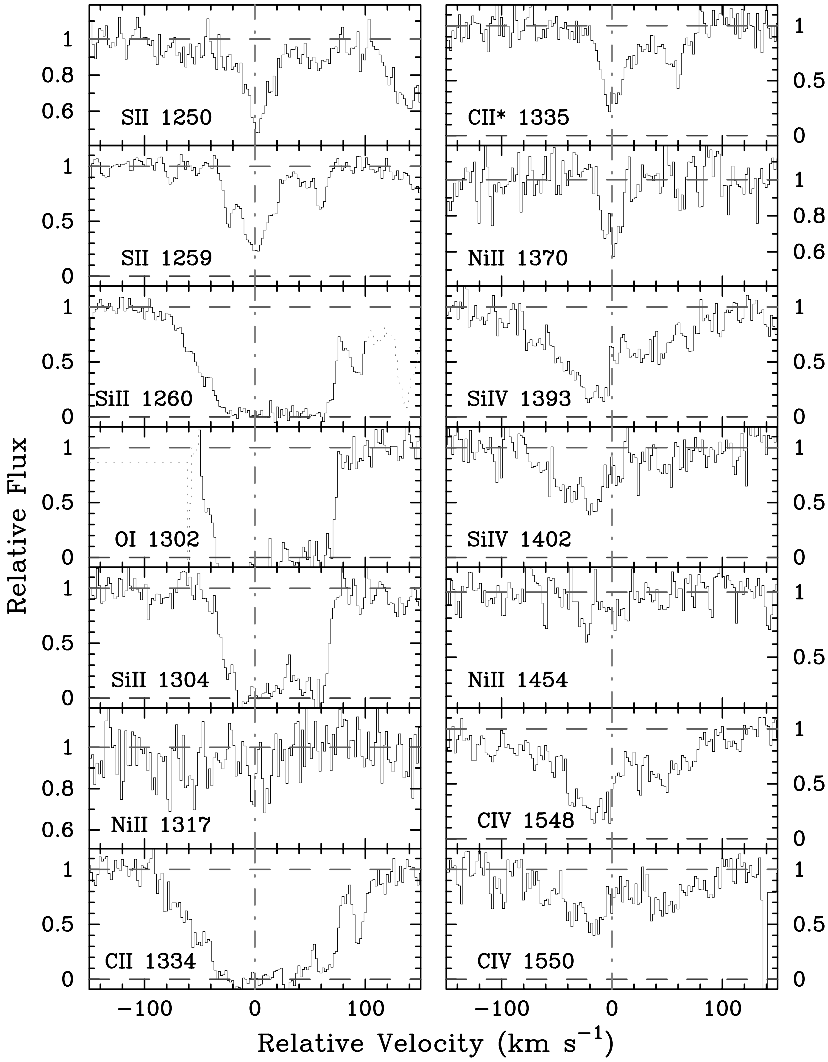

FIG. 9.—*Continued*

3.10. *HS 0741+47*, $z = 3.017$

The very bright QSO HS 0741+47 is taken from the Hamburg ESO QSO survey (Hagen, Engels, & Reimers 1999). Our wavelength coverage of the DLA system spans from 3600 to 7500 Å, and we have identified over 20 metal line profiles. Figure 12 plots the velocity profiles, and Table 13 presents all of the measurements. Unfortunately, our observations do not include the Zn II and Cr II transitions, although the $N(\mathrm{Si}^+)$ value indicates that it would require very high S/N to obtain a measurement.

TABLE 10—*Continued*

Ion	λ	AODM	$N_{\rm adopt}$	[X/H]
P II.......	1152	13.133±0.075	13.133±0.075	−1.597±0.125
S II.......	1250	15.118±0.022	14.994±0.011	−1.406±0.101
S II.......	1259	14.970±0.012	...	...
Ar I......	1048	>13.860	14.346±0.065	−1.374±0.119
Ar I......	1066	14.346±0.065	...	...
Fe II......	1081	14.879±0.055	14.905±0.033	−1.795±0.105
Fe II......	1125	14.920±0.046	...	...
Fe II......	1142	14.936±0.099	...	...
Fe II......	1144	>14.719	...	...
Ni II......	1317	<13.389	13.469±0.057	−1.981±0.115
Ni II......	1370	13.424±0.065	...	...
Ni II......	1454	13.880±0.091	...	...

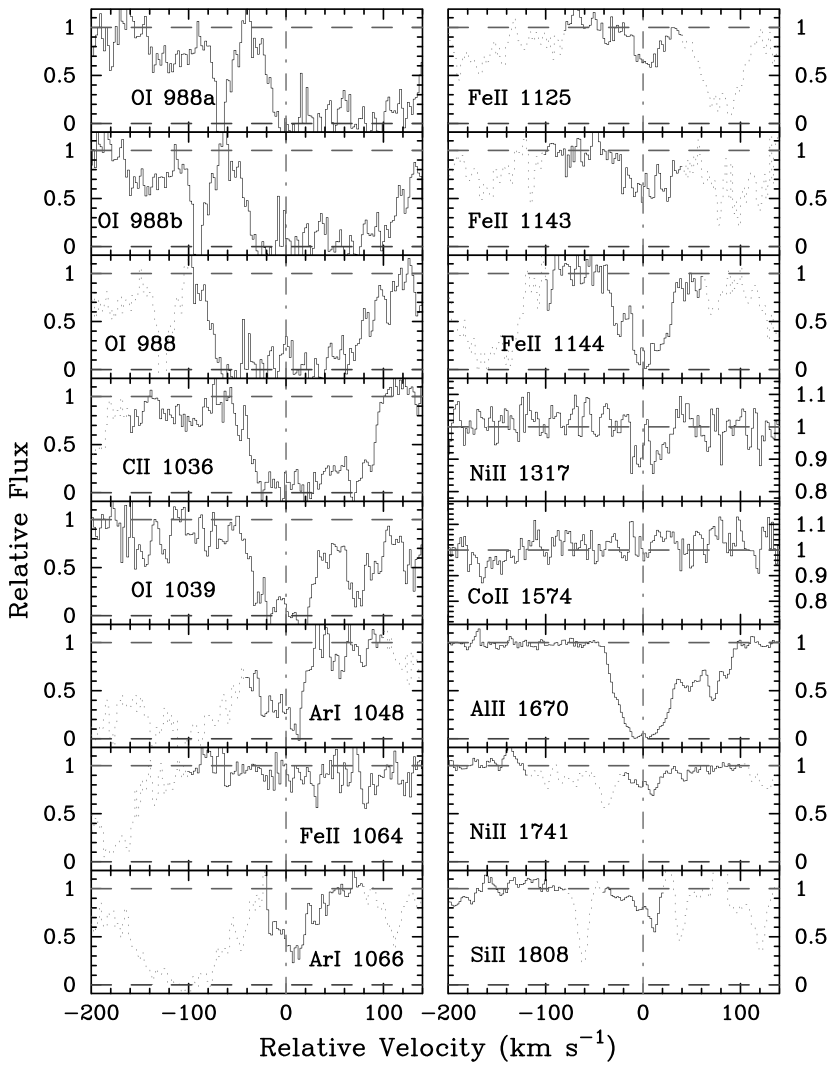

FIG. 10.—Velocity plot of several new metal line transitions for the DLA system at $z = 3.025$ toward Q0347−38. The vertical line at $v = 0$ corresponds to $z = 3.0247$. [*See the electronic edition of the Journal for a color version of this figure.*]

TABLE 11

Ionic Column Densities: Q0347−38, $z = 3.025$

Ion	λ	AODM	$N_{\rm adopt}$	[X/H]
H I........	1215	20.800 ± 0.100	...	...
C II	1036	>14.930	>15.065	>-2.285
C II	1334	>15.066	...	...
O I........	1039	>15.953	>15.953	>-1.717
O I........	1302	>15.449	...	...
Al II	1670	>13.408	>13.408	>-1.882
Si II.......	1260	>14.329	15.017 ± 0.026	-1.343 ± 0.103
Si II.......	1304	>14.889	...	...
Si II.......	1808	15.017 ± 0.026	...	...
S II........	1259	<14.760	<14.760	<-1.240
Ar I	1048	>14.063	14.282 ± 0.035	-1.038 ± 0.106
Ar I	1066	14.282 ± 0.035	...	...
Fe II	1063	14.763 ± 0.143	14.503 ± 0.007	-1.797 ± 0.100
Fe II	1125	14.453 ± 0.056	...	...
Fe II	1143	14.712 ± 0.040	...	...
Fe II	1608	14.501 ± 0.007	...	...
Fe II	1611	<14.447	...	...
Co II......	1574	<13.196	<13.196	<-0.514
Ni II	1317	13.034 ± 0.093	13.383 ± 0.031	-1.667 ± 0.105
Ni II	1370	13.115 ± 0.099	...	...
Ni II	1741	14.056 ± 0.019	...	...

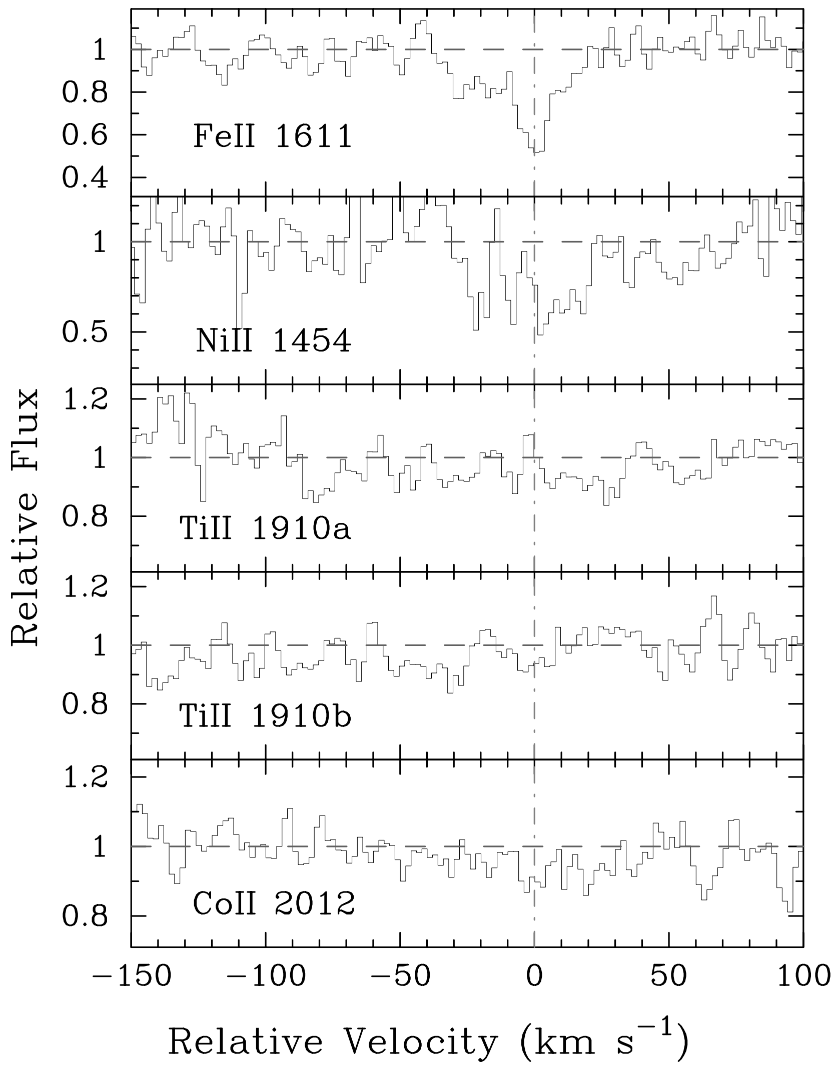

FIG. 11.—Velocity plot of several new metal line transitions for the DLA system at $z = 2.040$ toward Q0458−02. The vertical line at $v = 0$ corresponds to $z = 2.03955$. [*See the electronic edition of the Journal for a color version of this figure.*]

3.11. *Q0836+11*, $z = 2.465$

This DLA system is drawn from the LBQS survey (Wolfe et al. 1995), and we adopt the N(H I) value obtained from their analysis. Our observations cover a large number of transitions, many of which only provide upper limits owing to the relatively poor S/N (Fig. 13 and Table 14). In passing, we note that some of the Ni II upper limits are in contradiction with our adopted $N(\mathrm{Ni}^+)$ value. This might reflect an

TABLE 12

IONIC COLUMN DENSITIES: Q0458−02, $z = 2.040$

Ion	λ	AODM	N_{adopt}	[X/H]
H I........	1215	21.650 ± 0.090	...	...
C I........	1656	< 12.453	...	...
Mg I......	2026	13.117 ± 0.031	...	...
Ti II	1910	< 12.495	< 12.495	< −2.095
Co II......	2012	< 13.092	< 13.093	< −1.467
Ni II	1317	14.257 ± 0.024	14.181 ± 0.018	−1.719 ± 0.092
Ni II	1370	14.315 ± 0.071	...	...
Ni II	1454	14.187 ± 0.114	...	...
Ni II	1703	13.987 ± 0.090	...	...
Ni II	1709	14.158 ± 0.034	...	...
Ni II	1741	14.195 ± 0.032	...	...
Ni II	1751	14.170 ± 0.033	...	...
Zn II......	2026	13.134 ± 0.020	13.134 ± 0.020	−1.186 ± 0.092
Zn II......	2062	> 13.031	...	...

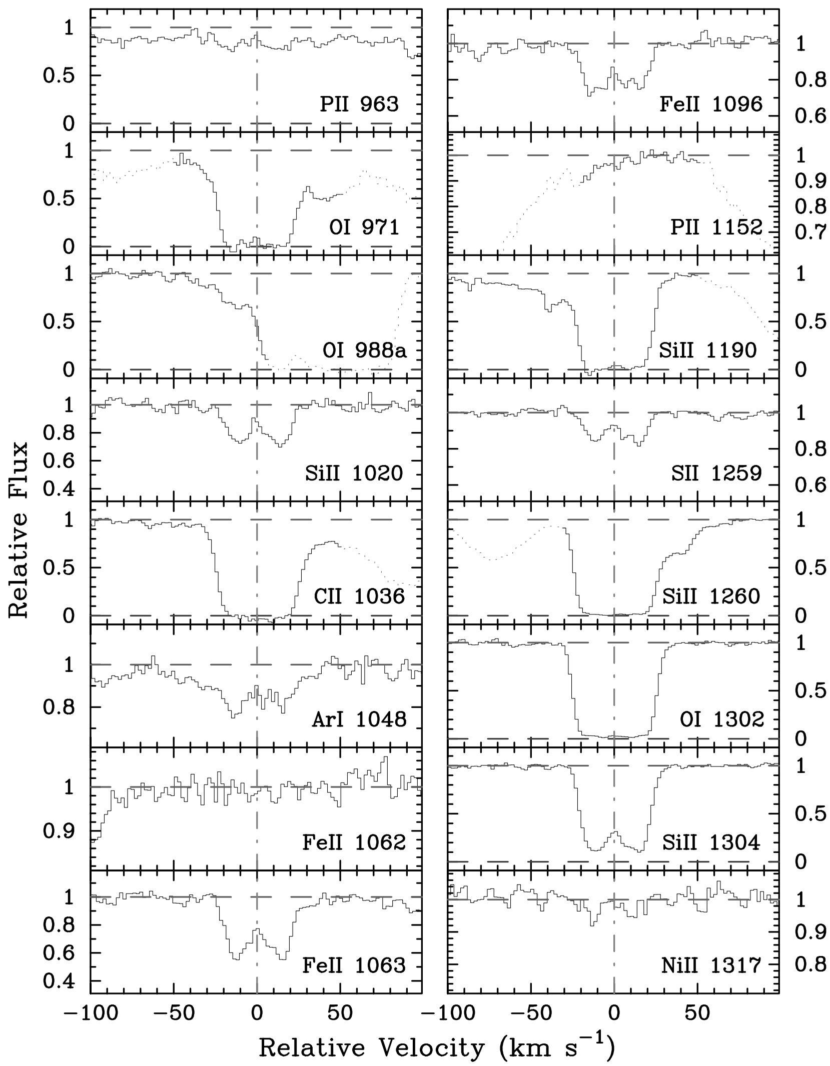

FIG. 12.—Velocity plot of the metal line transitions for the DLA system at $z = 3.017$ toward HS 0741 + 4741. The vertical line at $v = 0$ corresponds to $z = 3.017399$. [*See the electronic edition of the Journal for a color version of this figure.*]

TABLE 13

IONIC COLUMN DENSITIES: HS 0741+4741, $z = 3.017$

Ion	λ	AODM	$N_{\rm adopt}$	[X/H]
H I	1215	20.480 ± 0.100	...	...
C II	1036	>14.864	>14.864	>-2.166
C II	1334	>14.737	...	...
C II	1335	<12.554	...	...
C IV	1548	13.827 ± 0.005	...	...
C IV	1550	13.847 ± 0.009	...	...
O I	971	>15.711	>15.711	>-1.639
O I	1302	>15.229	...	...
Al II	1670	12.823 ± 0.005	12.824 ± 0.005	-2.146 ± 0.100
Al III......	1854	12.161 ± 0.043	...	...
Si II.......	1020	14.162 ± 0.019	14.354 ± 0.003	-1.686 ± 0.100
Si II.......	1260	>13.937	...	...
Si II.......	1304	14.368 ± 0.003	...	...
Si II.......	1526	>14.469	...	...
Si II.......	1808	14.395 ± 0.051	...	...
Si IV	1393	13.382 ± 0.006	...	...
Si IV	1402	13.376 ± 0.011	...	...
P II	1152	<12.080	<12.080	<-1.930

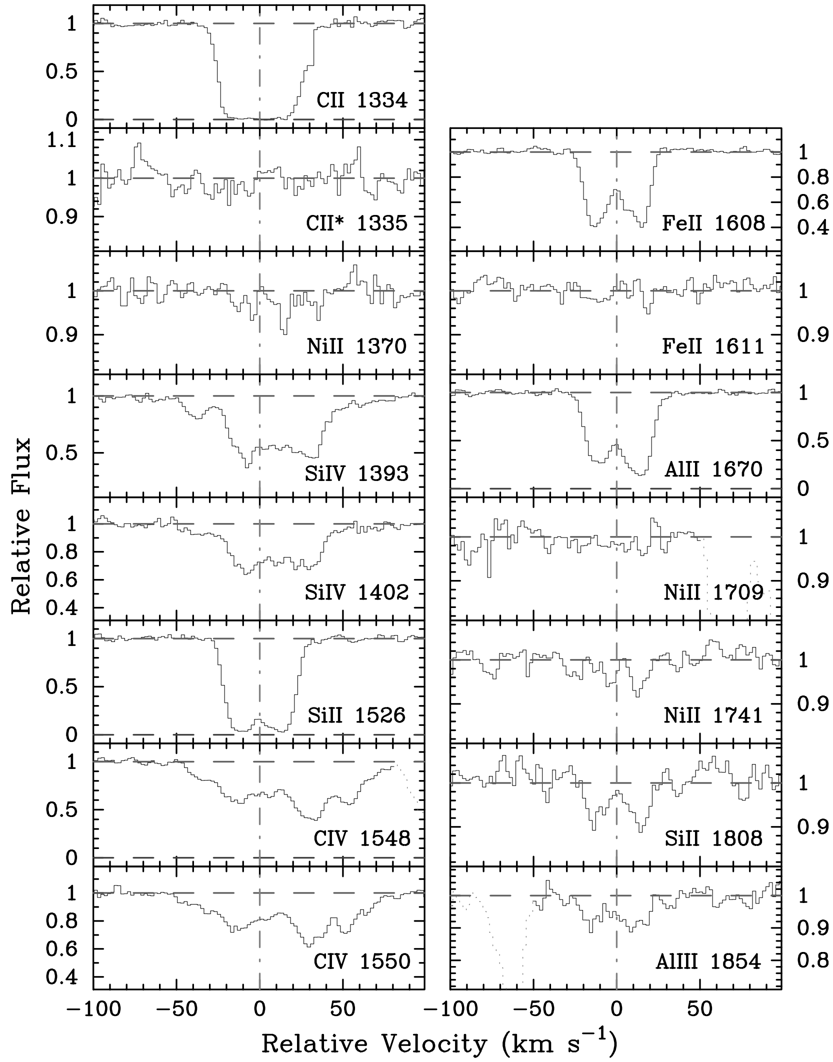

FIG. 12.—*Continued*

error in the relative *f*-values but more likely reflects the large error in the adopted value.

3.12. *Q0841+12, z = 2.375 and 2.476*

We augment the measurements presented in PW99 with a few additional Ni II transitions and several Co II and Ti II upper limits. These transitions are plotted in Figures 14 and 15 and tabulated in Tables 15 and 16. As discussed in PW99, we based the Fe abundance for the $z = 2.476$ system on the saturated Fe II $\lambda1608$ profile. We now choose to report the Fe II $\lambda1608$ column density as a lower limit on $N(\mathrm{Fe}^+)$ and adopt an Fe abundance based on averaging the lower and upper limits from Fe II $\lambda1608$ and Fe II $\lambda1611$, respectively: $\log N(\mathrm{Fe}^+) = 14.53 \pm 0.05$.

TABLE 13—*Continued*

Ion	λ	AODM	N_{adopt}	[X/H]
S II........	1259	14.000 ± 0.016	14.000 ± 0.016	-1.680 ± 0.101
Ar I.......	1048	13.166 ± 0.020	13.166 ± 0.020	-1.834 ± 0.102
Fe II	1063	14.075 ± 0.010	14.052 ± 0.005	-1.928 ± 0.100
Fe II	1096	14.068 ± 0.015	...	...
Fe II	1608	14.041 ± 0.006	...	...
Fe II	1611	<14.082	...	...
Co II......	1574	<12.958	<12.958	<-0.432
Ni II	1317	12.658 ± 0.110	12.758 ± 0.049	-1.972 ± 0.111
Ni II	1370	12.736 ± 0.081	...	...
Ni II	1454	<12.833	...	...
Ni II	1709	12.745 ± 0.144	...	...
Ni II	1741	12.943 ± 0.078	...	...

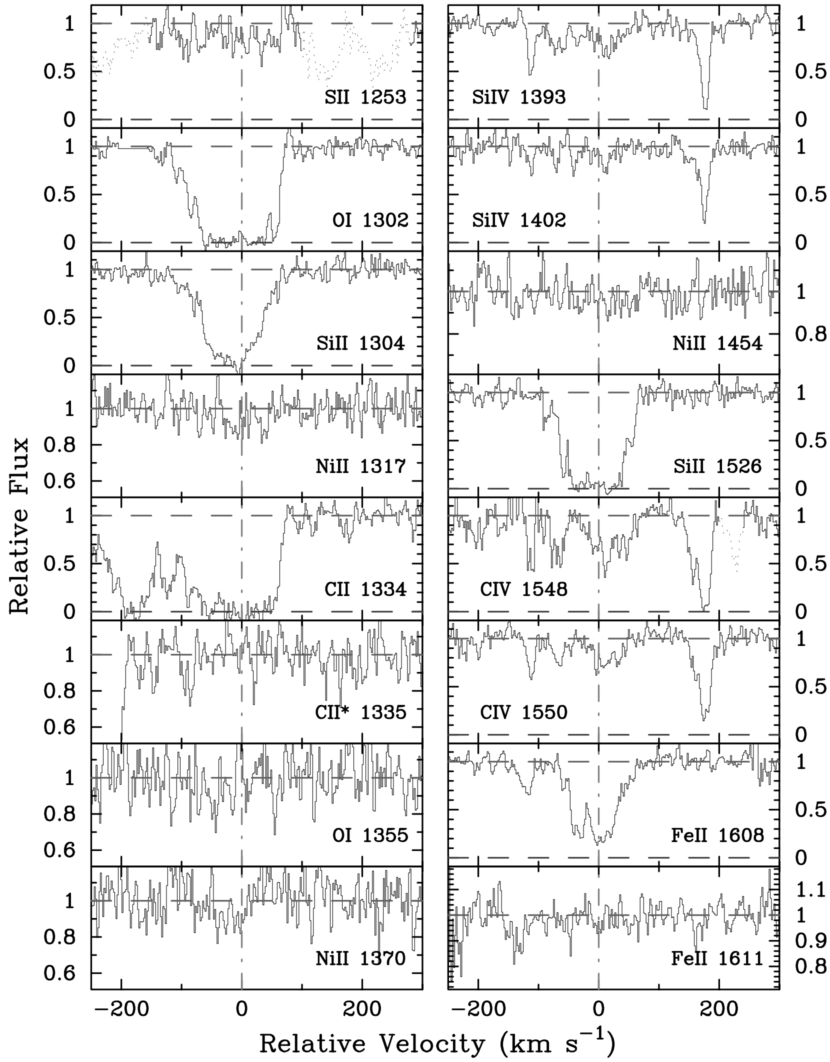

FIG. 13.—Velocity plot of the metal line transitions for the DLA system at $z = 2.465$ toward Q0836 + 11. The vertical line at $v = 0$ corresponds to $z = 2.46527$. [*See the electronic edition of the Journal for a color version of this figure.*]

TABLE 14

IONIC COLUMN DENSITIES: Q0836+11, $z = 2.465$

Ion	λ	AODM	$N_{\rm adopt}$	[X/H]
H I	1215	20.580 ± 0.100	...	...
C II	1334	>15.026	>15.026	>-2.104
C II	1335	<13.121	...	...
C IV	1548	>14.218	...	...
O I	1302	>15.485	>15.485	>-1.965
O I	1355	<18.186	...	...
Al III......	1854	12.459 ± 0.093	...	...
Al III......	1862	12.634 ± 0.076	...	...
Si II.......	1304	>14.918	14.987 ± 0.045	-1.153 ± 0.110
Si II.......	1526	>14.850	...	...
Si II.......	1808	14.987 ± 0.045	...	...
Si IV	1393	13.557 ± 0.024	...	...
Si IV	1402	13.592 ± 0.043	...	...
S II	1253	<14.660	<14.660	<-1.120
Ti II	1910	<12.537	<12.538	<-0.982
Cr II	2056	<12.898	<12.898	<-1.352
Cr II	2066	<13.230	...	...

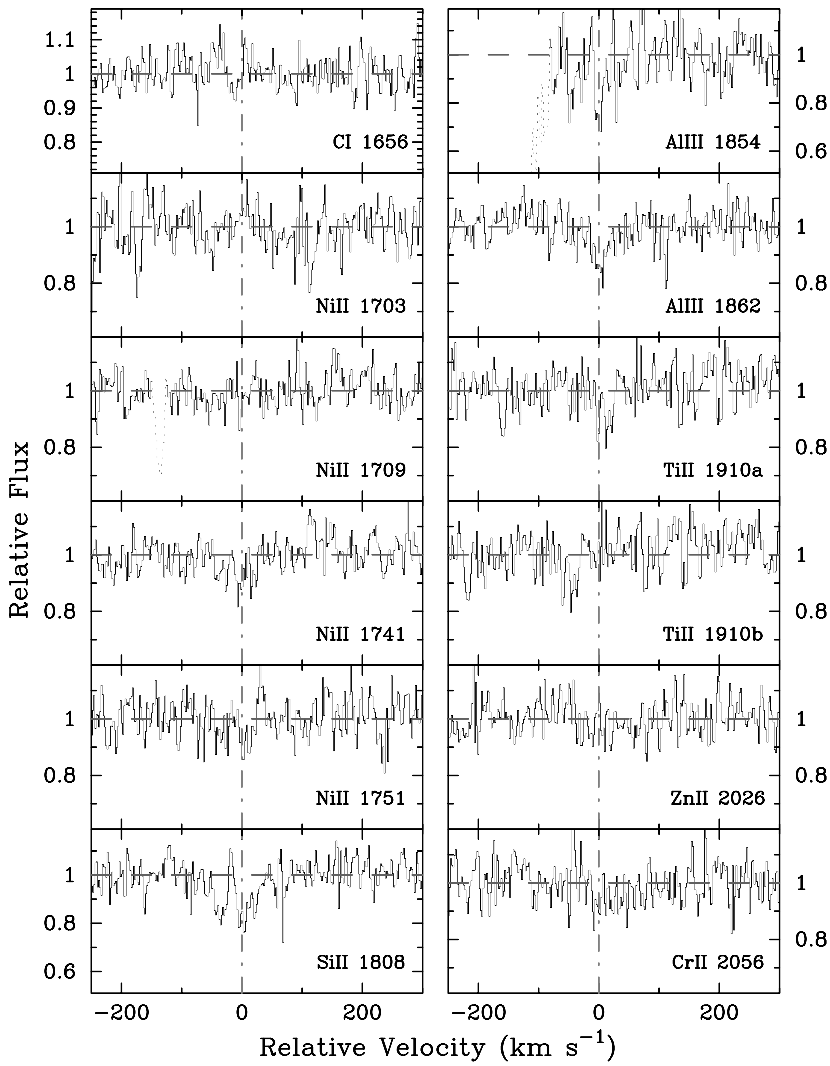

FIG. 13.—*Continued*

3.13. *BRI 0951−04*, $z = 3.857$ *and* 4.203

Our combined spectrum now includes a second setup with significant coverage blueward of the Lyα peak. Unfortunately, the new data add only a few unblended transitions to the analysis (Figs. 16 and 17 and Tables 17 and 18). With respect to PW99, we now suspect that the feature at 177 km s^{-1} in the $z = 3.857$ Ni II λ1370 profile is unrelated to that transition and obtain an upper limit on $N(\mathrm{Ni}^+)$. This value is in much better agreement with the Fe and Al abundances. In terms of the system at $z = 4.203$, we still have no reliable estimate of the Fe peak abundance. The combination of poor S/N and low H I column density has resulted in the

TABLE 14—*Continued*

Ion	λ	AODM	N_{adopt}	[X/H]
Fe II	1608	14.677±0.011	14.677±0.011	−1.403±0.101
Fe II	1611	<14.784	...	...
Co II......	1466	<13.383	<13.383	<−0.107
Co II......	1574	<13.442	...	...
Ni II	1317	13.364±0.105	13.388±0.065	−1.442±0.119
Ni II	1370	<13.339	...	...
Ni II	1454	<13.365	...	...
Ni II	1703	<14.058	...	...
Ni II	1709	<13.275	...	...
Ni II	1741	13.406±0.083	...	...
Ni II	1751	<13.393	...	...
Zn II	2026	<12.119	<12.119	<−1.131

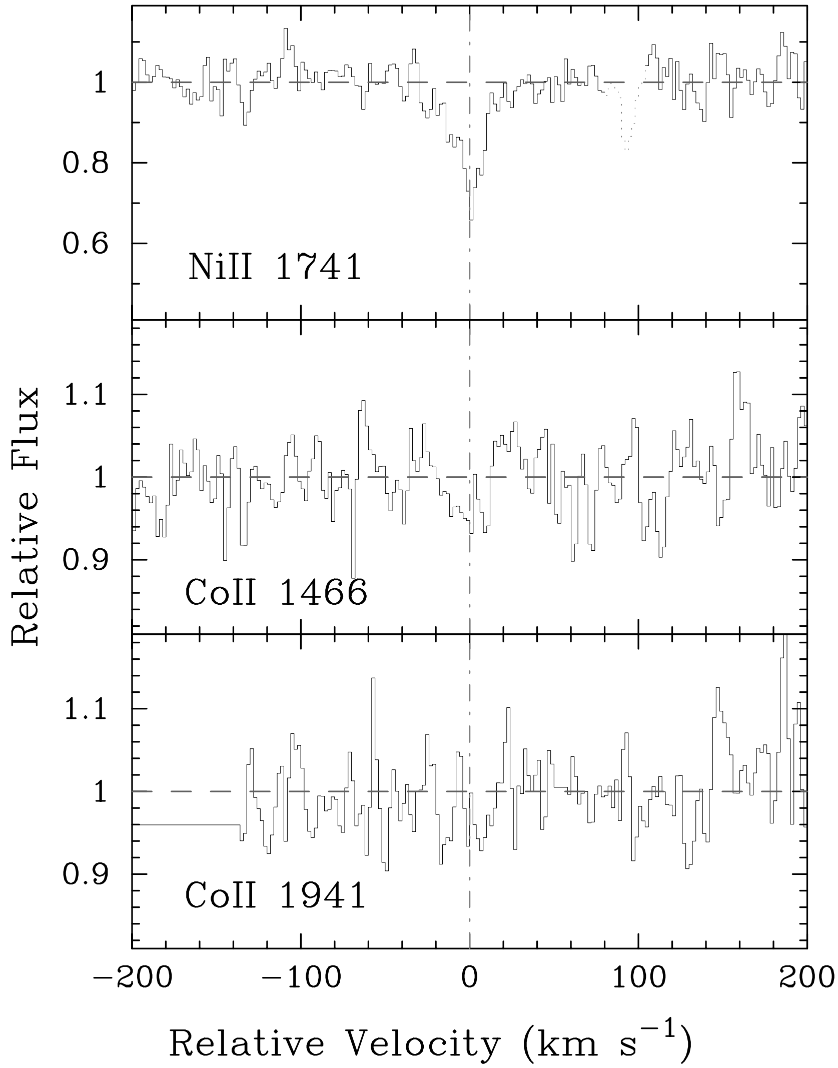

FIG. 14.—Velocity plot of two Co II profiles for the DLA system at $z = 2.375$ toward Q0841+12. For comparison, we also plot the Ni II λ1741 profile. The vertical line at $v = 0$ corresponds to $z = 2.374518$. [*See the electronic edition of the Journal for a color version of this figure.*]

nondetection of Fe II λ1608, and our observations did not cover C II λ1334 or Al II λ1670. Finally, we revise the oxygen abundance to account for the saturated O I λ1302 profile.

3.14. *BRI 0952−01*, $z = 4.024$

This DLA system was identified by Storrie-Lombardi et al. (1996) and confirmed with a follow-up LRIS spectrum by Storrie-Lombardi & Wolfe (2000). We adopt the N(H I) value from the latter analysis. Figure 18 presents the velocity profiles covered by our single setup. Unfortunately, a misestimate of the absorption redshift coupled with several line blends has limited our ionic column density measurements of this system (Table 19). As reported in Prochaska & Wolfe (2000), we estimate the Fe$^+$ column density by combining the unblended features observed for the Fe II $\lambda\lambda$1144 and 1608 profiles. With the updated oscillator strengths, we find $N(\mathrm{Fe}^+) = 14.187 \pm 0.07$.

TABLE 15

IONIC COLUMN DENSITIES: Q0841+12, $z = 2.375$

Ion	λ	AODM	N_{adopt}	[X/H]
H I........	1215	20.950 ± 0.087	...	...
Co II......	1466	< 13.047	< 12.990	< −0.870
Co II......	1941	< 12.990	...	...
Ni II	1454	13.415 ± 0.075	13.523 ± 0.030	−1.677 ± 0.092
Ni II	1741	13.560 ± 0.040	...	...
Ni II	1751	13.547 ± 0.055	...	...

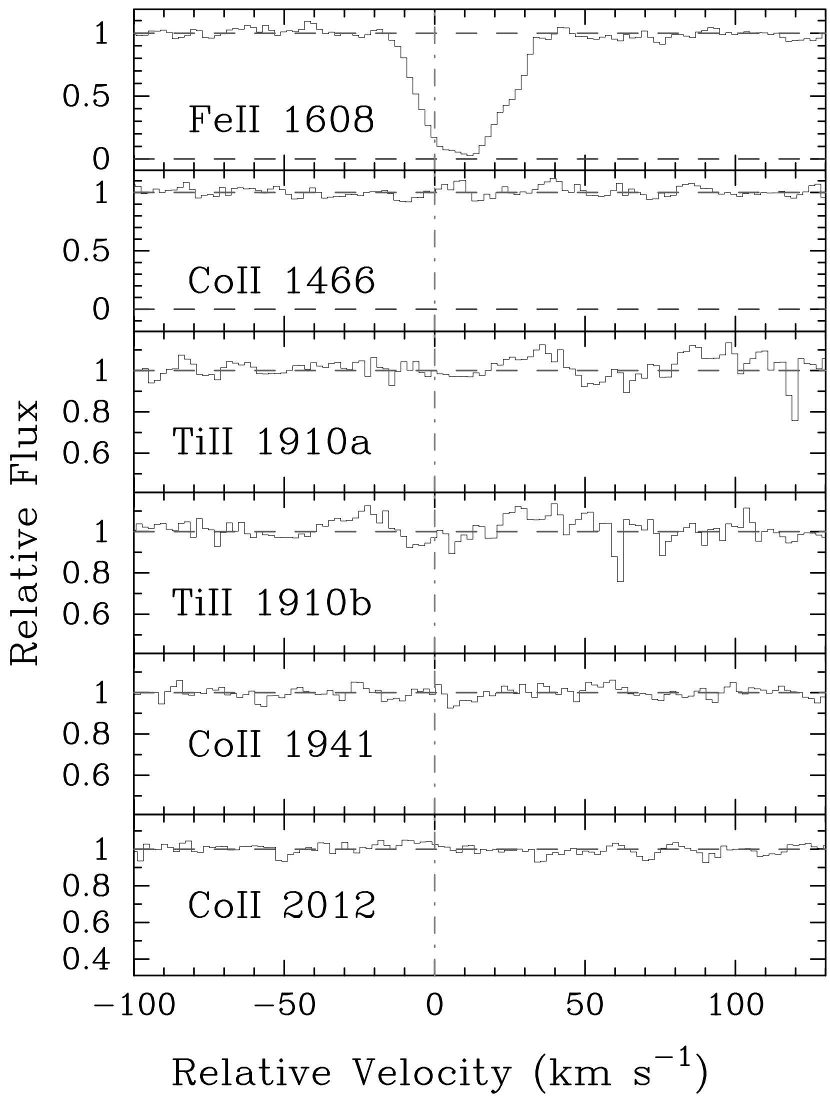

FIG. 15.—Velocity plot of the new metal line transitions for the DLA system at $z = 2.476$ toward Q0841+12. For comparison, we also plot the Fe II λ1608 profile. The vertical line at $v = 0$ corresponds to $z = 2.476219$. [*See the electronic edition of the Journal for a color version of this figure.*]

3.15. *PSS 0957+33, z = 3.279 and 4.178*

The two DLA systems toward this PSS quasar (Djorgovski et al. 1998) were discovered during the first night of our ongoing Echellette Spectrograph and Imager (ESI) project designed to discover and measure the metallicity of $z > 3$ damped systems (PGW01). Given the apparent brightness of this quasar we chose to obtain a HIRES spectrum. Figures 19 and 20 present the metal line transition identified in our HIRES spectrum, and Tables 20 and 21 give the ionic column densities.

To test the metallicities obtained with the ESI spectrum, we can compare the HIRES values with the Fe^{+} column densities adopted in PGW01 after correcting for the new

TABLE 16

IONIC COLUMN DENSITIES: Q0841+12, $z = 2.476$

Ion	λ	AODM	N_{adopt}	[X/H]
H I........	1215	20.780 ± 0.097	...	...
Ti II	1910	< 12.158	< 12.158	< −1.562
Fe II	1608	> 14.517	...	...
Fe II	1611	< 14.543	...	...
Co II......	1466	< 13.206	< 12.726	< −0.964
Co II......	1941	< 12.783	...	...
Co II......	2012	< 12.726	...	...
Ni II	1709	13.415 ± 0.060	13.355 ± 0.040	−1.675 ± 0.105
Ni II	1741	13.321 ± 0.054	...	...
Ni II	1751	< 13.348	...	...

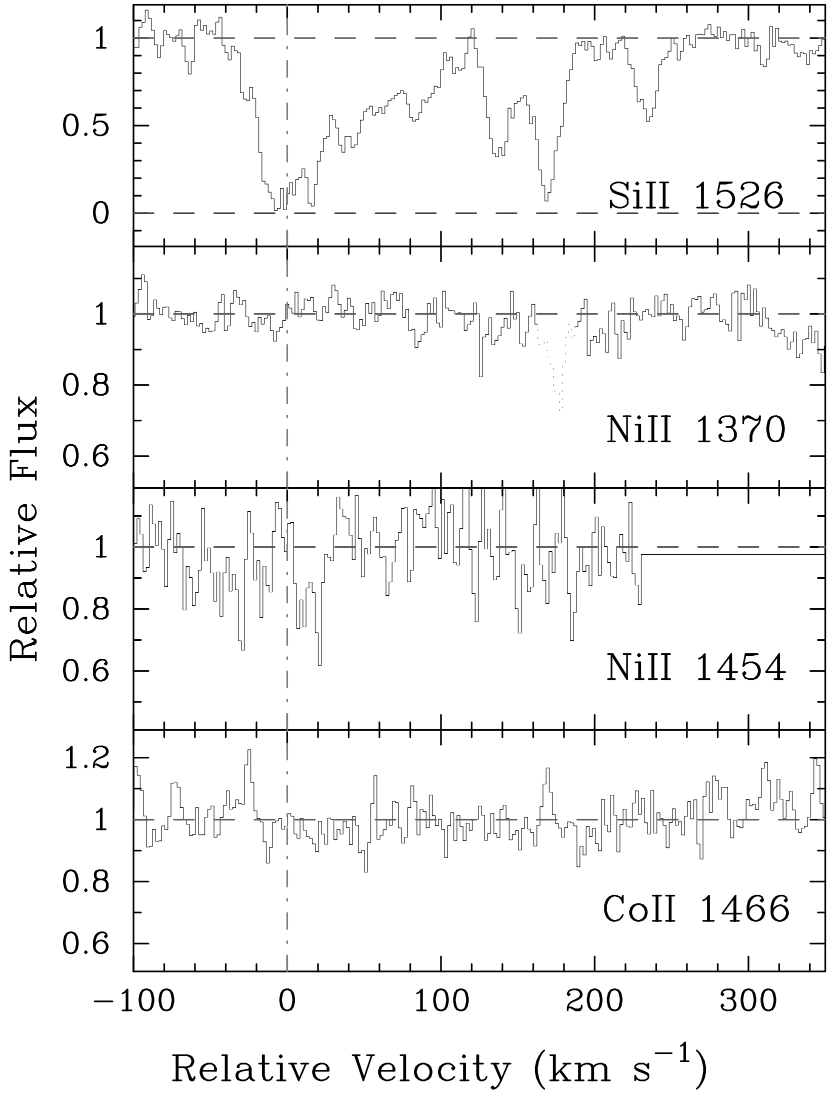

FIG. 16.—Velocity plot of the new metal line transitions for the DLA system at $z = 3.857$ toward BRI 0951−04. For comparison, we also plot the Si II λ1526 profile. The vertical line at $v = 0$ corresponds to $z = 3.856689$. [*See the electronic edition of the Journal for a color version of this figure.*]

oscillator strengths. For the system at $z = 3.279$, the Fe II λ1608 column densities are in excellent agreement, but because this transition is blended with telluric absorption, it might only provide an upper limit on $N(\mathrm{Fe^+})$. In PGW01, we derived the $\mathrm{Fe^+}$ column density from Fe II λ2344, which is redward of our HIRES coverage. We now suspect that this value was an underestimate of $N(\mathrm{Fe^+})$ as it implies [Ni/Fe] > 0.3 dex. For now, we adopt an $\mathrm{Fe^+}$ column density based on the Fe II λ1608 profile.

The system at $z = 4.178$ presents a more worrisome picture regarding column densities derived from ESI echellette observations. Comparing the column densities for Fe II λ1608, we find that we underestimated $N(\mathrm{Fe^+})$ by $\approx$0.3 dex with the ESI spectrum. It is somewhat puzzling given that the profile is not very strong (unlike the Si II profiles, for example) and the quality of the ESI data is high. The strongest features are relatively narrow, so the difference is probably an effect of the lower resolution. Another puzzling aspect of the $z = 4.178$ systems is the $\mathrm{S^+}$ column density derived from S II $\lambda\lambda$1250 and 1253. Although the S II λ1250 profile is partially blended with an unrelated C IV system ($z_{\mathrm{abs}} = 3.181$), we are confident that the absorption at

TABLE 17

IONIC COLUMN DENSITIES: BRI 0951−04, $z = 3.857$

Ion	λ	AODM	N_{adopt}	[X/H]
H I........	1215	20.600 ± 0.100		
Co II......	1466	< 13.597	< 13.597	< 0.087
Ni II	1370	< 12.977	< 12.977	< −1.873
Ni II	1454	< 13.927		

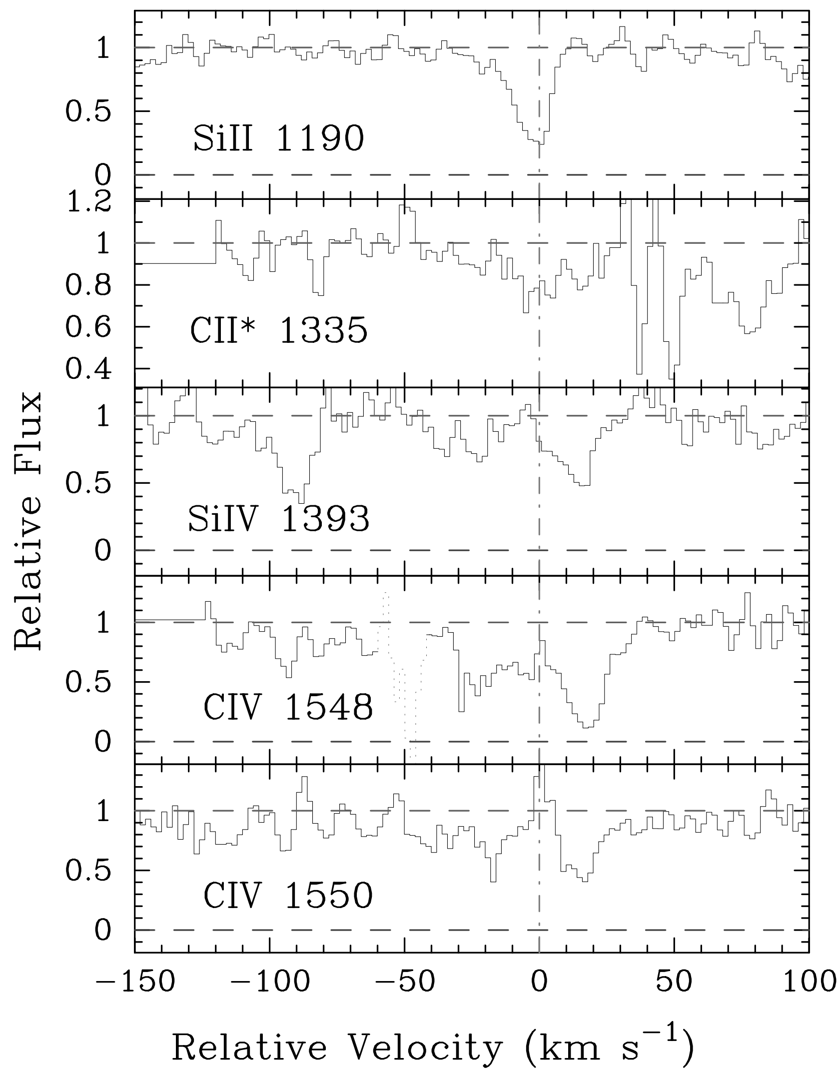

FIG. 17.—Velocity plot of the new metal line transitions for the DLA system at $z = 4.203$ toward BRI 0951−04. The vertical line at $v = 0$ corresponds to $z = 4.202896$. [*See the electronic edition of the Journal for a color version of this figure.*]

$-100 < v < 20$ km s^{-1} is free of contamination from the C IV system. In this case, N(S II λ1250) provides a lower limit on log $N(S^+) > 14.65$. This lower limit, however, is well in excess of the $N(S^+)$ value derived from the unblended S II λ1253 transition. The component at $v = 0$ km s^{-1} in the S II λ1250 profile is wider than its counterpart in the S II λ1253 profile, but there is no identifiable blend. Perhaps the difference suggests an extreme case of hidden saturation (Savage & Sembach 1991). If it is line saturation, this helps explain why the ESI data significantly underestimate the column densities in this case, and it also raises the possibility that the abundances derived from the HIRES observations are underestimates. This would be particularly surprising given that the spectra have a resolution of $R = 47{,}000$. Unfortunately, our HIRES spectrum did not cover any other pair of unsaturated transitions from the same ion to test this issue further. Furthermore, the difference even exists in a comparison of S II $\lambda\lambda$1250 and 1253 with respect to the

TABLE 18

IONIC COLUMN DENSITIES: BRI 0951−04, $z = 4.203$

Ion	λ	AODM	N_{adopt}	[X/H]
H I	1215	20.400 ± 0.100	...	...
C IV	1548		...	...
C IV	1550	13.945 ± 0.052	...	...
O I	1302	> 14.596	> 14.596	> −2.674
Si II	1190	13.417 ± 0.042	13.342 ± 0.030	−2.618 ± 0.104
Si II	1526	13.302 ± 0.056	...	...
Si IV	1393	12.918 ± 0.063	...	...

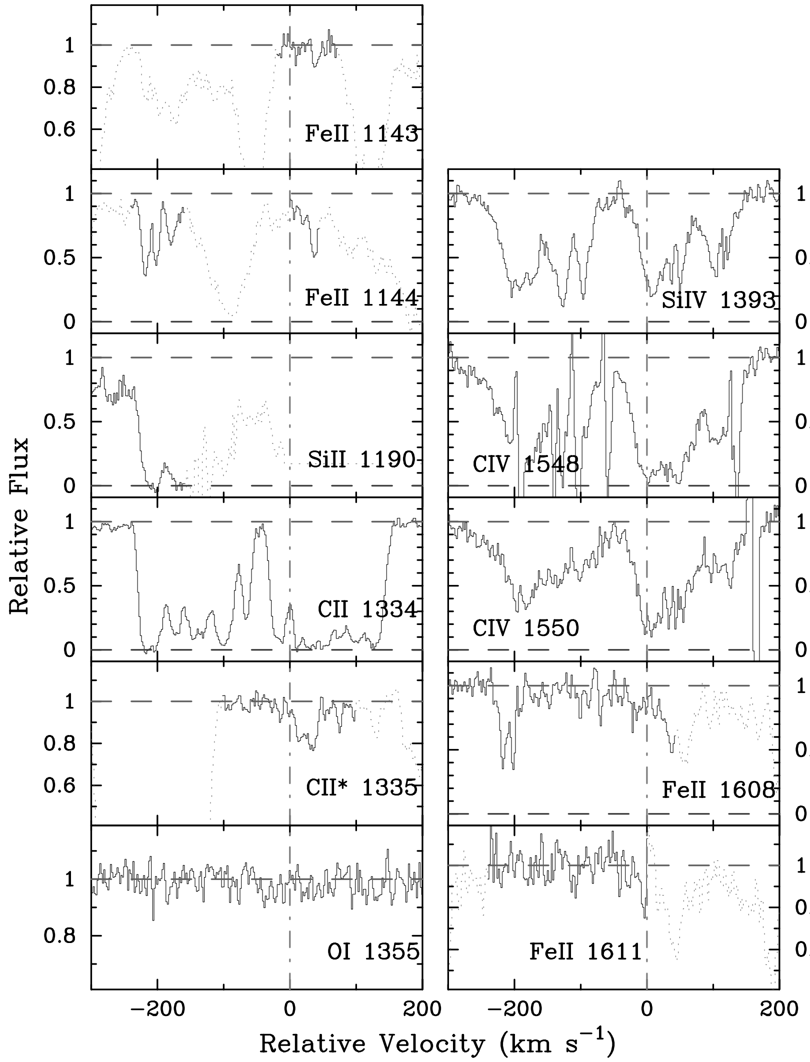

FIG. 18.—Velocity plot of the metal line transitions for the DLA system at $z = 4.024$ toward BRI 0952−01. The vertical line at $v = 0$ corresponds to $z = 4.024433$. [*See the electronic edition of the Journal for a color version of this figure.*]

feature at $v \approx -75$ km s^{-1}. Perhaps this is all the result of errors in the S II oscillator strengths, but it would have likely been identified by researchers who study the interstellar medium (ISM) (e.g., Howk, Savage, & Fabian 1999).

3.16. *BRI 1108−07*, $z = 3.608$

This DLA system was discovered and confirmed by Storrie-Lombardi et al. (1996). The quasar is relatively bright, and we obtained a reasonably high S/N HIRES spectrum. Figure 21 presents the velocity profiles, and Table 22 lists the ionic column densities. The Fe^+ and Si^+ column densities are well measured and indicate a very large Si/Fe ratio, perhaps indicative of substantial Type II supernova (SN) enrichment.

TABLE 19

IONIC COLUMN DENSITIES: BRI 0952−01, $z = 4.024$

Ion	λ	AODM	N_{adopt}	[X/H]
H I........	1215	20.550 ± 0.100	...	...
C II	1334	> 15.312	> 15.312	> −1.788
C II	1335	13.549 ± 0.024	...	...
C IV	1550	14.796 ± 0.009	...	...
Si IV	1393	14.134 ± 0.006	...	...
Fe II	1144	> 13.864	14.187 ± 0.076	−1.863 ± 0.126
Fe II	1608	> 13.746	...	...
Co II......	1574	< 13.750	< 13.750	< 0.290
Ni II	1454	< 13.439	< 13.439	< −1.361

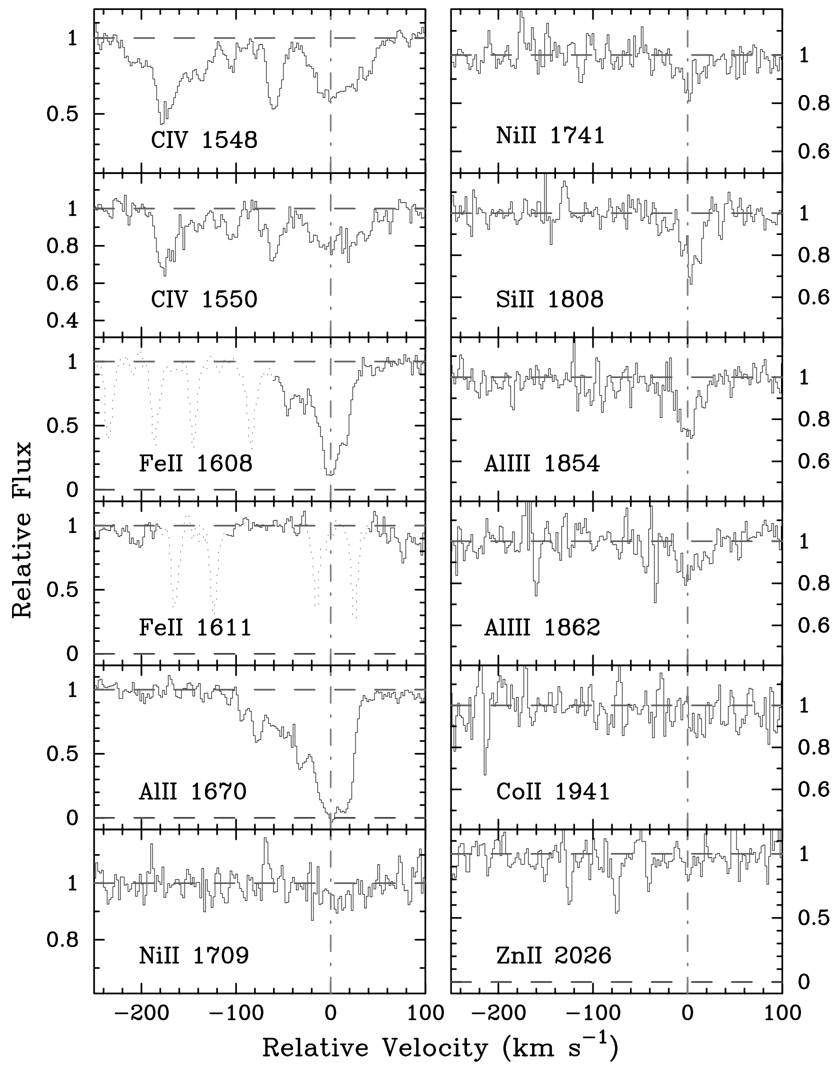

FIG. 19.—Velocity plot of the metal line transitions for the DLA system at $z = 3.279$ toward PSS 0957+33. The vertical line at $v = 0$ corresponds to $z = 3.279576$. [*See the electronic edition of the Journal for a color version of this figure.*]

3.17. *Q1210+17*, $z = 1.892$

This system is a member of the LBQS sample, and we have adopted the N(H I) value from their analysis. We plot all of the transitions covered by our observations in Figure 22 and list the column densities in Table 23. This damped system exhibits a relatively low Zn/Fe ratio, which suggests that it is largely free of dust depletion. In passing, we note a remarkable similarity between the relative abundances of

TABLE 20

IONIC COLUMN DENSITIES: PSS 0957+33, $z = 3.279$

Ion	λ	AODM	$N_{\rm adopt}$	[X/H]
H I........	1215	20.320 ± 0.080	...	...
C IV	1548	13.979 ± 0.009	...	...
C IV	1550	13.956 ± 0.019	...	...
Al II	1670	>13.322	>13.322	>-1.488
Al III......	1854	12.514 ± 0.048	...	...
Al III......	1862	12.578 ± 0.087	...	...
Si II	1808	14.880 ± 0.053	14.880 ± 0.053	-1.000 ± 0.096
Fe II	1608	14.367 ± 0.016	14.367 ± 0.016	-1.453 ± 0.082
Co II......	1941	<13.285	<13.285	<0.055
Ni II	1709	13.283 ± 0.122	13.318 ± 0.070	-1.252 ± 0.106
Ni II	1741	13.339 ± 0.085	...	...
Zn II......	2026	<12.127	<12.127	<-0.863

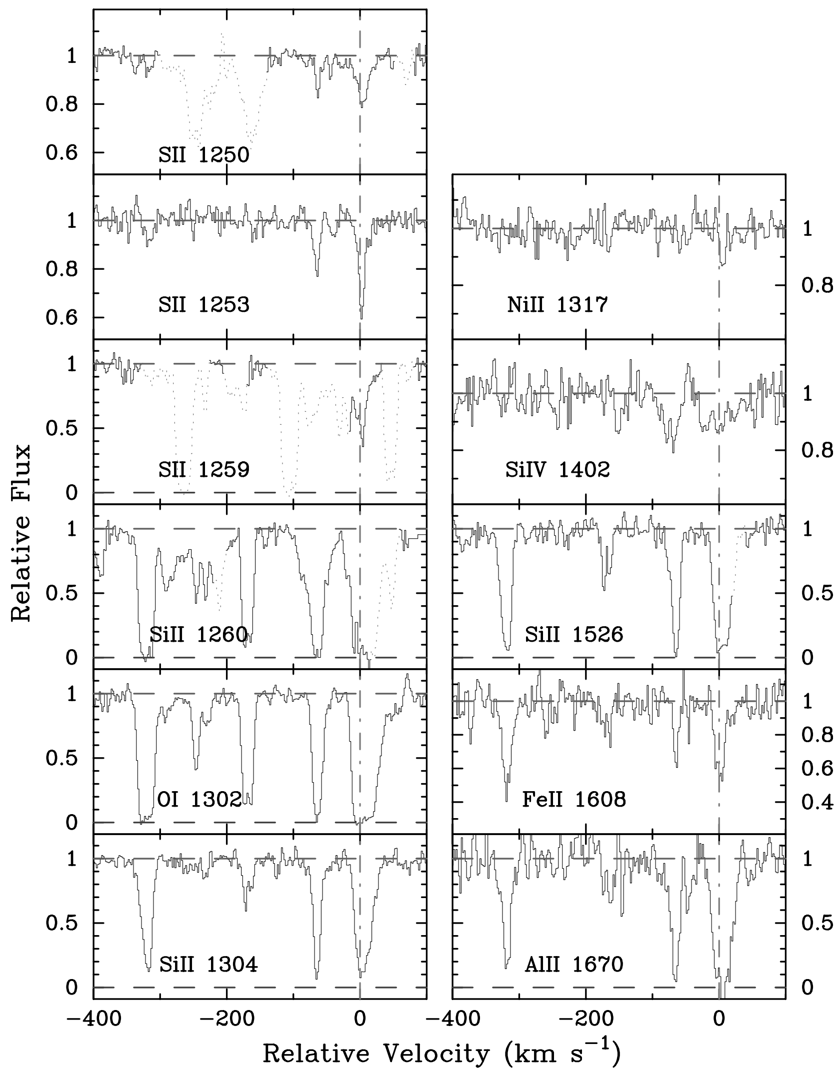

FIG. 20.—Velocity plot of the metal line transitions for the DLA system at $z = 4.178$ toward PSS 0957+33. The vertical line at $v = 0$ corresponds to $z = 4.179825$. [*See the electronic edition of the Journal for a color version of this figure.*]

TABLE 21

IONIC COLUMN DENSITIES: PSS 0957+33, $z = 4.178$

Ion	λ	AODM	N_{adopt}	[X/H]
H I........	1215	20.500 ± 0.100	...	...
O I........	1302	>15.344	>15.344	>-2.026
Al II	1670	>13.256	>13.256	>-1.734
Si II	1304	14.556 ± 0.012	14.556 ± 0.012	-1.504 ± 0.101
Si II	1526	>14.488	...	...
Si IV	1402	13.155 ± 0.049	...	...
S II........	1250	>14.647	14.392 ± 0.060	-1.308 ± 0.117
S II........	1253	14.392 ± 0.060	...	...
Fe II	1608	14.129 ± 0.045	14.129 ± 0.045	-1.871 ± 0.110
Co II......	1466	<13.648	<13.648	<0.238
Co II......	1574	<13.907	...	...
Ni II	1317	<12.910	<12.910	<-1.840

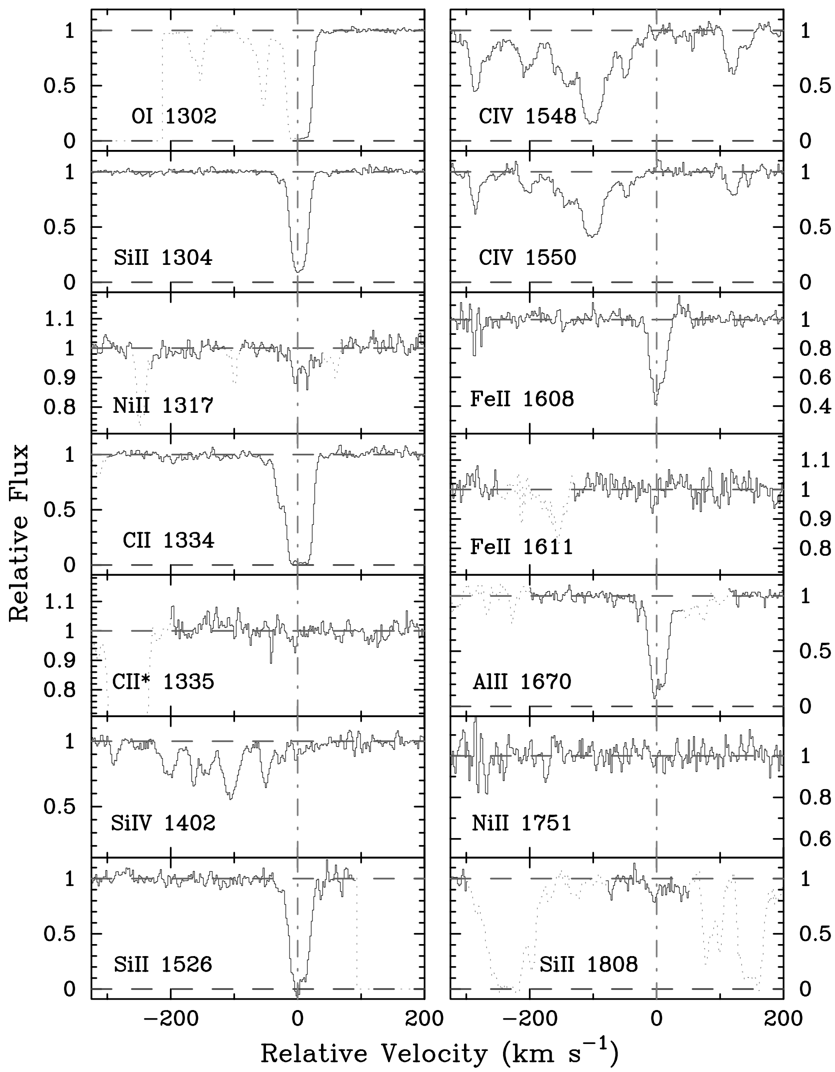

FIG. 21.—Velocity plot of the metal line transitions for the DLA system at $z = 3.608$ toward BRI 1108−07. The vertical line at $v = 0$ corresponds to $z = 3.607619$. [*See the electronic edition of the Journal for a color version of this figure.*]

TABLE 22

IONIC COLUMN DENSITIES: BRI 1108−07, $z = 3.608$

Ion	λ	AODM	$N_{\rm adopt}$	[X/H]
H I	1215	20.500 ± 0.100	...	...
C II	1334	> 14.675	> 14.675	> -2.375
C II	1335	< 12.341	...	...
C IV	1548	14.293 ± 0.006	...	...
C IV	1550	14.219 ± 0.011	...	...
O I	1302	> 14.873	> 14.873	> -2.497
Al II	1670	12.822 ± 0.015	12.822 ± 0.015	-2.168 ± 0.101
Si II	1304	14.262 ± 0.004	14.262 ± 0.004	-1.798 ± 0.100
Si II	1526	> 14.260	...	...
Si II	1808	< 14.665	...	...
Si IV	1402	13.685 ± 0.010	...	...
Fe II	1608	13.884 ± 0.014	13.884 ± 0.014	-2.116 ± 0.101
Fe II	1611	< 14.269	...	...
Ni II	1317	< 13.136	< 13.136	< -1.614
Ni II	1751	< 13.180	...	...

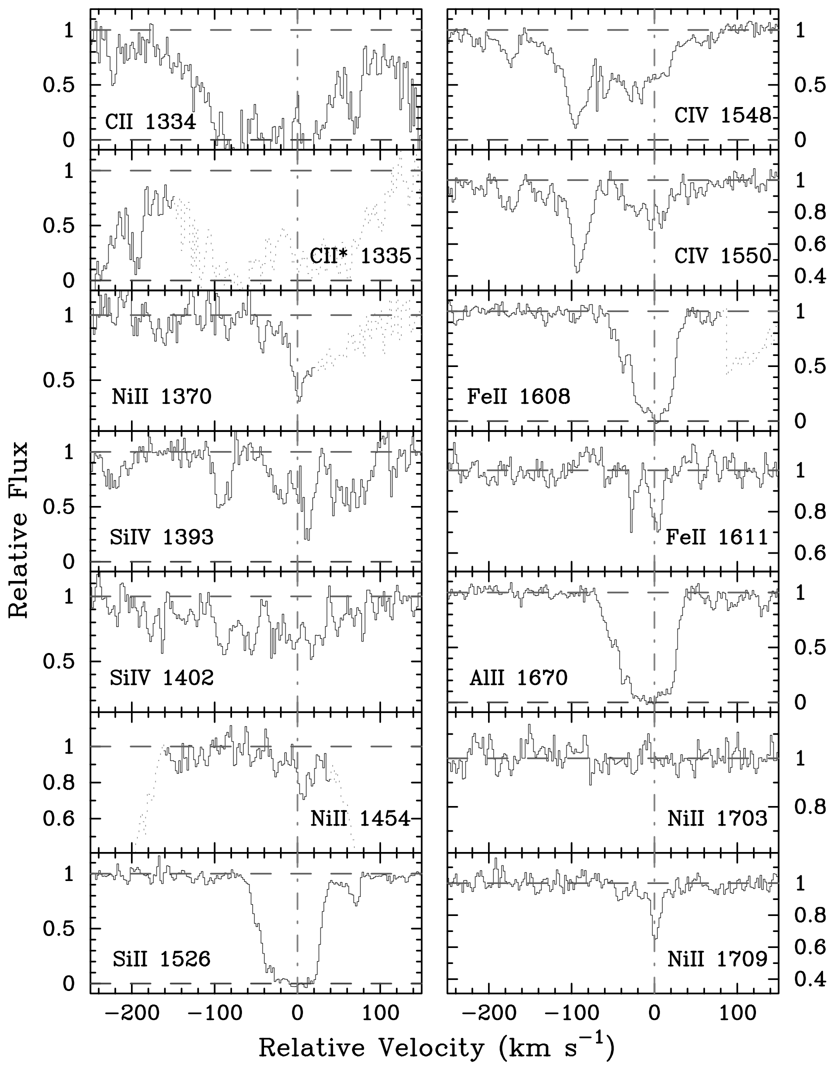

FIG. 22.—Velocity plot of the metal line transitions for the DLA system at $z = 1.892$ toward Q1210 + 17. The vertical line at $v = 0$ corresponds to $z = 1.891755$. [*See the electronic edition of the Journal for a color version of this figure.*]

Si, Ni, Cr, Fe, and Zn with the same pattern observed by Molaro et al. (2000) for the damped system toward Q0000−26, albeit at a much higher metallicity.

3.18. *Q1215+33*, $z = 1.999$

Although we presented a full analysis of this damped system in PW99, a number of transitions were overlooked, and we have revised the Fe abundance. Figure 23 plots the new transitions, and Table 24 lists the ionic column densities. We now report only a limit on $N(\mathrm{Fe}^+)$ because the Fe II λ1608 profile is saturated and the Fe II λ1611 transition is too weak to provide a reasonable measurement. In the subsequent analysis, we assume a value based on an average of the two limits: $N(\mathrm{Fe}^+) = 10^{14.748 \pm 0.05}$ cm^{-2}. Finally, we

TABLE 23

IONIC COLUMN DENSITIES: Q1210+17, $z = 1.892$

Ion	λ	AODM	N_{adopt}	[X/H]
H I	1215	20.600 ± 0.100	...	...
C IV	1548	< 14.230	...	...
C IV	1550	14.053 ± 0.017	...	...
Al II	1670	> 13.440	> 13.440	> −1.650
Al III......	1854	12.999 ± 0.017	...	...
Al III......	1862	13.005 ± 0.021	...	...
Si II.......	1526	> 14.780	15.285 ± 0.018	−0.875 ± 0.102
Si II.......	1808	15.285 ± 0.018	...	...
Si IV	1393	13.594 ± 0.025	...	...
Cr II	2056	13.291 ± 0.019	13.243 ± 0.016	−1.027 ± 0.101

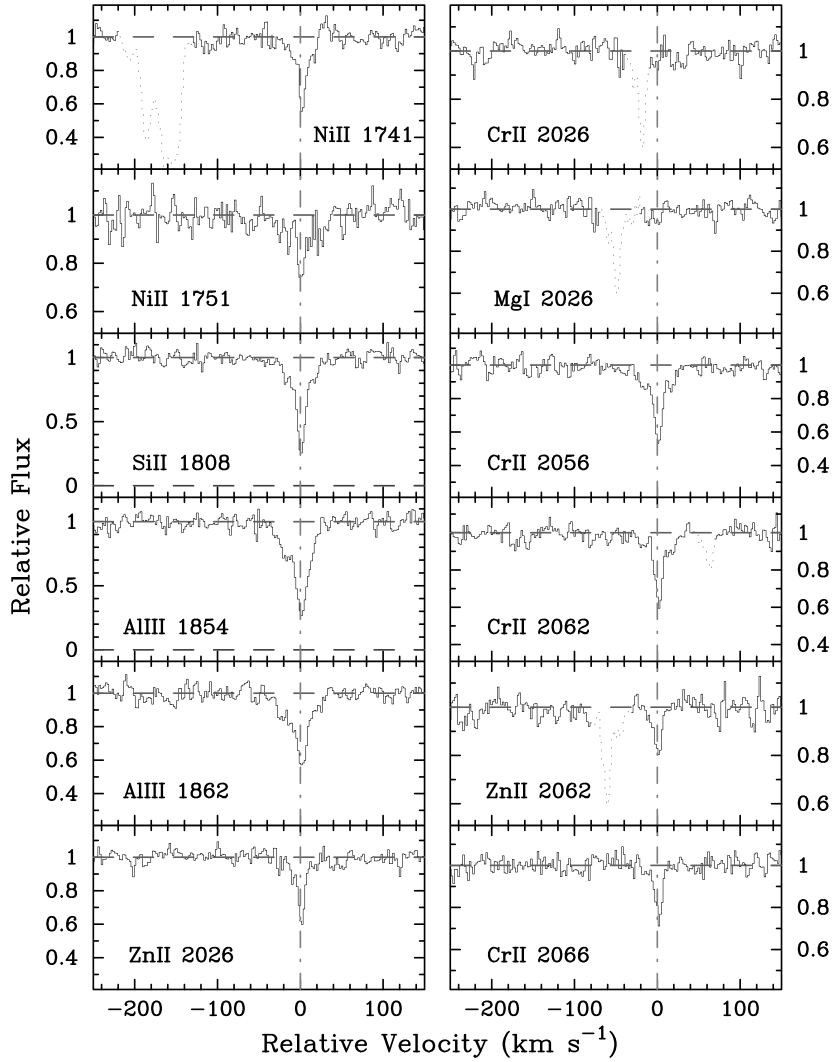

FIG. 22.—*Continued*

also report an upper limit on $N(\mathrm{Zn}^+)$ based on the Zn II λ2062 profile. It is 0.2 dex lower than the value derived from Zn II λ2026, which is difficult to understand aside from the fact that the Zn II λ2026 profile is noisy and the continuum is poorly constrained in that region. For now, we continue to adopt the value from Zn II λ2026.

3.19. *Q1223+17*, $z = 2.466$

The combination of a very large N(H I) value and extensive wavelength coverage allows for the analysis of a terrific number of transitions. Figure 24 and Table 25 present over 20 transitions including a large number of limits. One of the most interesting ratios is Ti/Fe, whose upper limit is less

TABLE 23—*Continued*

Ion	λ	AODM	N_{adopt}	[X/H]
Cr II	2062	13.219 ± 0.030	...	...
Cr II	2066	13.091 ± 0.058	...	...
Fe II	1608	> 14.780	14.951 ± 0.063	−1.149 ± 0.118
Fe II	1611	14.951 ± 0.063	...	...
Co II......	1574	< 13.513	< 12.728	< −0.782
Co II......	2012	< 12.728	...	...
Ni II	1370	< 13.964	13.632 ± 0.020	−1.218 ± 0.102
Ni II	1454	< 13.832	...	...
Ni II	1709	13.657 ± 0.031	...	...
Ni II	1741	13.628 ± 0.029	...	...
Ni II	1751	13.590 ± 0.049	...	...
Zn II......	2026	12.409 ± 0.032	12.370 ± 0.029	−0.900 ± 0.104
Zn II......	2062	12.263 ± 0.069	...	...

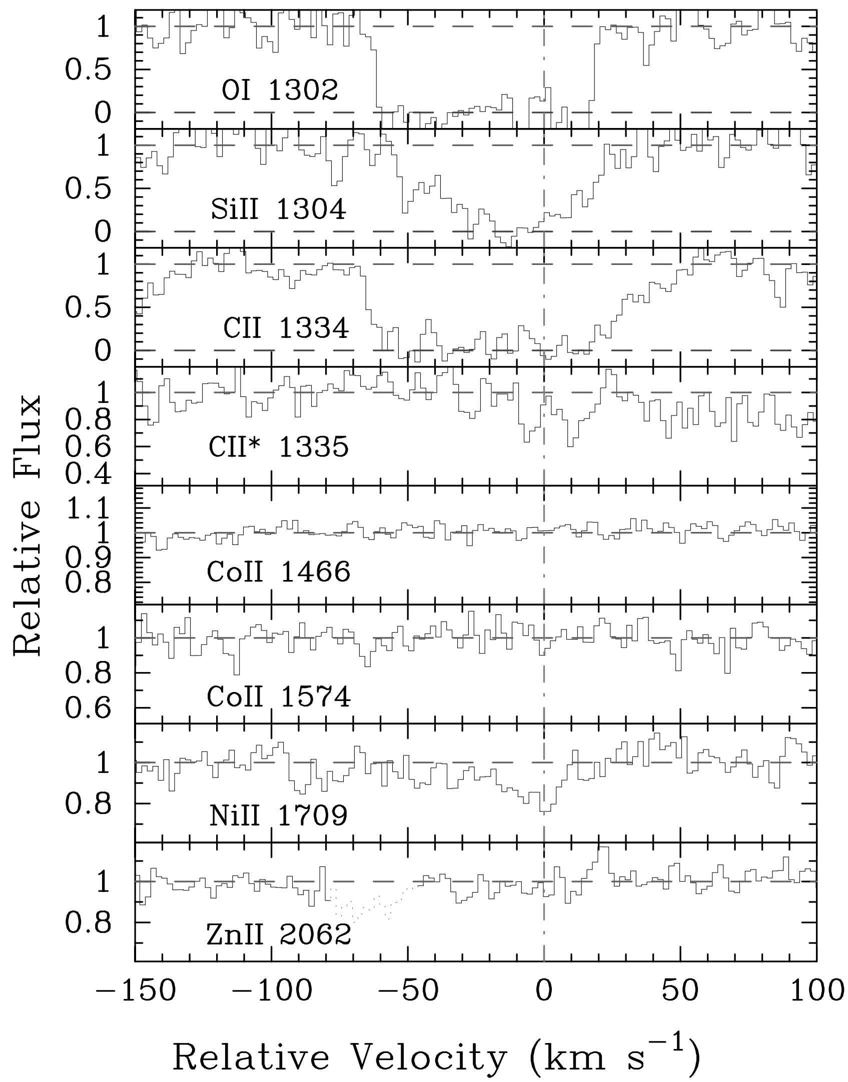

FIG. 23.—Velocity plot of the new metal line transitions for the DLA system at $z = 1.999$ toward Q1215+33. The vertical line at $v = 0$ corresponds to $z = 1.9991$. [*See the electronic edition of the Journal for a color version of this figure.*]

TABLE 24

IONIC COLUMN DENSITIES: Q1215+33, $z = 1.999$

Ion	λ	AODM	$N_{\rm adopt}$	[X/H]
H I........	1215	20.950 ± 0.067	...	...
C II	1334	>14.630	>14.630	>-2.870
C II	1335	<13.173	...	...
O I........	1302	>15.127	>15.127	>-2.693
O I........	1355	<18.065	...	...
Si II	1304	>14.617	15.030 ± 0.025	-1.480 ± 0.072
Si II	1526	>14.660	...	...
Si II	1808	15.030 ± 0.025	...	...
Fe II	1608	>14.696	14.748 ± 0.053	-1.702 ± 0.085
Fe II	1611	<14.800	...	...
Co II......	1466	<12.860	<12.860	<-1.000
Co II......	1574	<13.358	...	...
Ni II	1709	13.579 ± 0.061	13.594 ± 0.027	-1.606 ± 0.072
Ni II	1741	13.602 ± 0.039	...	...
Ni II	1751	13.592 ± 0.048	...	...
Zn II......	2026	12.330 ± 0.049	12.330 ± 0.049	-1.290 ± 0.083
Zn II......	2062	<12.138	...	...

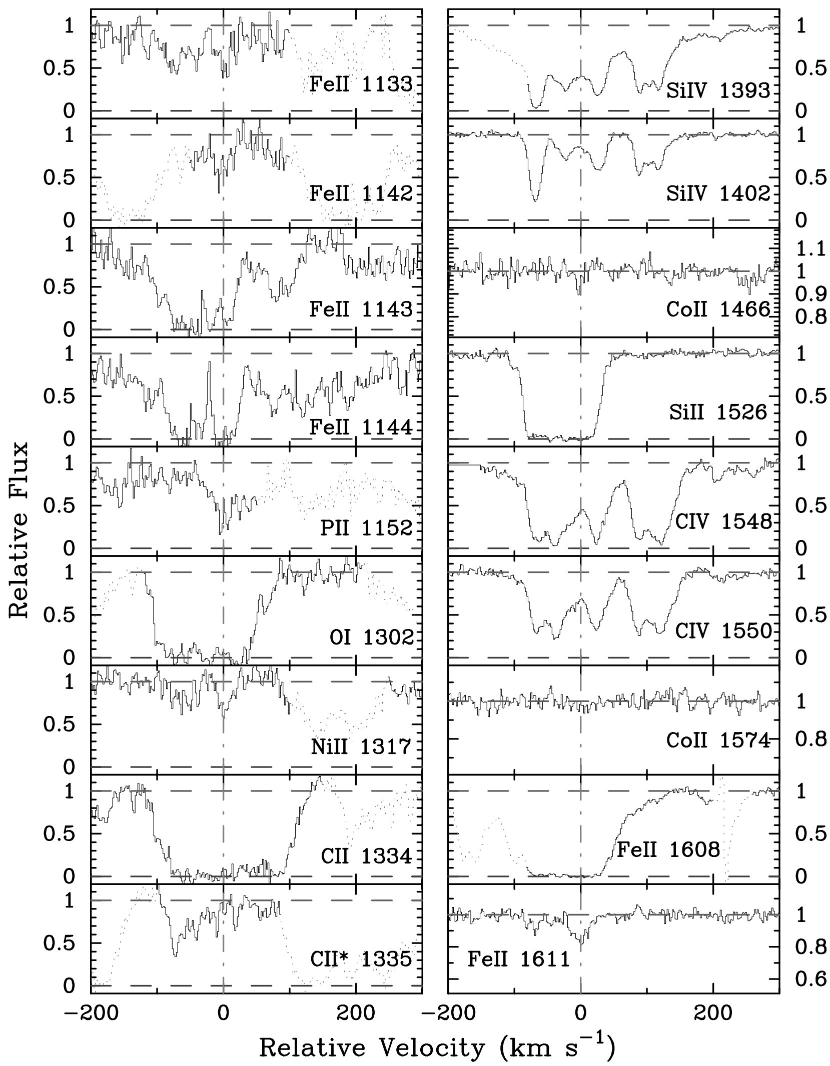

FIG. 24.—Velocity plot of the metal line transitions for the DLA system at $z = 2.466$ toward Q1223 + 17. The vertical line at $v = 0$ corresponds to $z = 2.466083$. [*See the electronic edition of the Journal for a color version of this figure.*]

TABLE 25

IONIC COLUMN DENSITIES: Q1223+17, $z = 2.466$

Ion	λ	AODM	$N_{\rm adopt}$	[X/H]
H I	1215	21.500 ± 0.100	...	...
C I	1656	< 12.426	...	...
C II	1334	> 15.155	> 15.155	> −2.895
C II	1335	< 14.007	...	...
C IV	1548	> 14.696	...	...
C IV	1550	14.658 ± 0.004	...	...
O I	1302	> 15.477	> 15.477	> −2.893
Al III	1862	12.909 ± 0.023	...	...
Si II	1526	> 15.037	15.468 ± 0.008	−1.592 ± 0.100
Si II	1808	15.468 ± 0.008	...	...
Si IV	1402	13.891 ± 0.004	...	...
P II	1152	< 13.883	< 13.883	< −1.147
Ti II	1910	< 12.252	< 12.252	< −2.188
Cr II	2056	13.521 ± 0.013	13.493 ± 0.010	−1.677 ± 0.100
Cr II	2062	13.480 ± 0.018	...	...
Cr II	2066	13.411 ± 0.032	...	...
Fe II	1133	15.098 ± 0.059	15.157 ± 0.022	−1.843 ± 0.102
Fe II	1142	15.258 ± 0.051	...	...
Fe II	1611	15.152 ± 0.027	...	...

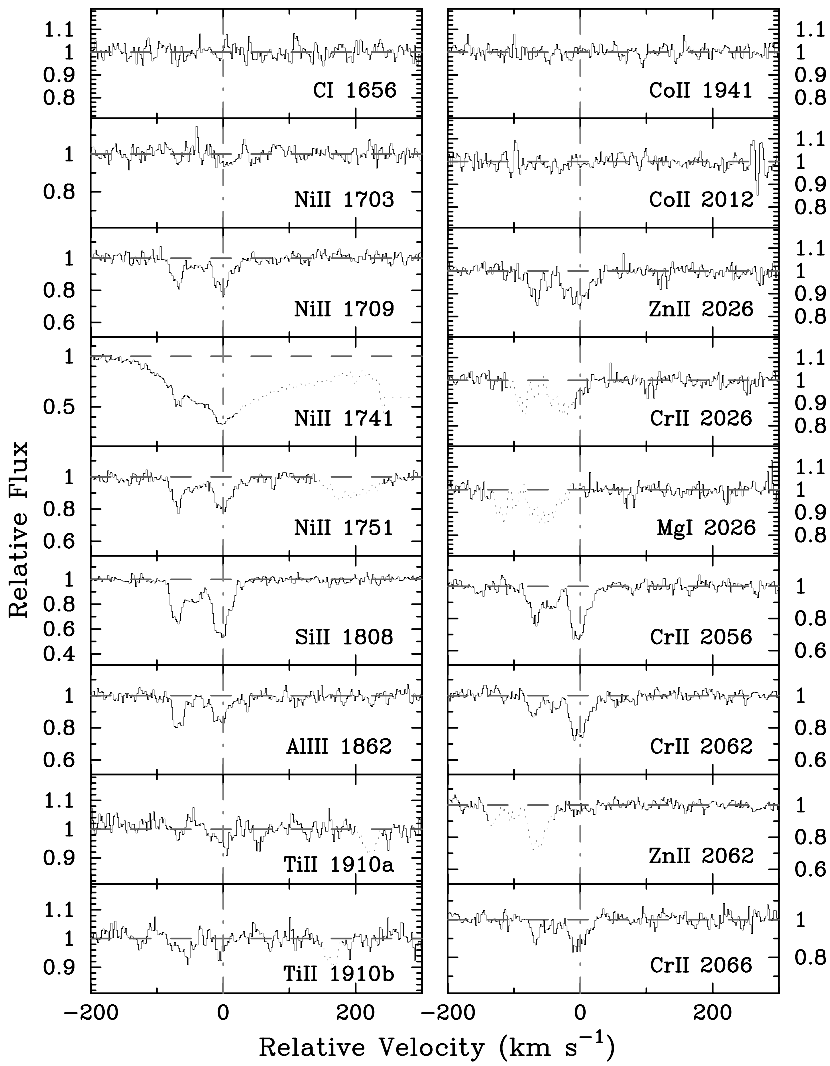

FIG. 24.—*Continued*

than $\frac{1}{2}$ the solar value ([Ti/Fe] < -0.4). In general, a subsolar Ti/Fe ratio implies significant dust depletion because Ti is more readily locked up into dust grains, but the Zn/Fe ratio is not particularly large as one would expect in a significantly dust depleted region ([Zn/Fe] $= 0.22$). Our observations also place a tight constraint on Co/Fe, which is described in greater detail in Ellison, Ryan, & Prochaska (2001).

3.20. *Q1331+17*, $z = 1.776$

An analysis of the damped system toward the very bright quasar Q1331+17 was given by PW99, but a number of transitions were missed (notably Ti II λ1910 and Co II λ2012). The new transitions are plotted in Figure 25, and the ionic column densities are given in Table 26.

With respect to the $N(Zn^{+})$ value presented by PW99, this system exhibits one of the largest Zn/Fe ratios of any

TABLE 25—*Continued*

Ion	λ	AODM	N_{adopt}	[X/H]
Co II......	1466	<13.174	<12.631	<−1.779
Co II......	1574	<13.122	...	...
Co II......	1941	<12.917	...	...
Co II......	2012	<12.631	...	...
Ni II	1317	13.853±0.051	13.949±0.011	−1.801±0.101
Ni II	1703	<13.817	...	...
Ni II	1709	13.901±0.020	...	...
Ni II	1751	14.000±0.014	...	...
Zn II......	2026	12.550±0.026	12.550±0.026	−1.620±0.103
Zn II......	2062	>11.785	...	...

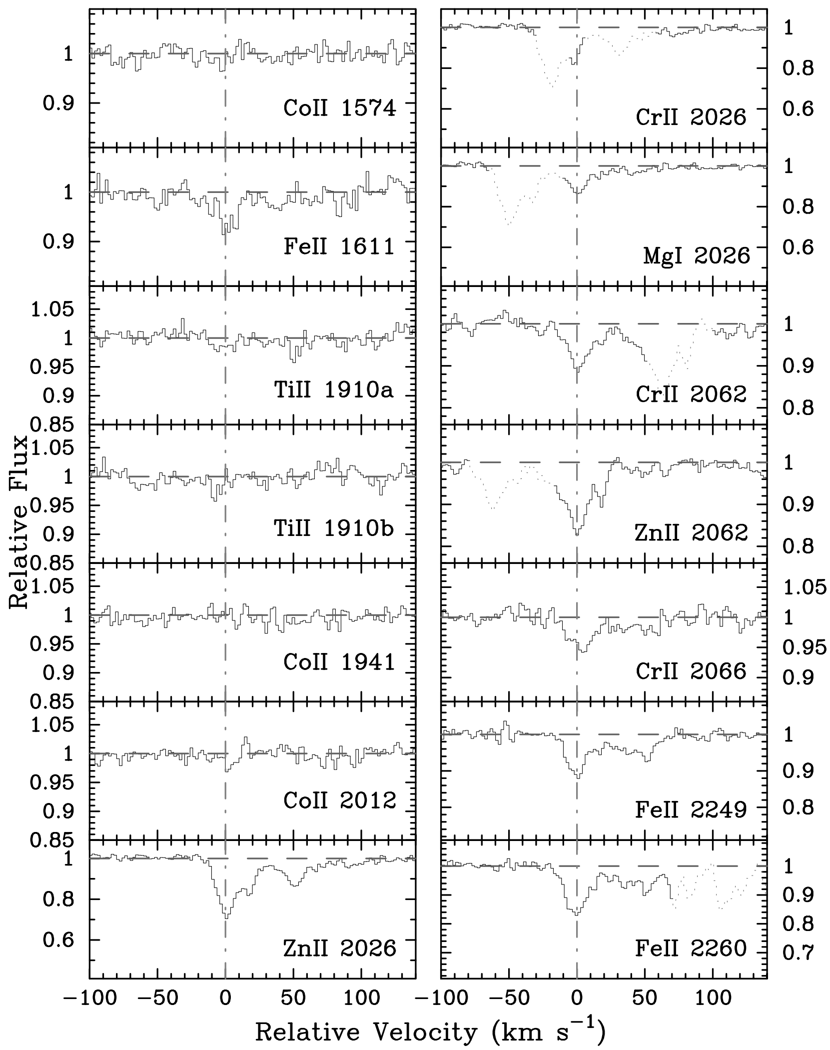

FIG. 25.—Velocity plot of the new metal line transitions for the DLA system at $z = 1.776$ toward Q1331+17. The vertical line at $v = 0$ corresponds to $z = 1.77636$. [*See the electronic edition of the Journal for a color version of this figure.*]

TABLE 26

IONIC COLUMN DENSITIES: Q1331+17, $z = 1.776$

Ion	λ	AODM	$N_{\rm adopt}$	[X/H]
H I........	1215	21.176 ± 0.041	...	...
C I........	1560	13.573 ± 0.013	...	...
C I........	1656	13.312 ± 0.012	...	...
Mg I......	2026	12.419 ± 0.048	...	...
Ti II	1910	11.836 ± 0.118	11.836 ± 0.118	-2.280 ± 0.125
Cr II	2056	12.957 ± 0.017	12.874 ± 0.012	-1.972 ± 0.043
Cr II	2066	12.834 ± 0.034	...	...
Fe II	1608	14.630 ± 0.003	14.618 ± 0.001	-2.058 ± 0.041
Fe II	1611	14.709 ± 0.046	...	...
Fe II	2249	14.595 ± 0.015	...	...
Fe II	2260	14.647 ± 0.010	...	...
Fe II	2344	>14.723	...	...
Fe II	2374	14.616 ± 0.002	...	...
Fe II	2382	>14.461	...	...
Co II......	1574	<12.659	<12.306	<-1.780
Co II......	1941	<12.367	...	...
Co II......	2012	<12.306	...	...
Zn II	2026[a]	12.542 ± 0.029	12.542 ± 0.029	-1.304 ± 0.050

[a] The Zn column density is based on a line profile analysis performed with the VPFIT software package.

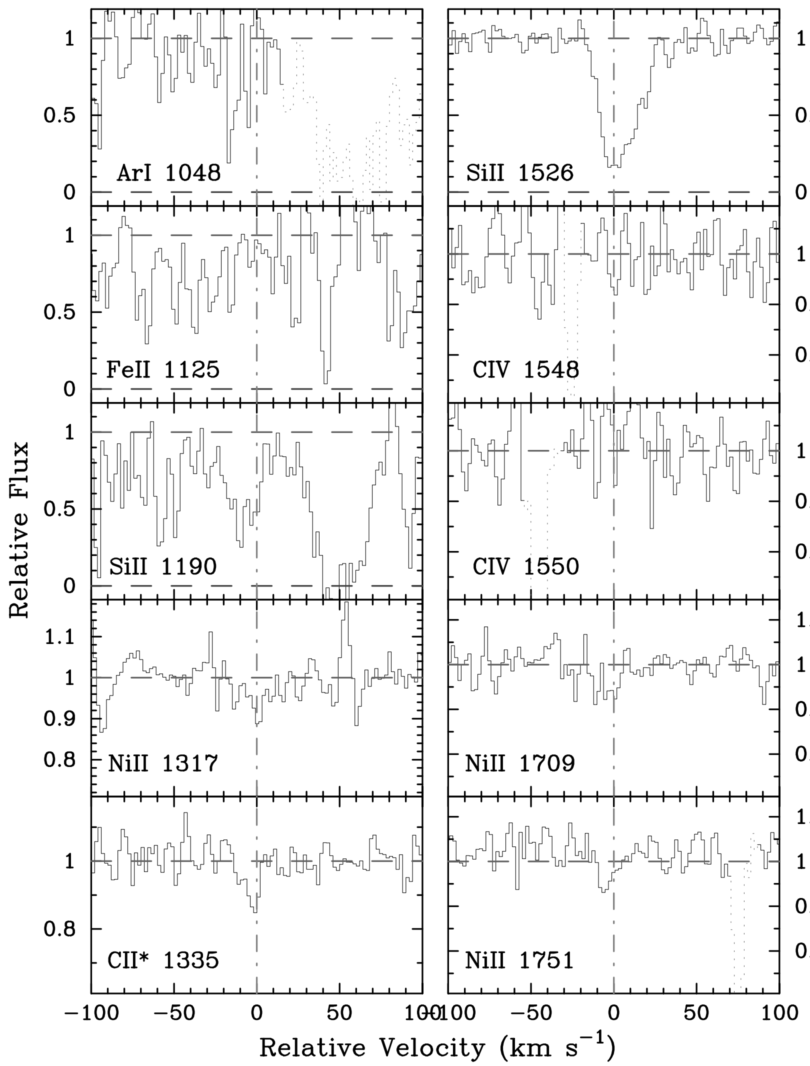

FIG. 26.—Velocity plot of the new metal line transitions for the DLA system at $z = 3.736$ toward BRI 1346−03. The vertical line at $v = 0$ corresponds to $z = 3.73583$. [*See the electronic edition of the Journal for a color version of this figure.*]

TABLE 27

IONIC COLUMN DENSITIES: BRI 1346−03, $z = 3.736$

Ion	λ	AODM	$N_{\rm adopt}$	[X/H]
H I........	1215	20.720 ± 0.100	...	...
C II	1335	12.550 ± 0.113	>14.486	>-2.784
C IV	1548	<12.717	...	...
C IV	1550	<13.146	...	...
O I........	1302	>15.018	>15.019	>-2.571
Si II	1190	13.430 ± 0.122	13.948 ± 0.009	-2.332 ± 0.100
Si II	1304	13.983 ± 0.009	...	...
Si II	1526	13.880 ± 0.026	...	...
Ar I	1048	<13.114	<13.113	<-2.127
Fe II	1125	<14.126	<14.126	<-2.094
Co II......	1574	<13.260	<13.260	<-0.370
Ni II	1317	<12.759	<12.760	<-2.210
Ni II	1370	<12.876	...	...
Ni II	1709	<13.345	...	...
Ni II	1741	<13.284	...	...
Ni II	1751	<13.428	...	...

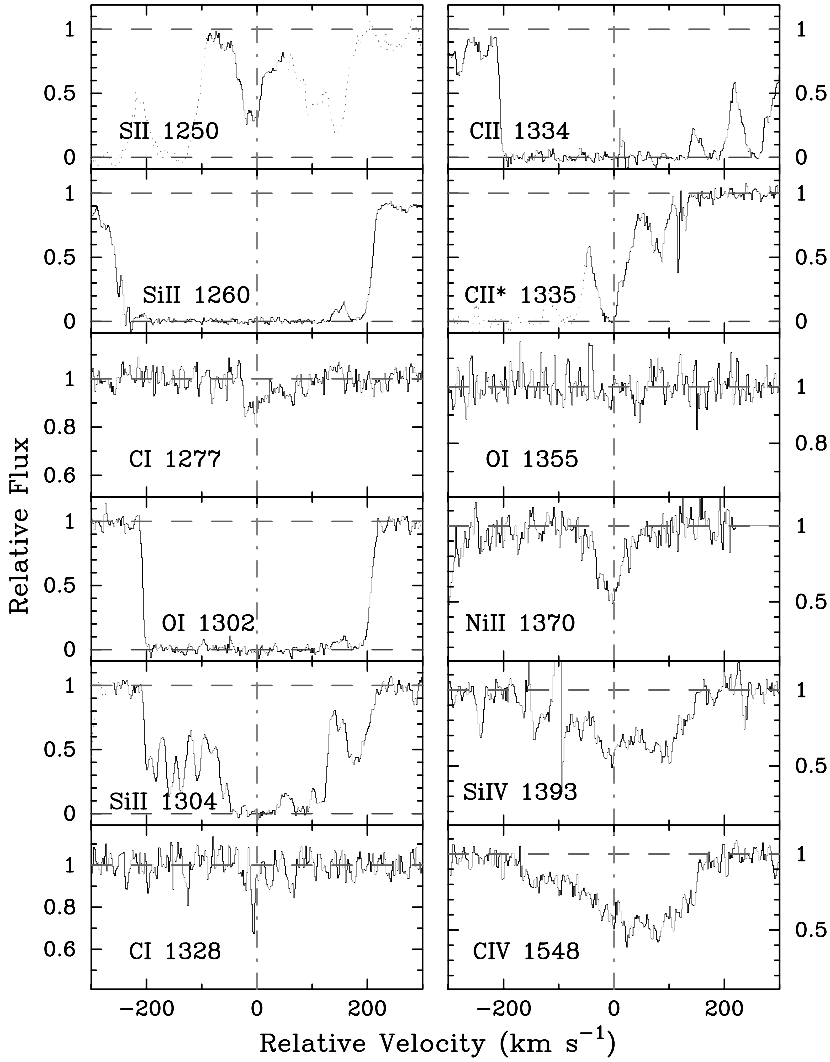

FIG. 27.—Velocity plot of the metal line transitions for the DLA system at $z = 4.224$ toward PSS 1443 + 27. The vertical line at $v = 0$ corresponds to $z = 4.224099$. [*See the electronic edition of the Journal for a color version of this figure.*]

TABLE 28

IONIC COLUMN DENSITIES: PSS 1443+27, $z = 4.224$

Ion	λ	AODM	N_{adopt}	[X/H]
H I........	1215	20.800 ± 0.100	...	...
C I........	1277	13.446 ± 0.037	...	...
C I........	1328	13.367 ± 0.090	...	...
C I........	1656	13.041 ± 0.133	...	...
C II	1334	> 15.613	> 15.612	> -1.738
C II	1335	> 14.709	...	...
C IV	1548	14.245 ± 0.009	...	...
C IV	1550	14.213 ± 0.017	...	...
O I........	1302	> 16.048	> 16.048	> -1.622
O I........	1355	< 17.734	...	...
Al II	1670	> 13.959	> 13.958	> -1.332
Si II.......	1304	> 15.434	> 15.434	> -0.926
Si IV	1393	13.706 ± 0.011	...	...
S II........	1253		...	...
Fe II	1608	> 15.101	15.204 ± 0.056	-1.096 ± 0.115
Fe II	1611	15.204 ± 0.056	...	...
Co II......	1574	< 13.508	< 13.509	< -0.201
Ni II	1370	14.079 ± 0.025	14.091 ± 0.024	-0.959 ± 0.103
Ni II	1709	14.229 ± 0.069	...	...
Ni II	1741	13.877 ± 0.074	...	...

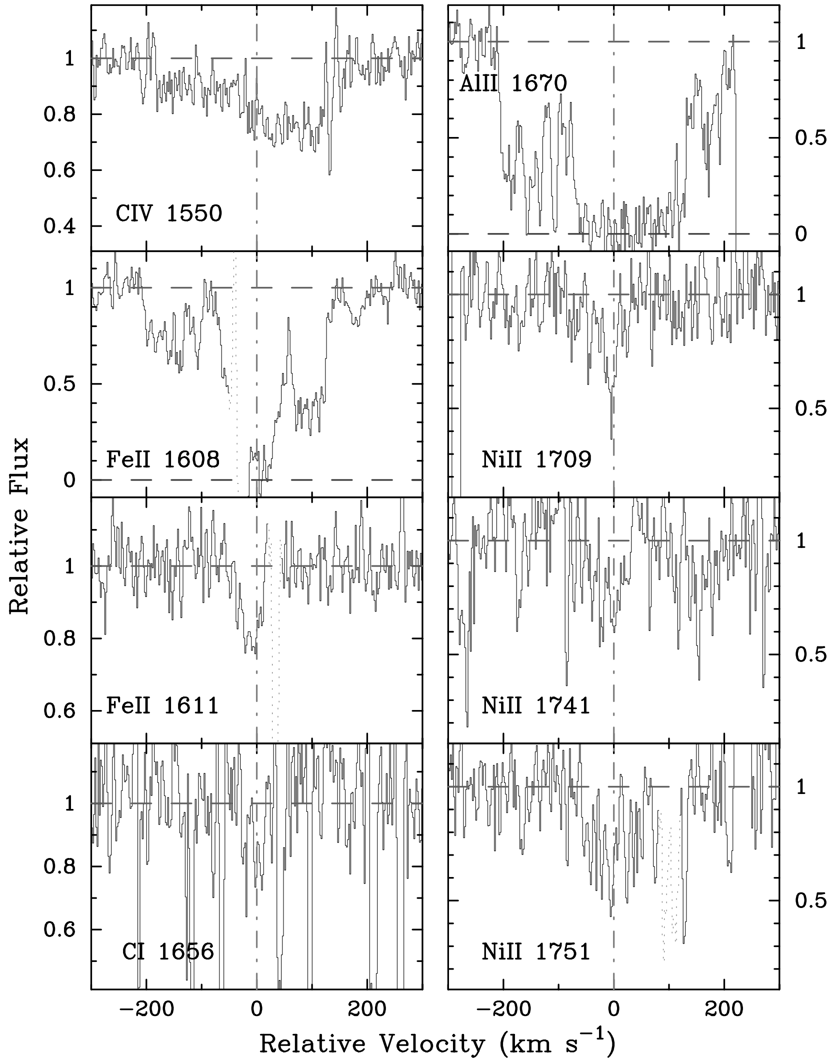

FIG. 27.—*Continued*

damped system. This $N(\mathrm{Zn}^+)$ value is nearly 0.3 dex higher than the value reported in Pettini et al. (1994), however, because we did not correct for possible contamination from the Mg I λ2026 transition. Although a significant feature is apparent at $v = 0$ km s^{-1} of the Mg I λ2026 profile, this feature is perfectly aligned with an absorption feature at $v = 52$ km s^{-1} in the unsaturated Fe II profiles. Furthermore, the $N(\mathrm{Zn}^+)$ value from Zn II λ2062 is identical to the value derived from Zn II λ2026 using the AODM method. We suspect, however, that this is a coincidence resulting from blending between the Zn II λ2062 and Cr II λ2062 profiles. Performing a detailed line profile analysis of the Zn and Cr lines and including Mg I λ2026, we find $\log N(\mathrm{Zn}^+) = 12.542 \pm 0.029$ and $\log N(\mathrm{Mg}^0) = 12.419 \pm 0.048$. We discuss this issue further and its impact on studies of Zn in Paper II, § 2.1.6.

In addition to the large Zn/Fe ratio, this system shows rarely observed C I absorption and a significant subsolar Ti/Fe ratio. Altogether the chemical abundances of this system represent the most compelling evidence for dust depletion in any DLA system. It is particularly important to note, therefore, that it is one of the brightest (apparent magnitude) quasars observed in our sample. In Paper II, § 5 we consider the obscuration of this quasar due to this damped system and the implications for dust obscuration in general.

This DLA system is one of the few cases in which one can derive $N(\mathrm{Fe}^+)$ values from both Fe II $\lambda\lambda$1608 and 1611. Furthermore, our observations also cover several of the Fe II transitions longward of 2000 Å, including Fe II $\lambda\lambda$2249 and 2260, which are the principal diagnostics of Fe^+ in the Galactic ISM. Examining Table 26, one notes that nearly all of the $N(\mathrm{Fe}^+)$ values are consistent at the 2 σ level and all are in accordance at 3 σ. One also notes that N(Fe II λ1611) exceeds all of the other measurements, suggesting that it is unlikely that the Raassen & Uylings (1998) analysis overestimated the Fe II λ1611 oscillator strength, at least relative to the other Fe II transitions.

3.21. *BRI 1346−03*, $z = 3.736$

Our additional observations blueward of the data presented in PW99 provide coverage of a few new transitions (Fig. 26 and Table 27). Unfortunately, we still do not have coverage of a single unsaturated Fe II profile or any other Fe peak metal transition. Therefore, we have adopted Al as a proxy for Fe (i.e., assume [Fe/H] = [Al/H]) and in this

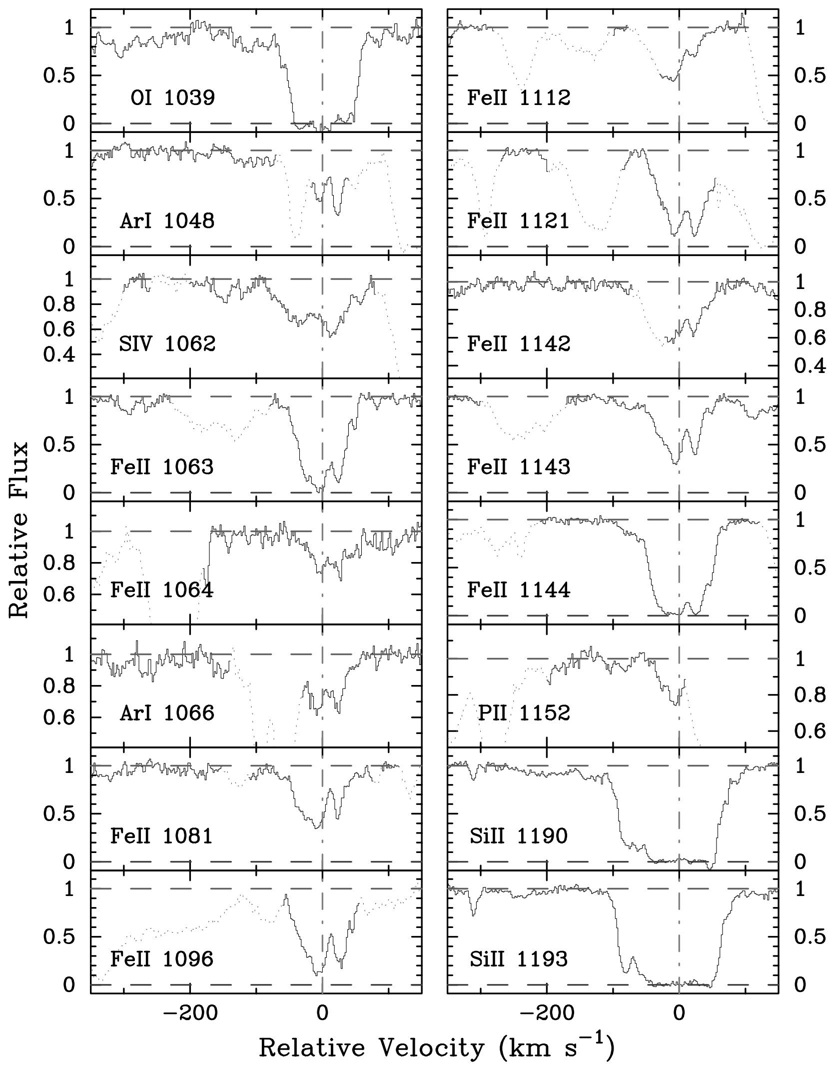

FIG. 28.—Velocity plot of the new metal line transitions for the DLA system at $z = 2.625$ toward Q1759 + 75. The vertical line at $v = 0$ corresponds to $z = 2.62530$. [*See the electronic edition of the Journal for a color version of this figure.*]

TABLE 29

IONIC COLUMN DENSITIES: Q1759+75, $z = 2.625$

Ion	λ	AODM	$N_{\rm adopt}$	[X/H]
H I	1215	20.800 ± 0.100	...	...
C I	1656	< 12.336	...	...
C II	1334	> 15.300	> 15.300	> -2.050
C II	1335	13.138 ± 0.032	...	...
O I	1039	> 16.261	> 16.261	> -1.409
O I	1302	> 15.759	...	...
Si II	1190	> 14.928	15.536 ± 0.008	-0.824 ± 0.100
Si II	1193	> 14.614	...	...
Si II	1260	> 14.396	...	...
Si II	1304	> 15.198	...	...
Si II	1808	15.536 ± 0.008	...	...
P II	1152	> 13.046	> 13.047	> -1.283
S II	1250	15.243 ± 0.009	15.243 ± 0.010	-0.757 ± 0.100
S II	1253	< 15.486	...	...
S II	1259	< 15.335	...	...
Ar I	1048	< 13.714	< 13.714	< -1.606
Ar I	1066	< 14.053	...	...
Fe II	1062	14.860 ± 0.037	15.091 ± 0.004	-1.209 ± 0.100

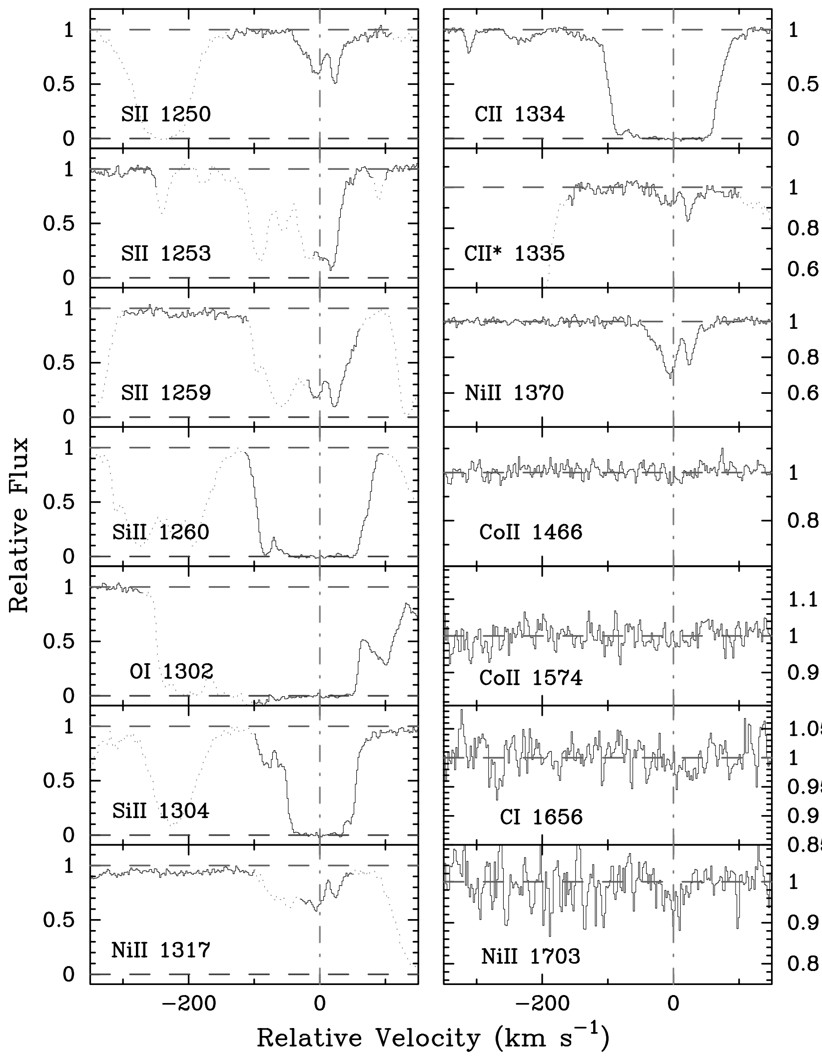

FIG. 28.—*Continued*

TABLE 29—*Continued*

Ion	λ	AODM	$N_{\rm adopt}$	[X/H]
Fe II	1063	>15.002	...	...
Fe II	1063	15.287 ± 0.020	...	...
Fe II	1081	15.182 ± 0.007	...	...
Fe II	1096	15.059 ± 0.007	...	...
Fe II	1112	<15.389	...	...
Fe II	1121	<15.260	...	...
Fe II	1142	<15.565	...	...
Fe II	1143	15.079 ± 0.005	...	...
Fe II	1144	>15.051	...	...
Fe II	1608	>15.077	...	...
Fe II	1611	14.923 ± 0.034	...	...
Co II	1466	<13.066	<13.019	<−0.691
Co II	1466	<13.019	...	...
Co II	1574	<13.108	...	...
Ni II	1317	<14.248	13.802 ± 0.007	−1.248 ± 0.100
Ni II	1370	13.766 ± 0.010	...	...
Ni II	1454	13.791 ± 0.039	...	...
Ni II	1703	<13.908	...	...
Ni II	1709	13.929 ± 0.020	...	...
Ni II	1741	13.841 ± 0.017	...	...
Ni II	1751	13.868 ± 0.021	...	...

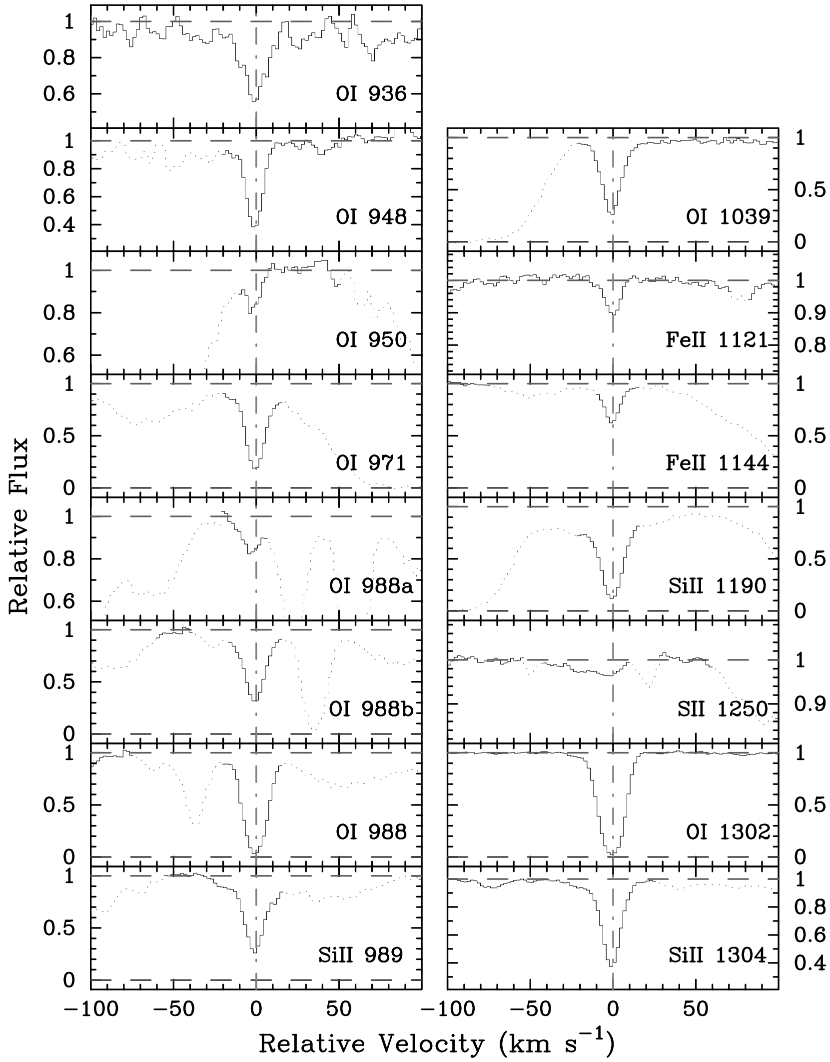

FIG. 29.—Velocity plot of the metal line transitions for the DLA system at $z = 2.844$ toward Q1946+76. The vertical line at $v = 0$ corresponds to $z = 2.8443$. [*See the electronic edition of the Journal for a color version of this figure.*]

manner include the system in the metallicity and relative abundance analyses of Paper II. The implied Si/Fe ratios match typical values. If the feature at $v = 0$ km s^{-1} in the Ni II λ1317 profile is not noise or a coincident metal line, it implies a very large Ni/Al ratio indicating that we might be underestimating $N(\mathrm{Fe}^+)$. For the moment, we consider it as an upper limit.

Our new observations also cover the C IV doublet at 1550

TABLE 30

IONIC COLUMN DENSITIES: Q1946+7658, $z = 2.844$

Ion	λ	AODM	N_{adopt}	[X/H]
H I	1215	20.270 ± 0.060	...	...
O I	936	15.036 ± 0.030	14.819 ± 0.007	−2.321 ± 0.060
O I	948	14.835 ± 0.025	...	...
O I	971	< 14.725	...	...
O I	988	< 15.244	...	...
O I	988	< 14.862	...	...
O I	988	> 14.627	...	...
O I	1039	14.811 ± 0.008	...	...
O I	1302	> 14.587	...	...
Si II	1190	< 13.579	13.602 ± 0.005	−2.228 ± 0.060
Si II	1304	13.602 ± 0.005	...	...
S II	1250	< 13.491	< 13.491	< −1.979
Fe II......	1121	13.241 ± 0.057	13.238 ± 0.009	−2.532 ± 0.061
Fe II......	1144	13.238 ± 0.009	...	...

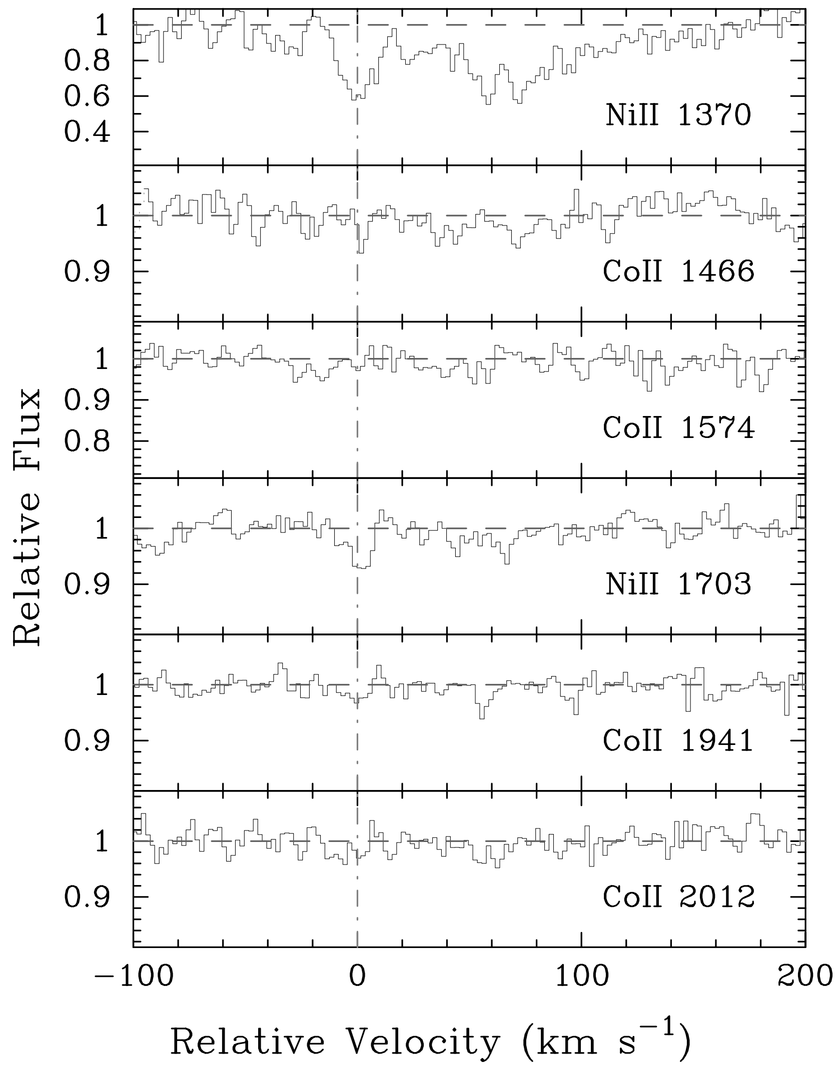

FIG. 30.—Velocity plot of the new metal line transitions for the DLA system at $z = 1.920$ toward Q2206−19. The vertical line at $v = 0$ corresponds to $z = 1.920$. [*See the electronic edition of the Journal for a color version of this figure.*]

TABLE 31

IONIC COLUMN DENSITIES: Q2206−19, $z = 1.920$

Ion	λ	AODM	$N_{\rm adopt}$	[X/H]
H I........	1215	20.653 ± 0.071	...	...
Al II	1670	> 14.070	> 14.070	> −1.073
Si II	1526	> 15.275	15.796 ± 0.005	−0.417 ± 0.071
Si II	1808	15.796 ± 0.005	...	...
Ti II	1910	12.768 ± 0.040	12.768 ± 0.040	−0.825 ± 0.081
Cr II	2056	13.627 ± 0.009	13.638 ± 0.007	−0.685 ± 0.071
Cr II	2066	13.665 ± 0.013	...	...
Fe II	1608	> 15.376	15.296 ± 0.018	−0.857 ± 0.073
Fe II	1611	15.296 ± 0.018	...	...
Co II......	1574	12.960 ± 0.139	12.960 ± 0.140	−0.603 ± 0.157
Co II......	1941	< 12.814	...	...
Co II......	2012	< 12.832	...	...
Ni II	1370	14.154 ± 0.022	14.232 ± 0.005	−0.671 ± 0.071
Ni II	1703	13.807 ± 0.116	...	...
Ni II	1709	14.221 ± 0.009	...	...
Ni II	1741	14.239 ± 0.006	...	...
Ni II	1751	14.266 ± 0.010	...	...
Zn II	2026	12.914 ± 0.009	12.914 ± 0.009	−0.409 ± 0.072

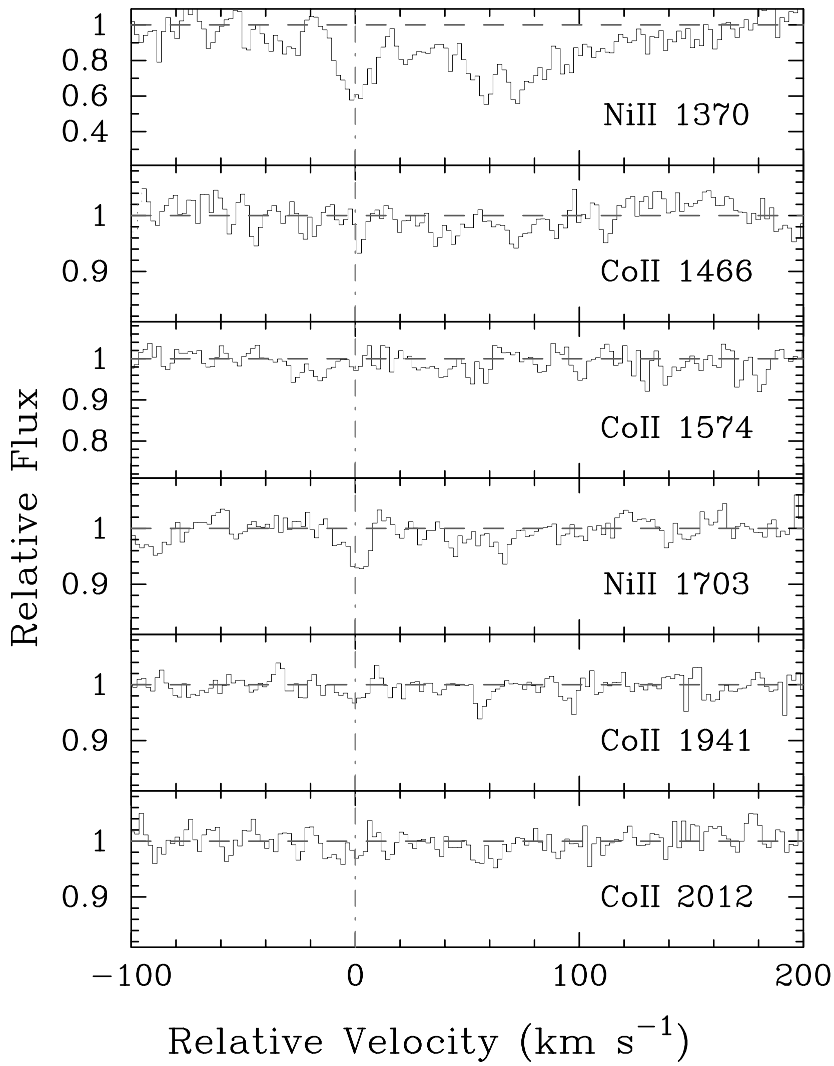

FIG. 31.—Velocity plot of the new metal line transitions for the DLA system at $z = 2.076$ toward Q2206−19. The vertical line at $v = 0$ corresponds to $z = 2.07623$. [*See the electronic edition of the Journal for a color version of this figure.*]

TABLE 32

IONIC COLUMN DENSITIES: Q2206−19, $z = 2.076$

Ion	λ	AODM	$N_{\rm adopt}$	[X/H]
H I	1215	20.431 ± 0.060	...	...
C II	1334	>14.207	>14.207	>-2.774
C II	1335	<13.157	...	...
C IV	1548	13.707 ± 0.005	...	...
C IV	1550	13.739 ± 0.008	...	...
O I	1302	>14.540	>14.540	>-2.761
Al II	1670	12.158 ± 0.012	12.158 ± 0.012	-2.763 ± 0.061
Al III......	1854	11.515 ± 0.098	...	...
Al III......	1862	11.719 ± 0.103	...	...
Si II.......	1304	13.682 ± 0.035	13.682 ± 0.035	-2.309 ± 0.069
Si IV	1402	12.845 ± 0.016	...	...
Cr II	2056	<11.911	<11.911	<-2.190
Cr II	2062	<12.158	...	...
Fe II	1608	13.325 ± 0.017	13.325 ± 0.017	-2.606 ± 0.062
Fe II	1611	<13.948	...	...
Ni II	1709	<12.585	<12.585	<-2.096
Ni II	1751	<12.591	...	...
Zn II......	2026	<11.199	<11.199	<-1.902

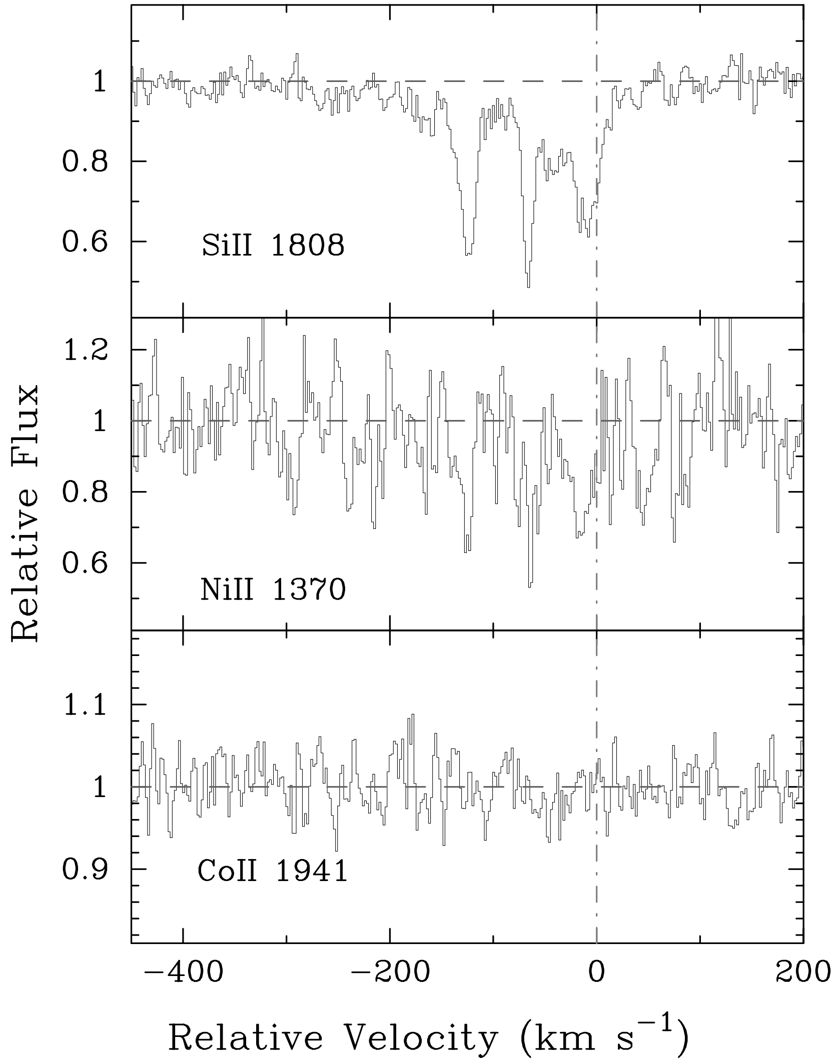

FIG. 32.—Velocity plot of C II* λ1335 transition for the DLA system at $z = 1.864$ toward Q2230+02. For comparison, we plot the Si II λ1304 and C II λ1334 profiles. The vertical line at $v = 0$ corresponds to $z = 1.864388$. [*See the electronic edition of the Journal for a color version of this figure.*]

Å. Although the spectra are particularly noisy over this region, there is no obvious C IV absorption. This marks the first DLA system with no detectable C IV absorption, and we note in passing a possible trend of weaker C IV absorption at $z > 3$.

3.22. *PSS 1443+27*, $z = 4.224$

This $z > 4$ DLA system was discovered by Storrie-Lombardi & Wolfe (2000), who determined the N(H I) value from a spectrum obtained using LRIS at Keck observatories. Its very high metallicity was first reported in Pro-

TABLE 33

IONIC COLUMN DENSITIES: Q2230+02, $z = 1.864$

Ion	λ	AODM	$N_{\rm adopt}$	[X/H]
H I........	1215	20.850 ± 0.084	…	…
Fe II	1608	> 15.160	15.184 ± 0.016	-1.166 ± 0.086
Fe II	1611	15.148 ± 0.084	…	…
Fe II	2249	15.119 ± 0.036	…	…
Fe II	2260	15.210 ± 0.019	…	…
Fe II	2344	> 15.039	…	…
Fe II	2374	> 15.213	…	…
Fe II	2382	> 14.744	…	…
Co II......	1941	< 13.118	< 13.118	< -0.642
Ni II	1370	14.161 ± 0.052	14.128 ± 0.011	-0.972 ± 0.085
Ni II	1709	14.171 ± 0.014	…	…
Ni II	1741	14.097 ± 0.023	…	…
Ni II	1751	14.049 ± 0.028	…	…

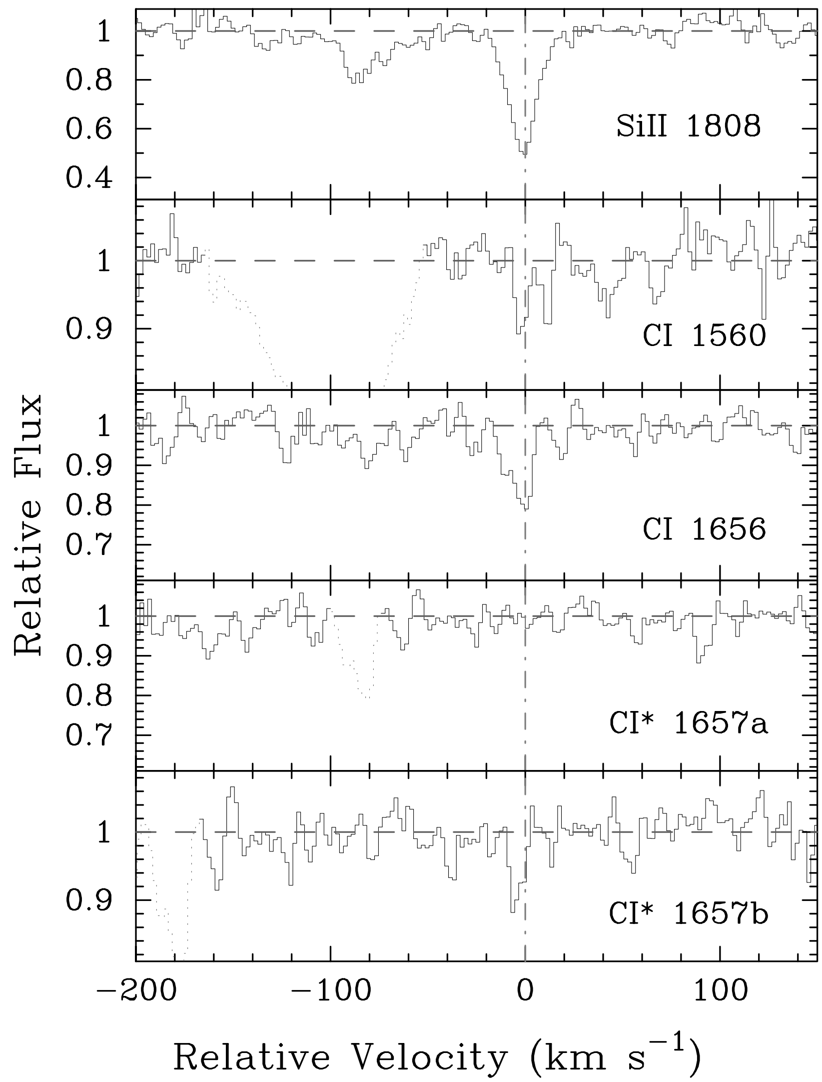

FIG. 33.—Velocity plot of the new metal line transitions for the DLA system at $z = 2.066$ toward Q2231−00. For comparison, we also plot the Si II λ1808 profile. The vertical line at $v = 0$ corresponds to $z = 2.066150$. [*See the electronic edition of the Journal for a color version of this figure.*]

chaska & Wolfe (2000). We have since acquired further observations of this system that confirm the [Fe/H] metallicity. In particular, we observed the Ni II $\lambda\lambda$1370, 1709, and 1741 transitions at reasonably high S/N and found [Ni/H] $\approx$ [Fe/H]. Figure 27 presents the transitions observed for this system, and the ionic column densities are presented in Table 28.

In passing, we note the remarkable C II* λ1335 profile, which is heavily saturated and suggests a large star formation rate for this system (Wolfe et al. 2001). In addition, we identify possible absorption from two C I profiles, which we expect is not due to coincident metal line systems. Unfortunately, our observations did not cover the stronger C II λ1556 profile, and the strongest C I λ1656 profile is located within a forest of sky lines.

3.23. *Q1759+75*, $z = 2.625$

This system was presented in PW99 and has been subsequently analyzed by Outram, Chaffee, & Carswell (1999). Here we present an analysis of our spectrum blueward of Lyα emission. Figure 28 presents the transitions and Table 29 the column densities.

TABLE 34

IONIC COLUMN DENSITIES: Q2231−002, $z = 2.066$

Ion	λ	AODM	$N_{\rm adopt}$	[X/H]
H I........	1215	20.560 ± 0.100	...	...
C I........	1656	12.701 ± 0.035	...	...
C I........	1657	12.662 ± 0.108	...	...
Co II......	1941	< 12.816	< 12.816	< −0.654

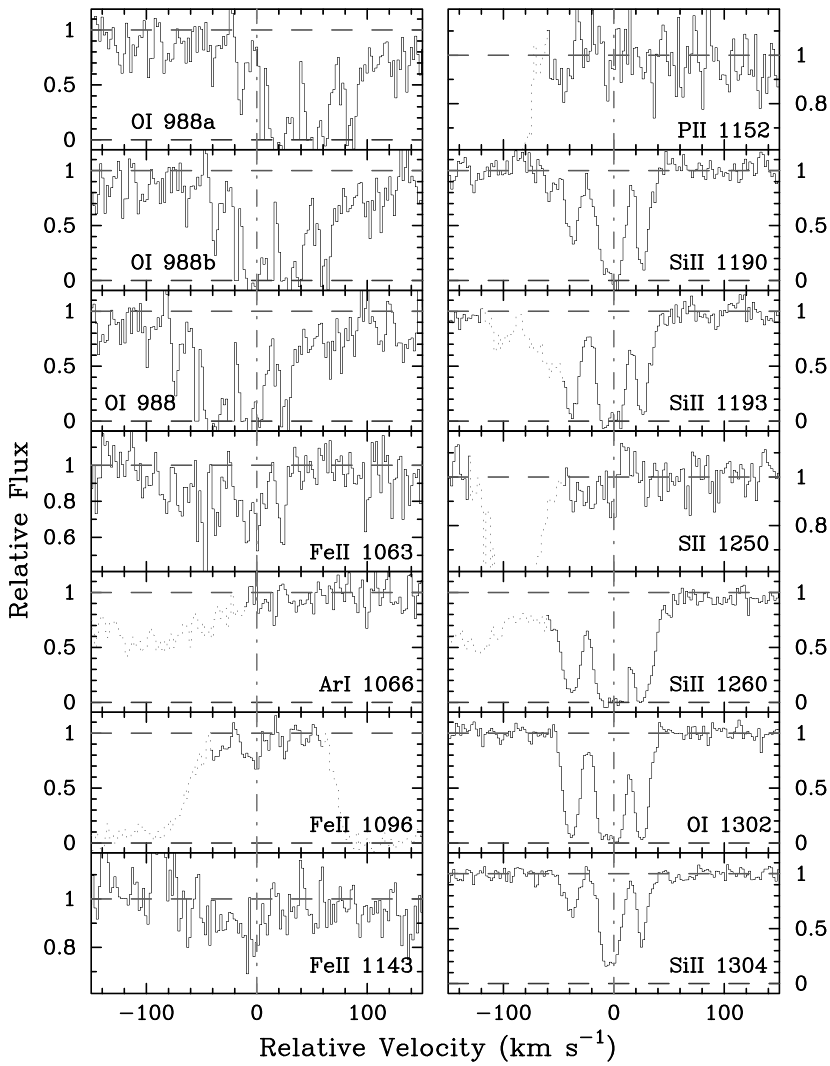

FIG. 34.—Velocity plot of the metal line transitions for the DLA system at $z = 2.538$ toward Q2344 + 12. The vertical line at $v = 0$ corresponds to $z = 2.53790$. [*See the electronic edition of the Journal for a color version of this figure.*]

TABLE 35

IONIC COLUMN DENSITIES: Q2344+12, $z = 2.538$

Ion	λ	AODM	$N_{\rm adopt}$	[X/H]
H I	1215	20.360 ± 0.100	...	...
C II	1334	>14.646	>14.645	>-2.265
C II	1335	<12.831	...	...
O I	988	>15.031	>15.031	>-2.199
O I	1302	>15.020	...	...
O I	1355	<17.814	...	...
Si II	1190	>14.131	14.179 ± 0.012	-1.741 ± 0.101
Si II	1193	>14.007	...	...
Si II	1260	>13.838	...	...
Si II	1304	14.179 ± 0.012	...	...
Si IV......	1393	12.569 ± 0.087	...	...
P II	1152	<12.744	<12.744	<-1.146
S II	1250	<14.201	<14.201	<-1.359
Ar I	1066	<13.262	<13.262	<-1.618
Fe II......	1063	14.021 ± 0.046	14.030 ± 0.032	-1.830 ± 0.105
Fe II......	1096	14.007 ± 0.053	...	...
Fe II......	1143	14.147 ± 0.077	...	...
Ni II......	1317	<12.814	<12.814	<-1.796
Ni II......	1370	<12.999	...	...

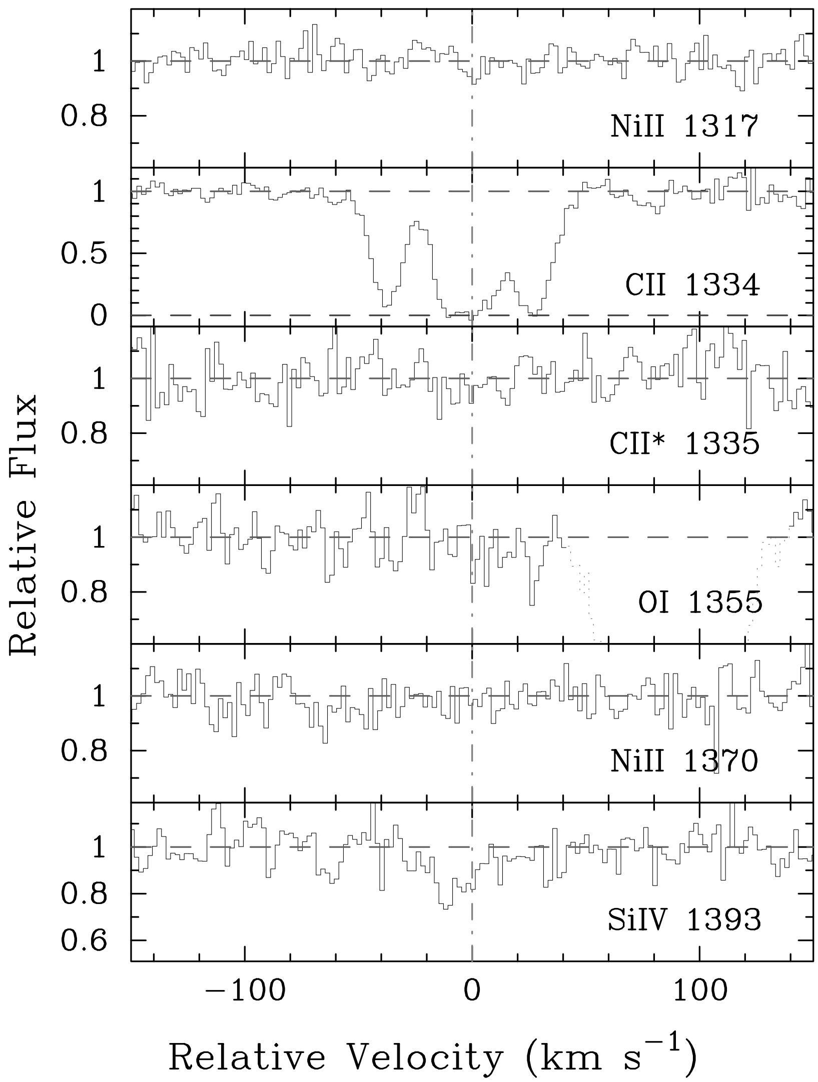

FIG. 34.—*Continued*

Our observations present measurements of a number of lines in the Lyα forest. In particular, we have excellent coverage of the far-ultraviolet (FUV) Fe II transitions, good measurements of the N I triplets at 1134 and 1200 Å, moderate limits on Ar I and O I, and an excellent measurement of $N(S^+)$. Regarding the Fe II lines, we find very good agreement between the many transitions, which confirms the f-values measured by Howk et al. (2000). The only exception is Fe II λ1062 (not analyzed by Howk et al. 2000), whose f-value appears to be systematically high. We recommend using a value $\approx$0.2 dex below the value reported by Morton (1991). Finally, we point out significant absorption at $v \approx -300$ km s^{-1} in the Si II $\lambda\lambda$1190 and 1193 transitions, which coincide with a strong feature in C IV and a weaker feature in Al II λ1670 (PW99). We suspect that this metal line system corresponds to a nearby Lyman limit system although there is no significant evidence for asymmetry in the Lyα profile.

3.24. *Q1946+76*, $z = 2.844$

Kirkman & Tytler (1997) analyzed this very high S/N spectrum of Q1946+76 to describe the Lyα forest at $z \sim 2.8$. Here we analyze the metal line transitions for the system at $z = 2.844$, ignoring the probably DLA system at $z = 1.73$ because we have no measure of its H I column density. Figure 29 presents the metal line profiles for the $z = 2.844$ system, and Table 30 summarizes the column density measurements. For the H I column density we adopt the value presented in L96. This system is notable for providing one of the few cases in which one can accurately determine $N(O^0)$. The observed O/Fe ratio is enhanced relative to solar, but at a lower level than metal-poor halo stars with comparable metallicity. Interestingly, the implied O/Si ratio is subsolar, which is almost never observed in metal-poor stars. Nevertheless, we believe that the $N(O^0)$ value is accurate. In a separate paper we examine the N/O ratio of this system.

3.25. *Q2206−19*, $z = 1.920$ *and* 2.076

In Figures 30 and 31 we show a number of transitions left unanalyzed by Prochaska & Wolfe (1997) and PW99 for the two DLA systems toward Q2206−19. Furthermore, we now consider only ionic column densities measured with the AODM in order to coincide with the rest of the data-

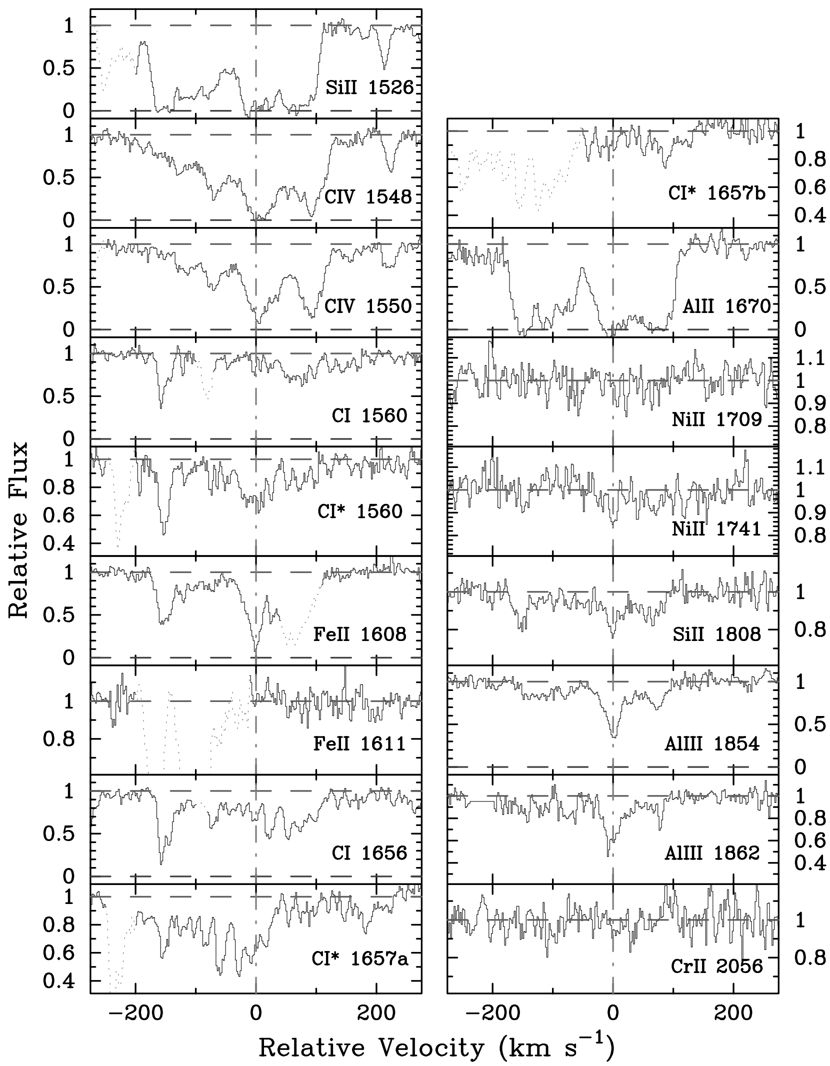

FIG. 35.—Velocity plot of the metal line transitions for the DLA system at $z = 2.426$ toward Q2348−01. The vertical line at $v = 0$ corresponds to $z = 2.426301$. [*See the electronic edition of the Journal for a color version of this figure.*]

base. As we showed in Prochaska & Wolfe (1997), there is very little difference between the abundances derived from a Voigt profile analysis and those from the AODM. All of the values are listed in Tables 31 and 32.

3.26. *Q2230+02*, $z = 1.864$

This system was extensively analyzed in PW99. We simply add a limit on $N(\mathrm{Co}^+)$ from the Co II λ1941 transition and a measurement for Ni II λ1370 (Fig. 32 and Table

TABLE 36
IONIC COLUMN DENSITIES: Q2348−01, $z = 2.426$

Ion	λ	AODM	$N_{\rm adopt}$	[X/H]
H I	1215	20.500 ± 0.100	...	...
C IV	1548	>14.705	...	...
C IV	1550	14.767 ± 0.008	...	...
Al II	1670	>13.939	>13.939	> −1.051
Al III......	1854	13.379 ± 0.011	...	...
Al III......	1862	13.515 ± 0.021	...	...
Si II	1526	>15.160	15.365 ± 0.022	−0.695 ± 0.102
Si II	1808	15.365 ± 0.022	...	...
Cr II	2056	<12.713	<12.713	< −1.457
Fe II	1608	14.614 ± 0.012	14.614 ± 0.012	−1.386 ± 0.101
Ni II	1709	13.434 ± 0.109	13.350 ± 0.104	−1.400 ± 0.144
Ni II	1741	13.350 ± 0.104	...	...

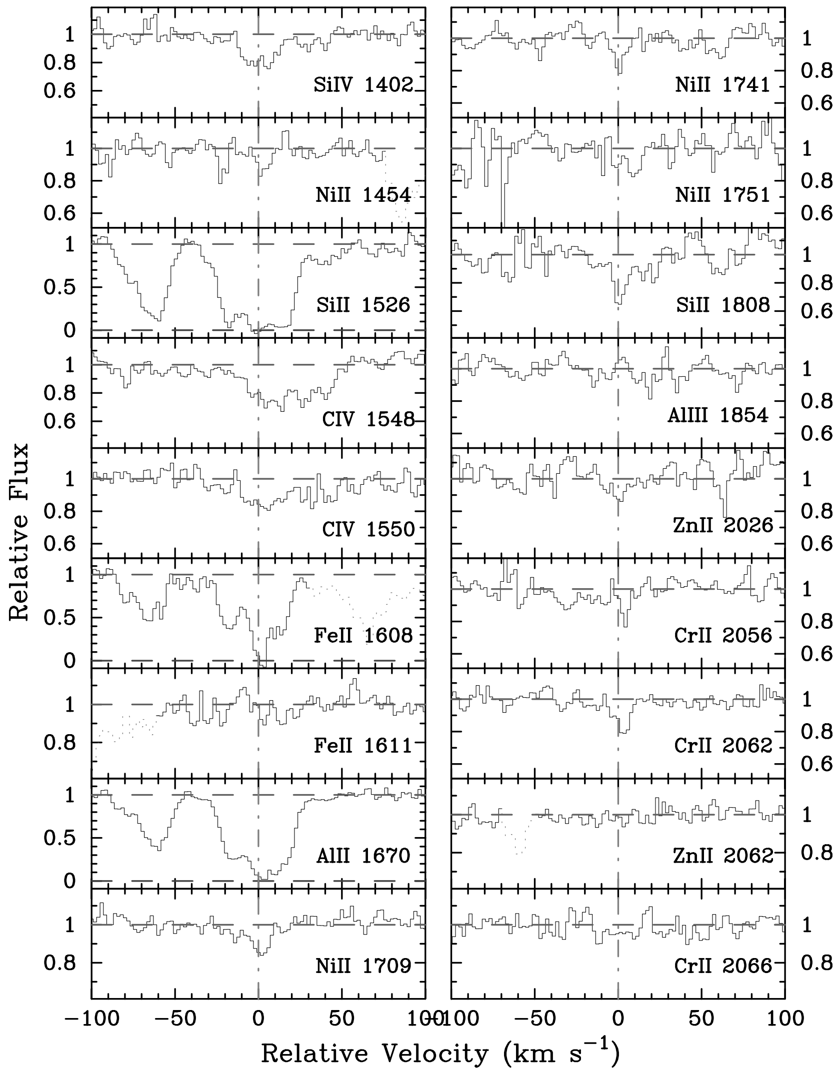

FIG. 36.—Velocity plot of the metal line transitions for the DLA system at $z = 2.615$ toward Q2348−01. The vertical line at $v = 0$ corresponds to $z = 2.614714$. [*See the electronic edition of the Journal for a color version of this figure.*]

TABLE 37

IONIC COLUMN DENSITIES: Q2348−01, $z = 2.615$

Ion	λ	AODM	$N_{\rm adopt}$	[X/H]
H I	1215	21.300 ± 0.100	...	...
C IV	1548	13.291 ± 0.024	...	...
C IV	1550	13.336 ± 0.046	...	...
Al II	1670	> 13.139	> 13.139	> −2.651
Al III......	1854	< 12.203	...	...
Si II	1526	> 14.562	14.892 ± 0.072	−1.968 ± 0.123
Si II	1808	14.892 ± 0.072	...	...
Si IV	1402	12.899 ± 0.051	...	...
Cr II	2056	12.619 ± 0.100	12.674 ± 0.060	−2.296 ± 0.117
Cr II	2062	12.718 ± 0.075	...	...
Fe II	1608	> 14.483	14.573 ± 0.088	−2.227 ± 0.133
Fe II	1611	< 14.663	...	...
Ni II	1454	13.121 ± 0.110	13.193 ± 0.074	−2.357 ± 0.124
Ni II	1709	13.296 ± 0.097	...	...
Ni II	1741	< 13.100	...	...
Zn II......	2026	< 11.871	< 11.871	< −2.099

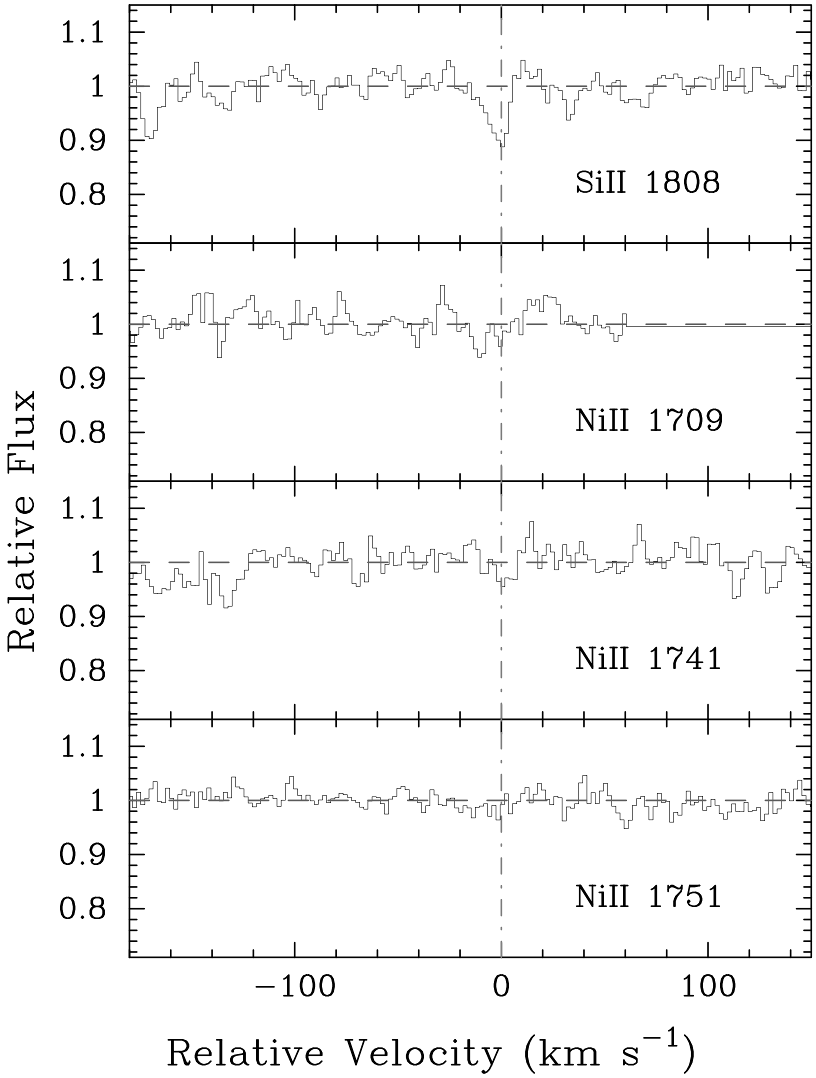

FIG. 37.—Velocity plot of the new metal line transitions for the DLA system at $z = 2.066$ toward Q2348−14. For comparison, we also plot the Si II λ1808 profile. The vertical line at $v = 0$ corresponds to $z = 2.066150$. [*See the electronic edition of the Journal for a color version of this figure.*]

33). We also include the new values for $N(\mathrm{Fe}^+)$ as the extensive wavelength coverage provides a comparison between the Fe II $\lambda\lambda$1611, 2249, and 2260 transitions. All three values are in good agreement, which indicates that the relative *f*-values are reasonably accurate.

3.27. *Q2231−00*, $z = 2.066$

This damped system was analyzed in PW99. At the time we considered possible absorption from the C I λ1656 and C I* λ1657 transitions but were unconvinced that the profiles were associated with the DLA system. Figure 33 presents the two transitions and the Si II λ1808 profile for comparison, and Table 34 presents the column densities. We are now reasonably confident that these profiles arise in the DLA system and their relative strengths place constraints on the temperature of the cosmic microwave background (CMB) at this redshift (J. X. Prochaska, J. M. O'Meara, & A. M. Wolfe 2001, in preparation).

3.28. *Q2344+12*, $z = 2.538$

This system has been observed previously by Lu, Sargent, & Barlow (1997), and they presented an [Fe/H] metallicity

TABLE 38

IONIC COLUMN DENSITIES: Q2348−14, $z = 2.279$

Ion	λ	AODM	N_{adopt}	[X/H]
H I	1215	20.560 ± 0.075	...	...
Ni II	1709	<12.752	<12.583	<-2.227
Ni II	1741	<12.583	...	...
Ni II	1751	<12.704	...	...

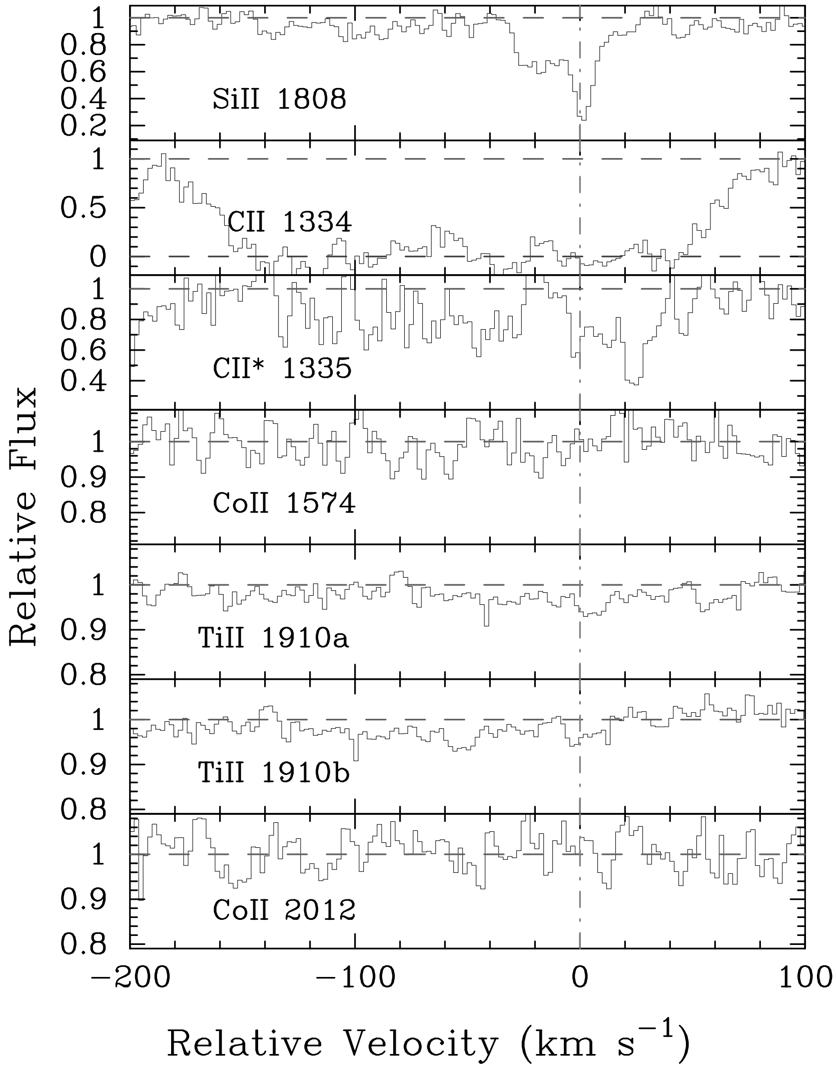

FIG. 38.—Velocity plot of the new metal line transitions for the DLA system at $z = 2.095$ toward Q2359−02. For comparison, we also plot the Si II λ1808 profile. The vertical line at $v = 0$ corresponds to $z = 2.095067$. [*See the electronic edition of the Journal for a color version of this figure.*]

and an N(H I) value. We adopt their measurement of the H I column density and have an independent measurement of $N(\mathrm{Fe}^+)$ from several FUV Fe II transitions. In addition, our blue spectra cover a number of transitions in the Lyα forest (Fig. 34 and Table 35).

3.29. *Q2348−01, z = 2.426 and 2.615*

The two damped systems along this sight line were first identified by Turnshek et al. (1989) and are both part of the LBQS statistical sample. This quasar is very faint, and the S/N of our 4.5 hr spectrum is relatively poor. Figures 35 and 36 and Tables 36 and 37 present the transitions and column densities for the two systems. With respect to the system at $z = 2.426$, the Fe II λ1608 profile is blended at $v > 40$ km s^{-1} and we estimate the $N(\mathrm{Fe}^+)$ value by integrating this profile at $v < 40$ km s^{-1}. Therefore, the value is strictly a lower limit, although the Fe II λ1611 indicates that the column density at $v > 40$ km s^{-1} is less than $10^{14.46}$ cm^{-2}. The system at $z = 2.426$ is special for showing absorption from C I and C I*. In a companion paper we analyze these

TABLE 39

IONIC COLUMN DENSITIES: Q2359−02, $z = 2.095$

Ion	λ	AODM	N_{adopt}	[X/H]
H I........	1215	20.700±0.100	...	...
C II	1334	>15.147	>15.147	>−2.103
C II	1335	13.704±0.061	...	...
Ti II	1910	12.330±0.055	12.330±0.055	−1.310±0.114
Co II......	1574	<<13.398	<12.828	<−0.782
Co II......	2012	<12.828	...	...

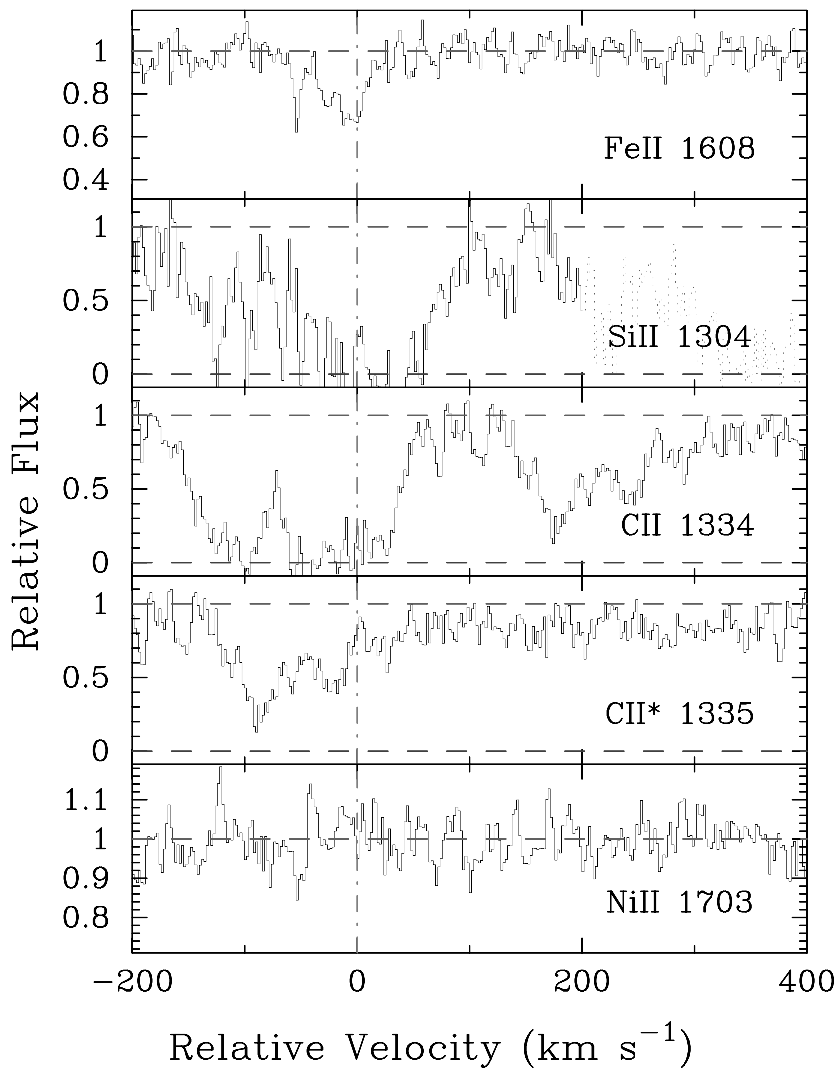

FIG. 39.—Velocity plot of the new metal line transitions for the DLA system at $z = 2.154$ toward Q2359−02. For comparison, we also plot the Fe II λ1608 profile. The vertical line at $v = 0$ corresponds to $z = 2.153934$. [*See the electronic edition of the Journal for a color version of this figure.*]

transitions to place a limit on the temperature of the CMB radiation at $z = 2.4$ (J. X. Prochaska, J. M. O'Meara, & A. M. Wolfe 2001, in preparation). The system at $z = 2.615$ is notable for exhibiting a very low metallicity ([Fe/H] ~ -2.2, [Ni/H] ~ -2.5). In fact, this is the only system with N(H I) $> 10^{21}$ cm^{-2}, which also has a metallicity less than 1/100 solar. For the Fe$^+$ column density, we have averaged the lower and upper limits established by Fe II $\lambda\lambda$1608 and 1611, respectively.

3.30. *Q2348−14*, $z = 2.279$

The abundances for this damped system were first measured by Pettini, Lipman, & Hunstead (1995) and subsequently by PW99. We now include a limit on N(Ni$^+$) from the nondetection of two Ni II transitions (Fig. 37 and Table 38).

3.31. *Q2359−02*, $z = 2.095$ *and* 2.154

Although these two systems were analyzed in PW99, we have now identified several new profiles including measurements for C II* λ1335 for the two systems. The C II* column density for the $z = 2.154$ is very high and, as we discuss in Wolfe et al. (2001), may indicate a high star formation rate in this DLA system. The C II* profile is within the Lyα forest, however, and may be significantly blended with an

TABLE 40

IONIC COLUMN DENSITIES: Q2359−02, $z = 2.154$

Ion	λ	AODM	$N_{\rm adopt}$	[X/H]
H I	1215	20.300 ± 0.100	...	...
C II.......	1334	> 14.991	> 14.991	> −1.859
C II.......	1335	14.475 ± 0.020	...	...
Si II	1304	> 15.098	14.277 ± 0.015	−1.583 ± 0.101
Ni II......	1703	< 14.171	< 13.208	< −1.342

TABLE 41

Abundance Summary

Name	z_{abs}	N(H I)	[C/H]	[O/H]	[Al/H]	[Si/H]	[P/H]	[S/H]	[Ar/H]	[Ti/H]	[Cr/H]	[Fe/H]	[Co/H]	[Ni/H]	[Zn/H]
Q0000−2619	3.390	21.41	...	...	...	−1.884	...	...	...	...	...	−2.160	...	−2.295	...
BR 0019−15	3.439	20.92	...	...	...	−1.057	...	...	...	...	...	> −1.631	...	−1.487	...
PH 957..............	2.309	21.40	...	< −0.596	...	> −2.241	...	...	...	< −2.133	−1.686	−1.929	< −1.146	−1.778	−1.623
Q0149+33..........	2.141	20.50	> −2.406	< 0.428	> −2.017	−1.488	...	...	...	< −1.271	−1.450	−1.770	...	−1.581	−1.674
Q0201+36..........	2.463	20.38	...	...	> −0.737	−0.406	...	...	...	< −1.124	−0.802	−0.870	< −0.333	−0.608	−0.286
J0255+00...........	3.253	20.70	...	...	> −1.311	−0.937	...	...	...	< −0.835	...	−1.436	< −0.352	−1.342	...
J0255+00...........	3.915	21.30	> −3.118	> −3.003	...	> −2.667	...	−1.779	...	...	...	−2.050	< −0.998	−2.279	...
Q0336−01..........	3.062	21.20	> −2.792	> −1.130	...	> −1.619	−1.597	−1.406	−1.374	...	...	−1.795	...	−1.981	...
Q0347−38..........	3.025	20.80	> −2.285	> −1.717	> −1.882	−1.343	...	< −1.240	−1.038	...	...	−1.797	< −0.514	−1.667	...
Q0458−02..........	2.040	21.65	...	> −3.110	> −2.377	> −1.167	...	...	...	< −2.095	−1.501	−1.767	< −1.467	−1.719	−1.186
HS 0741+4741.....	3.017	20.48	> −2.166	> −1.639	−2.146	−1.686	< −1.930	−1.680	−1.834	...	...	−1.928	< −0.432	−1.972	...
Q0836+11..........	2.465	20.58	> −2.104	> −1.965	...	−1.153	...	< −1.120	...	< −0.982	< −1.352	−1.403	< −0.107	−1.442	< −1.131
Q0841+12..........	2.375	20.95	...	...	> −2.105	−1.271	...	...	...	...	−1.548	...	< −0.870	−1.677	−1.507
Q0841+12..........	2.476	20.78	...	...	> −2.054	> −1.845	...	...	...	< −1.562	−1.608	−1.750	< −0.964	−1.675	−1.401
BRI 0951−04	3.857	20.60	...	...	−1.814	> −1.535	...	...	...	...	...	−1.997	< 0.087	< −1.873	...
BRI 0951−04	4.203	20.40	...	> −2.674		−2.618	...	...	...	...	...	< −2.591	...	−1.730	...
BRI 0952−01	4.024	20.55	> −1.788	...	...	...	...	...	...	...	...	−1.863	< 0.290	< −1.361	...
PSS 0957+33	3.279	20.32	...	...	> −1.488	−1.000	...	...	...	...	...	−1.453	< 0.055	−1.252	< −0.863
PSS 0957+33	4.178	20.50	...	> −2.026	> −1.734	−1.504	...	−1.308	...	...	...	−1.871	< 0.238	< −1.840	...
BRI 1108−07	3.608	20.50	> −2.375	> −2.497	−2.168	−1.798	...	...	...	...	...	−2.116	...	< −1.614	...
Q1210+17..........	1.892	20.60	...	...	> −1.650	−0.875	...	...	...	...	−1.027	−1.149	< −0.782	−1.218	−0.900
Q1215+33..........	1.999	20.95	> −2.870	> −2.693	> −2.039	−1.480	...	...	...	...	−1.516	−1.702	< −1.000	−1.606	−1.290
Q1223+17..........	2.466	21.50	> −2.895	> −2.893	...	−1.592	< −1.147	...	...	< −2.188	−1.677	−1.843	< −1.779	−1.801	−1.620
Q1331+17..........	1.776	21.18	...	...	> −1.927	−1.451	...	...	...	−2.280	−1.972	−2.058	< −1.780	−1.890	−1.304
BRI 1346−03	3.736	20.72	> −2.784	> −2.571	−2.634	−2.332	...	...	< −2.127	...	...	< −2.094	< −0.370	< −2.210	...
PSS 1443+27	4.224	20.80	> −1.738	> −1.622	> −1.332	> −0.926	...	...	...	...	...	−1.096	< −0.201	−0.959	...
Q1759+75..........	2.625	20.80	> −2.050	> −1.409	...	−0.824	> −1.283	−0.757	< −1.606	...	−1.259	−1.209	< −0.691	−1.248	> −1.782
Q1946+7658	2.844	20.27	...	−2.321	...	−2.228	...	< −1.979	...	...	...	−2.532	...	...	...
Q2206−19..........	1.920	20.65	...	...	> −1.073	−0.417	...	...	...	−0.825	−0.685	−0.857	−0.603	−0.671	−0.409
Q2206−19..........	2.076	20.43	> −2.774	> −2.761	−2.763	−2.309	...	...	...	...	< −2.190	−2.606	...	< −2.096	< −1.902
Q2230+02..........	1.864	20.85	...	...	...	−0.754	...	...	...	−1.175	−1.117	−1.166	< −0.642	−0.972	−0.720
Q2231−002	2.066	20.56	...	> −1.877	...	−0.873	...	...	...	−1.022	−1.065	−1.402	< −0.654	−1.206	−0.882
Q2344+12..........	2.538	20.36	> −2.265	> −2.199	...	−1.741	< −1.146	< −1.359	< −1.618	...	...	−1.830	...	< −1.796	...
Q2348−01..........	2.426	20.50	...	...	> −1.051	−0.695	...	...	...	...	< −1.457	−1.386	...	−1.400	...
Q2348−01..........	2.615	21.30	...	...	> −2.651	−1.968	...	...	...	...	−2.296	−2.227	...	−2.357	< −2.099
Q2348−14..........	2.279	20.56	> −2.459	> −2.581	−2.393	−1.917	...	−2.035	...	...	...	−2.238	...	< −2.227	...
Q2359−02..........	2.095	20.70	> −2.103	...	> −1.476	−0.777	...	...	...	−1.310	−1.550	−1.655	< −0.782	−1.526	−0.775
Q2359−02..........	2.154	20.30	> −1.859	...	−1.625	−1.583	...	...	...	...	−1.368	−1.877	...	< −1.342	< −1.069

TABLE 42

Relative Abundance Summary

Name	z_{abs}	N(H I)	[C/Fe]	[O/Fe]	[Al/Fe]	[Si/Fe]	[P/Fe]	[S/Fe]	[Ar/Fe]	[Ti/Fe]	[Cr/Fe]	[Co/Fe]	[Ni/Fe]	[Zn/Fe]
Q0000−2619[a]	3.390	21.41	...	...	...	0.411	...	...	...	...	...	...	...	...
BR 0019−15[a]	3.439	20.92	...	...	...	0.430	...	...	...	...	...	...	...	...
PH 957	2.309	21.40	...	<1.333	...	>−0.312	...	...	...	<−0.204	0.243	<0.783	0.151	0.306
Q0149+33	2.141	20.50	>−0.636	<2.198	>−0.247	0.282	...	...	...	<0.499	0.320	...	0.189	0.096
Q0201+36	2.463	20.38	...	...	>0.133	0.464	...	...	...	<−0.254	0.068	<0.537	0.262	0.584
J0255+00	3.253	20.70	...	...	>0.125	0.499	...	...	...	<0.601	...	<1.084	0.094	...
J0255+00	3.915	21.30	>−1.068	>−0.953	...	>−0.617	...	0.271	...	...	...	<1.052	−0.229	...
Q0336−01	3.062	21.20	>−0.997	>0.665	...	>0.176	0.198	0.389	0.421	...	...	...	−0.186	...
Q0347−38	3.025	20.80	>−0.488	>0.080	>−0.085	0.454	...	<0.557	0.759	...	...	<1.283	0.130	...
Q0458−02	2.040	21.65	...	>−1.343	>−0.610	>0.600	...	...	...	<−0.328	0.266	<0.300	0.048	0.581
HS 0741+4741	3.017	20.48	>−0.238	>0.289	−0.218	0.242	<−0.002	0.248	0.094	...	...	<1.496	−0.044	...
Q0836+11	2.465	20.58	>−0.701	>−0.562	...	0.250	...	<0.283	...	<0.421	<0.051	<1.296	−0.039	<0.272
Q0841+12[a]	2.375	20.95	...	...	>−0.428	0.406	...	...	...	...	0.129	<0.807	...	0.170
Q0841+12	2.476	20.78	...	...	>−0.304	>−0.095	...	...	...	<0.188	0.142	<0.786	0.075	0.349
BRI 0951−04	3.857	20.60	...	...	0.183	>0.462	...	...	...	...	...	<2.084	<0.124	...
BRI 0951−04	4.203	20.40	...	...	...	...	...	...	...	...	...	...	...	...
BRI 0952−01	4.024	20.55	>0.075	...	...	...	...	...	...	...	...	<2.153	<0.502	...
PSS 0957+33	3.279	20.32	...	...	>−0.035	0.453	...	...	...	...	...	<1.508	0.201	<0.590
PSS 0957+33	4.178	20.50	...	>−0.155	>0.137	0.367	...	0.563	...	...	...	<2.109	<0.031	...
BRI 1108−07	3.608	20.50	>−0.259	>−0.381	−0.052	0.318	...	...	...	...	...	...	<0.502	...
Q1210+17	1.892	20.60	...	...	>−0.501	0.274	...	...	...	...	0.122	<0.367	−0.069	0.249
Q1215+33	1.999	20.95	>−1.168	>−0.991	>−0.337	0.222	...	...	...	...	0.186	<0.702	0.096	0.412
Q1223+17	2.466	21.50	>−1.052	>−1.050	...	0.251	<0.696	...	...	<−0.345	0.166	<0.064	0.042	0.223
Q1331+17	1.776	21.18	...	...	>0.131	0.607	...	...	...	−0.222	0.086	<0.278	0.168	0.754
BRI 1346−03[b]	3.736	20.72	>−0.150	>0.063	...	0.302	...	...	<0.507	...	...	<2.264	<0.424	...
PSS 1443+27	4.224	20.80	>−0.642	>−0.526	>−0.236	>0.170	...	...	...	...	...	<0.895	0.137	...
Q1759+75	2.625	20.80	>−0.841	>−0.200	...	0.385	>−0.074	0.452	<−0.397	...	−0.050	<0.518	−0.039	>−0.573
Q1946+7658	2.844	20.27	...	0.211	...	0.304	...	<0.553	...	...	...	...	...	...
Q2206−19	1.920	20.65	...	...	>−0.216	0.440	...	...	...	0.032	0.172	0.254	0.186	0.448
Q2206−19	2.076	20.43	>−0.168	>−0.155	−0.157	0.297	...	...	...	...	<0.416	...	<0.510	<0.704
Q2230+02	1.864	20.85	...	...	...	0.412	...	...	...	−0.009	0.049	<0.524	0.194	0.446
Q2231−002	2.066	20.56	...	>−0.475	...	0.529	...	...	...	0.380	0.337	<0.748	0.196	0.520
Q2344+12	2.538	20.36	>−0.435	>−0.369	...	0.089	<0.684	<0.471	<0.212	...	...	...	<0.034	...
Q2348−01	2.426	20.50	...	...	>0.335	0.691	...	...	...	...	<−0.071	...	−0.014	...
Q2348−01[a]	2.615	21.30	...	...	>−0.294	0.389	...	...	...	...	0.061	...	...	<0.258
Q2348−14	2.279	20.56	>−0.221	>−0.343	−0.155	0.321	...	0.203	...	...	...	...	<0.011	...
Q2359−02	2.095	20.70	>−0.448	...	>0.179	0.878	...	...	...	0.345	0.105	<0.873	0.129	0.880
Q2359−02	2.154	20.30	>0.018	...	0.252	0.294	...	...	...	...	0.509	...	<0.535	<0.808

[a] Ni is serving as a proxy for Fe.

[b] Al is serving as a proxy for Fe.

Lyα forest cloud. We also report a tentative measurement of Ti II λ1910 for the system at $z = 2.095$. Given the very large Zn/Fe ratio for this system, the enhanced Ti/Fe ratio is strongly suggestive of Type II SN enrichment. Figures 38 and 39 present all of the new transitions, and Tables 39 and 40 list the column densities.

4. SUMMARY

Tables 41 and 42 present a summary of the absolute and relative abundances of the 38 DLA systems in our complete database. Regarding Table 42, where we present abundances relative to Fe, in a few cases we have considered Ni, Cr, or Al as a proxy for Fe, as noted.

We have presented ionic column density measurements for our complete sample of DLA systems. With the exception of a few important transitions that exhibit blends with other profiles, we have measured each column density with the apparent optical depth method. In general, therefore, all of the data have been reduced and analyzed with an identical approach. We have used the most up-to-date atomic data and will continue to update the database as new information becomes available. Visit the Web site mentioned in footnote 6 for tables, figures, and updated measurements. A series of companion papers (in particular, Paper II) present new scientific results based on this database.

We thank T. Barlow for providing the HIRES reduction package. We also thank Jim Lawler and Chris Howk for helpful discussions. We acknowledge the Keck support staff for their efforts in performing these observations. We thank R. Carswell and J. Webb for providing the VPFIT software package. J. X. P. acknowledges support from a Carnegie postdoctoral fellowship. A. M. W. was partially supported by NASA grant NAGW-2119 and NSF grant AST 86-9420443.

REFERENCES

Bergeson, S. D., & Lawler, J. E. 1993a, ApJ, 408, 382
———. 1993b, ApJ, 414, L137
Bergeson, S. D., Mullman, K. L., & Lawler, J. E. 1994, ApJ, 435, L157
Bergeson, S. D., Mullman, K. L., Wickliffe, M. W., Lawler, J. E., Litzen, U., & Johansson, S. 1996, ApJ, 464, 1044
Djorgovski, S. G., Gal, R. R., Odewahn, S. C., de Carvalho, R. R., Brunner, R., Longo, G., & Scaramella, R. 1998, in Wide Field Surveys in Cosmology, ed. S. Colombi & Y. Mellier, (Paris: Editions Frontieres), 89
Edmunds, M. G., & Phillips, S. 1997, MNRAS, 292, 733
Ellison, S. L., Ryan, S., & Prochaska, J. X. 2001, MNRAS, in press
Fan, X., et al. 1999, AJ, 118, 1 (SDSS Collaboration)
Fedchak, J. A., & Lawler, J. E. 1999, ApJ, 523, 734
Fedchak, J. A., Wiese, L. M., & Lawler, J. E. 2000, ApJ, 538, 773
Grevesse, N., Noels, A., & Sauval, A. J. 1996, in Cosmic Abundances, ed. S. Holt & G. Sonneborn (San Francisco: BookCrafters), 117
Hagen, H. J., Engels, D., & Reimers, D. 1999, A&AS, 134, 483
Howk, J. C., Savage, B. D., & Fabian, D. 1999, ApJ, 525, 253
Howk, J. C., Sembach, K. R., Roth, K. C., & Kruk, J. W. 2000, ApJ, 544, 867
Kirkman, D., & Tytler, D. 1997, ApJ, 484, 672
Lanzetta, K. M., Wolfe, A. M., & Turnshek, D. A. 1995, ApJ, 440, 435
Lu, L., Sargent, W. L. W., & Barlow, T. A. 1999, in ASP Conf. Ser. 156, Highly Redshifted Radio Lines, ed. C. Carilli, S. Radford, K. Menten, & G. Langston (San Francisco: ASP), 132
Lu, L., Sargent, W. L. W., Barlow, T. A., Churchill, C. W., & Vogt, S. 1996, ApJS, 107, 475 (L96)
Molaro, P., Bonifacio, P., Centurión, M., D'Odorico, S., Vladilo, G., Santin, P., & Di Marcantonio, P. 2000, ApJ, 541, 54
Molaro, P., Levshakov, S. A., D'Oderico, S., Bonifacio, P., & Centurion, M. 2001, ApJ, 549, 90
Morton, D. C. 1991, ApJS, 77, 119
Mullman, K. L., Lawler, J. E., Zsargo, J., & Federman, S. R. 1998, ApJ, 500, 1064
Outram, P. J., Chaffee, F. H., & Carswell, R. F. 1999, MNRAS, 310, 289
Pettini, M., Ellison, S. L., Steidel, C. C., Shapley, A. E., & Bowen, D. V. 2000, ApJ, 532, 65
Pettini, M., Lipman, K., & Hunstead, R. W. 1995, ApJ, 451, 100
Pettini, M., Smith, L. J., Hunstead, R. W., & King, D. L. 1994, ApJ, 426, 79
Pettini, M., Smith, L. J., King, D. L., & Hunstead, R. W. 1997, ApJ, 486, 665
Prochaska, J. X., Gawiser, E., & Wolfe, A. M. 2001, ApJ, 552, 99 (PGW01)
Prochaska, J. X., & Wolfe, A. M. 1996, ApJ, 470, 403
———. 1997, ApJ, 474, 140
———. 1999, ApJS, 121, 369 (PW99)
———. 2000, ApJ, 533, L5
———. 2001, ApJ, submitted (Paper II)
Raassen, A. J. J., & Uylings, P. H. M. 1998, A&A, 340, 300
Savage, B. D., & Sembach, K. R. 1991, ApJ, 379, 245
Schectman, R. M., Povolny, H. S., & Curtis, L. J. 1998, ApJ, 504, 921
Storrie-Lombardi, L. J., Irwin, M. J., & McMahon, R. G. 1996, MNRAS, 282, 1330
Storrie-Lombardi, L. J., & Wolfe, A. M. 2000, ApJ, 543, 552
Tripp, T. M., Lu, L., & Savage, B. D. 1996, ApJS, 102, 239
Turnshek, D. A., Wolfe, A. M., Lanzetta, K. M., Briggs, F. H., Cohen, R. D., Foltz, C. B., Smith, H. E., & Wilkes, B. J. 1989, ApJ, 344, 567
Verner, D. A. 1996, At. Data Nucl. Data Tables, 64, 1
Verner, D. A., Barthel, P. D., & Tytler, D. 1994, A&AS, 108, 287
Vogt, S. S., et al. 1994, Proc. SPIE, 2198, 362
Wiese, L. M., Fedchak, J. A., & Lawler, J. E. 2001, ApJ, 547, 1178
Wolfe, A. M., Fan, X.-M., Tytler, D., Vogt, S. S., Keane, M. J., & Lanzetta, K. M. 1994, ApJ, 435, L101
Wolfe, A. M., Lanzetta, K. M., Foltz, C. B., & Chaffee, F. H. 1995, ApJ, 454, 698
Wolfe, A. M., & Prochaska, J. X. 2000, ApJ, 545, 591
Wolfe, A. M., Prochaska, J. X., & Gawiser, E. 2001, ApJ, submitted
Wolfe, A. M., Turnshek, D. A., Smith, H. E., & Cohen, R. D. 1986, ApJS, 61, 249